

Regulation of synaptic signaling following environmental enrichment and local secretory trafficking in neuronal dendrites

Dissertation

zur Erlangung des akademischen Grades

doctor rerum naturalium (Dr. rer. nat.)

genehmigt durch die Fakultät für Naturwissenschaften der Otto-von-Guericke-Universität

Magdeburg

von Master of Science Maximilian Karl Borgmeyer

geb. am 05.08.1992 in Hamburg

Gutachter:

Prof. Dr. Daniela Dieterich

Prof. Dr. Andreas Grabrucker

eingereicht am: 26.08.2021

verteidigt am: 04.02.2022

Summary

A hallmark of the brain is its plasticity. To achieve this, the brain must be able to react to internal and external stimuli, either by changing or modifying molecular components of its neural cells or by altering connections between neurons. In the first part of this thesis a novel proteomics and lipidomics approach is used to analyze the protein and lipid composition of murine synapses. The second part of my thesis deals with the question how some of these synaptic proteins are processed and transported locally in dendrites. In fact, membrane lipids are important components of synaptic junctions. Compelling evidence suggests their participation in fundamental processes of synaptic neurotransmission. However, our knowledge about the lipid composition of synaptic membranes is still sparse. The protein and lipid content of synapses can be analyzed using mass spectrometry. The combination of both proteomics and lipidomics in a multiomics approach allows for the generation of novel hypotheses, which could not be achieved by applying only one of the techniques. In this study this approach is tested by applying it to a well-established mild stimulation protocol. To do this, mice were raised in an enriched environment (EE) with toys, housing, and social interactions. It is well known that this intervention results in improved physical and mental performance, while the molecular changes in the synapse which accompany these changes are poorly understood. A multiomics approach revealed a regulation of synaptic endocannabinoid signaling on both protein and lipid level following exposure to EE. Mice raised in EE showed a significant reduction of the synaptic levels of the signaling lipid 2-Arachidonoylglycerol (2-AG), which is the main agonist of the Cannabinoid receptor 1 (CB1R) in the hippocampus. A parallel proteomics approach revealed a regulation of two postsynaptic enzymes involved in endocannabinoid signaling. Fatty acid amide hydrolase (FAAH), an enzyme responsible for the degradation of 2-AG and N-arachidonylethanolamine (AEA), was significantly upregulated following EE. In contrast alpha/beta-Hydrolase domain containing 6 (ABHD6) a second enzyme responsible for the degradation of 2-AG was significantly downregulated. Based on further experimental work I propose that alterations in the postsynaptic association of ABHD6 and FAAH (catabolizing enzymes of 2-AG exclusively expressed in 30% of excitatory CA1/CA3 synapses) interact with lowered levels of 2-AG to facilitate endocannabinoid signaling (ECS)-sensitive forms of plasticity at a subset of CA1-CA3 synapses in EE. In brief, lower postsynaptic 2-AG levels appear to negatively influence the postsynaptic localization of ABHD6. This in turn increases surface expression of AMPARs following LTP induction as ABHD6 is an auxiliary subunit of AMPARs that negatively regulates surface expression. The increased synaptic activity will elevate postsynaptic FAAH levels and decrease 2-AG. Lower 2-AG levels will reduce CB1R signaling and the postsynaptic expression of ABHD6. These changes will only affect a subset of CB1R positive synapses in the Schaffer collateral pathway and will lower the threshold for the induction of certain forms of plasticity (metaplasticity). Many proteins involved in this pathway are synaptic transmembrane proteins, which have to undergo a complex series of quality controls and modifications following their exit from the endoplasmic reticulum (ER).

This process exists in all eukaryotic cells, but is especially challenging for neurons, since they are highly arborized and polarized cells. The soma makes up only 5% of the total cell volume and only 1% of membrane proteins are localized to the somatic cell membrane. This

morphological complexity poses a major challenge for neurons since they need to process and modify proteins far from the soma, in dendrites and axons which harbor up to 10000 synapses. Synaptic receptors such as AMPARs and NMDARs, as well as cell adhesion molecules that connect pre- and postsynapse undergo a complex series of quality controls and modification following their synthesis in the ER. The ER is continuous throughout the dendrites and many components of the secretory system, such as ERGIC and Retromer are abundant in dendrites. Mature glycosylation of surface proteins requires transport through Golgi membranes. The Golgi apparatus is located in the soma, while glycosylation machinery-containing Golgi satellites are present throughout the dendritic arbor. This ubiquitous distribution sets them apart from Golgi outposts, which are only found in a subset of primary apical dendrites. Calneuron 1 which is localized in Golgi satellites and the TGN and regulates the export of membranes from the Golgi in a calcium dependent manner. The number of Golgi satellites is reduced following Calneuron 1 KO. Loss of Calneurons also resulted in a loss of synapses predominantly in distal dendrites, suggesting a crucial role for Calneurons in these distal dendrites. This result points to an important role for Calneurons in stabilization and maintenance of Golgi satellites. Lectin stainings demonstrate that Golgi satellites contain O- and N- glycosylated proteins. A specific glycosylation, with a crucial function in synaptic plasticity, is the polysialylation of the cell adhesion molecule NCAM. Golgi satellites contain PSA-NCAM as well as the enzyme that catalyzes the polysialylation. Loss of Calneuron 1 results in loss of PSA-NCAM in distal dendrites. This confirms the importance of Calneuron 1 for the function of Golgi satellites and suggests an important role for Golgi satellites in synaptic plasticity relevant glycosylation in dendrites.

Zusammenfassung

Membranlipide sind wichtige Komponenten der synaptischen Membran. Überzeugende Hinweise legen nahe, dass sie eine fundamentale Rolle in der synaptischen Neurotransmission spielen. Allerdings ist das Wissen über die Lipidzusammensetzung der synaptischen Membran immer noch begrenzt. Die Protein- und Lipidzusammensetzung kann mit Hilfe von Massenspektrometrie untersucht werden. Die Kombination von Lipidomik und Proteomik in einem Multiomicsansatz, ermöglicht es neue Hypothesen zu generieren, die nicht durch die Verwendung nur einer der Methoden hätten erreicht werden können. Hierzu wurden Mäuse in einem sogenannten *enriched environment* (EE) mit Spielzeug, Versteckmöglichkeiten und sozialen Interaktionen gehalten. Es ist bekannt, dass diese Intervention in einer gesteigerten körperlichen und mentalen Leistungsfähigkeit resultiert, die damit einhergehenden molekularen Änderungen der Synapse sind nicht ausreichend geklärt. Der in dieser Arbeit verwendete Multiomicsansatz offenbarte eine Regulation der synaptischen Endocannabinoid-abhängigen Signalweiterleitung sowohl auf Protein- als auch auf Lipidebene infolge von EE. Die Mäuse zeigen eine signifikante Reduktion der synaptischen Konzentration des Signallipids 2-Arachidonoylglycerol (2-AG), wobei es sich um den Hauptagonisten des Cannabinoid-Rezeptors 1 (CB1R) im Hippocampus handelt. Ein paralleler Proteomikansatz offenbarte die Regulation zweier postsynaptischer Enzyme die an der Regulation der endocannabinoidabhängigen Signalweiterleitung beteiligt sind. FAAH ein Enzym, das sowohl für die Degradation von 2-AG als auch AEA verantwortlich ist, ist in Folge von EE deutlich hochreguliert. Im Gegensatz dazu war die synaptische Konzentration von ABHD6 in Folge von EE herunterreguliert. Basierend auf weiteren Versuchen schlage ich vor, dass die Assoziation von ABHD6 und FAAH (katabolische Enzyme von 2-AG, die in 30% der exzitatorischen CA1-CA3 Synapsen exprimiert werden) mit der Postsynapse mit verringerten Konzentrationen von 2-AG interagiert, was in Folge von EE zu einer Endocannabinoid-Signalübertragung (ECS)-sensitiven Form von Plastizität in einer Untergruppe von CA1-CA3 Synapsen führt. Kurz gesagt, geringere postsynaptische 2-AG Konzentrationen scheinen die postsynaptische Lokalisation von ABHD6 negativ zu beeinflussen. Dies wiederum führt zu einer verstärkten Oberflächenexpression von AMPARs infolge von LTP, da ABHD6 eine auxilare Untereinheit von AMPARs ist, die deren Oberflächenexpression negativ beeinflusst. Der Anstieg in synaptischer Aktivität erhöht postsynaptische FAAH Level und reduziert damit die Konzentration von 2-AG. Reduzierte 2-AG Level reduzieren die Signalweiterleitung durch CB1R und die postsynaptische Expression von ABHD6. Diese Änderungen betreffen nur eine Untergruppe von CB1R positiven Synapsen in der Schaffer-Kollaterale und reduzieren die Schwelle für die Induktion bestimmter Formen der Plastizität (Metaplastizität). Bei vielen Proteinen, die an diesem Prozess beteiligt sind, handelt es sich um synaptische Transmembranproteine, die eine komplexe Abfolge von Qualitätskontrollen und Modifikationen unterlaufen müssen, nachdem sie aus dem Endoplasmatische Retikulum (ER) exportiert wurden. Dieser Prozess existiert in allen eukaryotischen Zellen, stellt aber eine besondere Herausforderung für Neurone dar, da es sich bei ihnen um stark arborisierte und polarisierte Zellen handelt. Das Soma macht nur 5% des gesamten Zellvolumens aus und nur 1% der Membranproteine befinden sich in somatischen Zellmembranen. Diese morphologische Komplexität stellt Neurone vor eine große Herausforderung, da sie Proteine in großer Entfernung zum Soma in Dendriten und Axonen modifizieren müssen, auf denen

sich bis zu 10000 Synapsen befinden. Synaptische Rezeptoren, wie AMPARs und NMDARs, sowie Zelladhäsionsmoleküle, die Prä- und Postsynapsen verbinden, müssen nach ihrer Synthese im ER eine komplexe Reihe von Qualitätskontrollen und Modifikationen durchlaufen. Das ER ist durchgehend in den Dendriten verbreitet, wichtige Komponenten des sekretorischen Systems, wie ERGIC und Retromer sind ebenfalls weit verbreitet. Diese ubiquitäre Verteilung unterscheidet sie von Golgi-Außenposten, die nur in einer Untergruppe von primären apikalen Dendriten zu finden sind. Calneuron 1 lokalisiert zu Golgisatelliten und dem TGN und reguliert den Export von Vesikeln aus dem *trans*-Golgi-Netzwerk in Abhängigkeit von der freien Calciumkonzentration. Die Anzahl von Golgisatelliten ist in den Dendriten von Calneuron 1 Knockout Mäusen reduziert. Der Verlust von Calneuron führte zu einem Verlust von Synapsen, vor allem in distalen Dendriten. Diese Ergebnisse unterstützen die Annahme, dass Calneuron 1 eine wichtige Rolle für den Membrantransport und die Strukturhaltung von Golgisatelliten spielt. Lectin-Färbungen zeigen, dass Golgisatelliten O-, N- und *Core*-glykosylierte Proteine enthalten. Eine spezifische Glykosylierung, mit einer entscheidenden Funktion für synaptischer Plastizität ist die Polysialylierung des Zelladhäsionsmoleküls NCAM. Golgisatelliten enthalten PSA-NCAM sowie mindestens ein Enzym, dass die Polysialylation katalysiert. Verlust von Calneuron 1 führt zum Verlust von PSA-NCAM in distalen Dendriten. Dies bestätigt die Bedeutung von Calneuron 1 für die Funktion von Golgisatelliten und lässt vermuten, dass sie eine Rolle für plastizitätsrelevante Glykosylierung in Dendriten spielen.

Contents

| | |
|---|----|
| 1 Introduction | 4 |
| 1.1 The complex morphology of neurons poses a challenge for protein proteostasis..... | 4 |
| 1.2 Modern proteomics and the study of synaptic function..... | 5 |
| 1.3 A major technological advance: Multiomics | 6 |
| 1.4 The endocannabinoid system is a prominent example for lipid signaling in the brain..... | 8 |
| 1.5 Secretory trafficking of synaptic transmembrane proteins | 11 |
| 1.6 Polysialylation of the neuronal cell adhesion molecule (NCAM) | 12 |
| 1.7 The discovery of Golgi-satellites..... | 14 |
| 1.8 The hippocampus plays a crucial role in learning and memory and has been studied widely in the context of the cell biology of pyramidal neurons | 16 |
| 1.9 Aims | 17 |
| 2 Materials and Methods | 18 |
| 2.1 Materials and reagents..... | 18 |
| 2.1.1 Table 1 Drugs..... | 18 |
| 2.1.2 Table 2 Antibodies..... | 18 |
| 2.1.3 Table 3 Lectins | 20 |
| 2.1.4 Table 4 Constructs..... | 20 |
| 2.1.5 Table 5 Software..... | 21 |
| 2.1.6 Table 6 Solutions and Kits..... | 21 |
| 2.1.7 Table 7 Buffers and Media | 21 |
| 2.1.8 Table 8 Molecular cloning reagents | 23 |
| 2.2 Methods | 24 |
| 2.2.1 Bacterial culture and molecular cloning..... | 24 |
| 2.2.2 Competent bacteria..... | 24 |
| 2.2.3 Transformation..... | 24 |
| 2.2.4 Plasmid preparation | 24 |
| 2.2.5 Molecular cloning | 24 |
| 2.2.6 Cell culture..... | 25 |
| 2.2.6.1 Coating of coverslips | 25 |
| 2.2.6.2 Cell lines..... | 25 |
| 2.2.6.3 Transfection of cell lines..... | 25 |
| 2.2.6.4 Hippocampal rat primary culture..... | 25 |
| 2.2.6.5 Mouse hippocampal primary cultures | 26 |

| | |
|--|----|
| 2.2.6.6 Transfection of hippocampal primary neurons..... | 26 |
| 2.2.6.7 Treatments | 26 |
| 2.2.6.8 Release systems | 26 |
| 2.2.6.9 Organotypic slice preparation | 27 |
| 2.2.6.10 AAV production and transduction..... | 27 |
| 2.2.7 Cell culture stainings | 27 |
| 2.2.7.1 Immunocytochemistry (ICC)..... | 27 |
| 2.2.7.2 Lectin staining..... | 27 |
| 2.2.8 Immunohistochemistry (IHC) | 28 |
| 2.2.8.1 Perfusion | 28 |
| 2.2.8.2 Immunostaining of cryosections | 28 |
| 2.2.8.3 Lectin staining of cryosections | 28 |
| 2.2.9 Histology and electron microscopy | 29 |
| 2.2.9.1 Nissl staining..... | 29 |
| 2.2.9.2 Section preparation for transmission electron microscopy | 29 |
| 2.2.10 Subcellular fractionation experiments | 29 |
| 2.2.11. SDS-PAGE and western blot | 30 |
| 2.2.11.1 Protein measurement | 30 |
| 2.2.11.2 SDS-PAGE..... | 30 |
| 2.2.11.3 Immunoblotting..... | 30 |
| 2.2.12 Southern blot..... | 31 |
| 2.2.12 Mutant and transgenic mouse breeding..... | 31 |
| 2.2.12.1 Pronucleus injection | 31 |
| 2.2.12.2 Implantation | 32 |
| 2.2.12.3 Single cell embryo electroporation | 33 |
| 2.2.12.4 Environmental enrichment | 34 |
| 2.2.12.5 Genotyping | 35 |
| 2.2.13 Acute hippocampal slice preparation and electrophysiology | 35 |
| 2.2.14 Imaging..... | 36 |
| 2.2.14.1 Confocal imaging | 36 |
| 2.2.14.2 STED imaging | 36 |
| 2.2.14.3 Live cell imaging (TIRF, wide field) | 36 |
| 2.2.14.4 Electron microscopy | 36 |
| 2.2.14.5 Image analysis | 37 |
| 3 Results | 38 |

| | |
|---|----|
| 3.1 A novel multiomics approach using mice raised in an enriched environment | 38 |
| 3.1.1 Subcellular fractionation experiments | 41 |
| 3.1.2 No gross structural alterations occur in synaptic connectivity in response to EE | 42 |
| 3.1.3 Results of the multiomics screen | 44 |
| 3.1.4 Endocannabinoid-dependent plasticity is altered by EE | 45 |
| 3.1.5 Expression of catabolic enzymes of the endocannabinoid pathway are regulated following EE | 46 |
| 3.1.6 Localization and regulation of catabolic enzymes of the endocannabinoid pathway | 51 |
| 3.1.7 ABHD6 regulates the surface expression of AMPARs | 56 |
| 3.2 A functional characterization of Golgi satellites | 61 |
| 3.2.1 A GoltmCherry expressing mouse line, to label GS <i>in vivo</i> | 61 |
| 3.2.2 What is the role of Calneuron 1 in the assembly, maintenance and function of GS? | 66 |
| 3.2.3 Polysialylation of NCAM in GS..... | 70 |
| 4 Discussion | 75 |
| 4.1 Synaptoneurolipidomics is a novel research area and multiomics is well suited to generate novel hypothesis on synaptic function in plasticity | 75 |
| 4.2 ECS is altered in mice exposed to an EE | 77 |
| 4.2 Further characterization of Golgi-satellites in dendrites | 79 |
| 4.3 The needs of a synapse: How Golgi satellites serve synaptic function | 80 |
| 5 References | 82 |
| 6 Abbreviations | 94 |

1 Introduction

1.1 The complex morphology of neurons poses a challenge for protein proteostasis

Neurons are highly polarized with a complex cytoarchitecture. The number of synapses is typically very large; they harbor a complex arbor of dendrites and an axon that can project over long distances. This holds true in particular for projection neurons like pyramidal cells of the hippocampus. Their dendrites are covered with more than 10.000 spine synapses. Intriguingly, the somata of such neurons contribute less than 5% to the entire volume and their share of membrane is negligible (Rosenberg et al., 2014; Dieterich and Kreutz, 2016). These figures nicely illustrate the unique challenges for protein synthesis, sorting, modification, and transport in particular of membrane proteins. To function properly, proteins must pass through a complex secretory system that ensures correct protein folding and various posttranslational modifications (Barlowe and Miller, 2013). These highly regulated processes are crucial for synaptic function in light of the fact that chemical synapses have to maintain a complex balance between stability and plasticity (Abraham and Robins, 2005; Ohline and Abraham, 2019a). More than 2000 different proteins reportedly have a synaptic localization and several hundred different proteins can arguably be present in a single spine synapse (Dieterich and Kreutz, 2016). Synapses are the most complex cell-cell junctions in the body from a proteomics perspective. The synaptic junction consists of the presynapse, the synaptic cleft and the postsynapse. The cell-cell contact is established by a variety of cell adhesion molecules (e.g. Missler et al., 2012). The organization of transmembrane proteins in the synaptic membrane is accomplished on both sides by a specialized cytoskeleton, the cytomatrix of the presynaptic active zone and the so-called postsynaptic density (PSD) of the postsynapse (Banker et al., 1974; Blomberg et al., 1977). The PSD is assembled by various scaffolding proteins that serve to anchor neurotransmitter receptors, ion channels and cell adhesion molecules in the postsynaptic membrane. They link the spine synapse to the filamentous actin (F-actin) cytoskeleton and they target signaling machinery to the synapse (Bär et al., 2016). The receptors are typically activated upon neurotransmitter release from the presynapse. The neurotransmitter will then bind to ligand-gated ion channels in the postsynaptic membrane, which then results in channel opening and ion influx (Eric R. Kandel 2013). The second type of receptor belongs to the so-called G protein-coupled receptors, which can activate a large number of signal cascades in the postsynaptic cell. Chemical synapses can be separated into two classes. Inhibitory synapses are typically located on the dendritic shaft or the soma of the neuron. Their main scaffolding protein is Gephyrin, which recruits GABA receptors to the postsynapse and forms a lattice of oligomers (Grønberg et al., 2010). GABA receptors are permeable to chloride ions and therefore transmit an inhibitory signal in mature neurons. Glutamatergic synapses on the other hand are excitatory with their main receptors being the calcium and sodium conducting NMDARs and AMPARs, which are to a large degree sodium channels (Eric R. Kandel 2013). The receptors are anchored in a complex scaffold of matrix proteins, with the most important ones being the membrane-associated guanylate kinases (MAGUKs) and here critically PSD95 and the ProSAPShanks family (Dieterich and Kreutz, 2016).

The vast majority of excitatory synapses in the forebrain are so-called spine synapses. Spines are made up of a thin spine neck ensuring chemical and electrical isolation and a spine head

that contains the PSD. As the name PSD already suggests molecular crowding creates an electron-dense structure that it is visible as a dark structure in the electron microscope (EM). As mentioned above, the pre- and the postsynapse are connected across the synaptic cleft by a variety of cell adhesion molecules whose extracellular domains interact with each other. These proteins do not only connect both sides of the synapse but regulate signaling across the synapse (Missler et al., 2012; Duncan et al., 2021). Spines exhibit a high level of functional and structural plasticity; they can rapidly change their size and shape as well as surface expression of glutamate receptors and the organization of the PSD. The mechanism by which spines are potentiated is known as long term potentiation (LTP), which is believed to be the molecular basis for learning and memory. Induction of postsynaptic LTP has been shown to require calcium influx through NMDARs, which are present in all glutamatergic synapses. This initial influx of calcium triggers calcium-dependent proteins that further facilitate changes in the synapse, including Ca^{2+} /calmodulin-dependent protein kinase II (CaMKII). The potentiation of the synapse is facilitated by structural and functional changes. Globular actin polymerizes to form F-Actin expanding the synapse and enabling the trafficking of AMPARs. F-Actin is stabilized by Capping protein in calcium-dependent manner (Mikhaylova et al., 2018). The AMPAR receptors (GluA1-4) are assembled in different combinations into tetramers, which form the functional channel. In *cornu ammonis* 1 (CA1) pyramidal neurons 80% of synaptic AMPARs are composed of GluA1/A2 heteromers. GluA3/A2 heterodimers make up 10% of the total population (Yu et al., 2021). Less than 10% synaptic AMPARs in CA1 pyramidal neurons are GluA1 homomers but these are thought to play a crucial role in synaptic plasticity and might be recruited first during LTP formation (Plant et al., 2006; Liu and Zukin, 2007; Shepherd, 2012). AMPARs require mature glycosylation and have to undergo the secretory pathway (see below). AMPARs lacking mature glycosylation are not fully functional and undergo rapid lysosomal degradation (Kandel et al., 2018). Specific glycosylation sites necessary for proper assembly and surface expression have been identified for both GluA1 and GluA2 (Takeuchi et al., 2015; Kandel et al., 2018). LTP is maintained by anchoring AMPARs into the PSD by binding to scaffolding proteins, including PSD95. During LTP the PSD is enlarged as more scaffolding proteins are recruited into the synapse along with increased surface expression of AMPAR (Henley and Wilkinson, 2016; Park, 2018).

1.2 Modern proteomics and the study of synaptic function

The understanding of the molecular composition of synapses has been greatly advanced by mass spectrometry (MS) based proteomics (Bayés and Grant, 2009; Distler et al., 2014; Dieterich and Kreutz, 2016), which eventually revealed the complexity of the synaptic proteome. Just recently a database that was annotated and curated by experts has gone online (Koopmans et al., 2019). This SynGO database provides a comprehensive catalogue of the components of the synaptic proteome. To gain a more detailed understanding of the distribution of proteins within synapses individual complexes and sub-compartments have been analyzed in detail. Quantitative and stoichiometric models have been developed. The composition of synaptic vesicles from both glutamatergic and GABAergic synapses have been analyzed (Grønberg et al., 2010). The content of the synaptic cleft and the complexes of

multiple cell adhesion molecules have been characterized (Tanaka et al., 2012; Kang et al., 2014). More recent work based on these proteomic studies was focused on the topology of the synapse with nanoscopic resolution (Yang and Annaert, 2021). In addition, NMDAR and AMPAR complexes have been characterized, the subunit composition has been revealed as well as posttranslational modifications and auxiliary subunits (Bissen et al., 2019).

MS of AMPARs at different stages of transport and assembly revealed the components and the time line of this process in more detail (Brechet et al., 2017).

1.3 A major technological advance: Multiomics

The suffix -omics describes a comprehensive, or global, assessment of a set of molecules (<http://omics.org/>). In addition to the aforementioned proteomics analyzing proteins this includes genomics, epigenomics, transcriptomics, metabolomics and lipidomics (Hasin et al., 2017). Since the characterization of the synapse has been mostly focused on protein composition, there is now an effort to extend the omics approach beyond this and to integrate datasets of multiple molecule classes from a single sample. This approach is known as multiomics. Especially in the context of disease genomics, epigenomics and transcriptomics are widely used and combined (Zheng et al., 2019). MS has become the main tool for the analysis of lipids. Consequently, MS has undergone large scale technical progress with regards to speed, sensitivity and resolution (Yang and Sun, 2021). In parallel advanced lipid databases and search engines (Herzog et al., 2011; Peng et al., 2017) have enabled the identification of the detected lipid species. The brain is a highly lipid-rich organ with a complex lipid composition, which is based on a high chemical diversity (O'Brien and Sampson, 1965; Breckenridge et al., 1972; Chavko et al., 1993). Neurolipidomics aims to understand the interplay of lipids and proteins, their specific metabolism, and subcellular localization within brain regions to explore the basic dynamics of the neuronal lipidome (Han, 2007). The central role of lipids inter alia derives from their function to mediate fundamental neuronal processes including membrane formation and fusion (Bayés and Grant, 2009), myelin packing (Riccio et al., 2000) and direct lipid mediated signal transmission (Distler et al., 2014). Moreover, compelling evidence exists for a specific role of lipids in synaptic signal transduction. Neurotransmission for instance requires several specific trace lipids, including phosphatidylinositol phosphates (PtdInsPs) and negatively charged phosphatidylserine (PtdSer) in the cytosolic face of the plasma membrane, function at multiple steps of the synaptic vesicle cycle. In addition, at synaptic junctions lipids determine collective molecular dynamics of membrane shape and motion, which can in turn regulate ion channel activity (Koopmans et al., 2019), influence presynaptic protein interaction (Grønberg et al., 2010) and control the endocytosis machinery and receptor activity (Tanaka et al., 2012). Since most lipid mediators are direct or indirect products of polyunsaturated phospholipids, sufficient molar content of complex polyunsaturated lipids must be located at synaptic junctions to guarantee lipid mediator formation and neurotransmitter release (Kang et al., 2014). Finally, several lines of evidence suggest that the lipid composition of synapses might be dynamic (Jurado et al., 2010; Martin et al., 2014a). It is also clear that lipids impact on cellular functions and it is therefore of fundamental importance to correlate lipid dynamics with proteins that are essential for the synthesis, modification and turnover of lipids. Hence, it is not less than

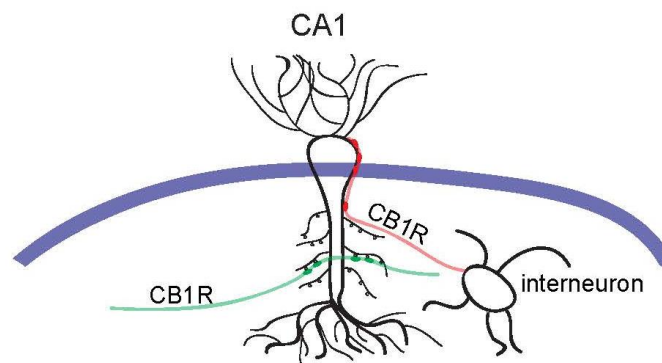
astonishing that neither a quantitative lipid inventory nor a detailed proteomic map of the lipid metabolism of the synaptic junction is available. Lipidomics of brain tissue is still in its infancy. The existence of more than 40 different lipids known to modulate signaling and/or to influence membrane geometry in neurons, synapses, and synaptic vesicles (Dieterich and Kreutz, 2016) demands for a systematic large scale study of lipid abundance and functional regulation in neuronal subcompartments. Modern lipidomic tools can provide access to understand the complexity of lipids, their homeostatic regulation, and their role in neuronal plasticity and in synaptic diseases (Steindel et al., 2013; Ellis et al., 2018). Thus, studies are ultimately warranted that break ground and provide a lipid inventory of synapses and synaptodendritic organelles and that address whether corresponding lipid alterations occur in brain disease states. During the past decade MS has evolved into a state-of-the-art technology for lipid analysis to address such questions. The technical progress regarding sensitivity, speed and resolution in MS, combined with advances in systems biology (Molenaar et al., 2019), the accessibility to lipid databases and search engines (Herzog et al., 2011) along with the availability of lipid standards for quantification nowadays allow us to address complex questions related to lipid function and regulation (Peng et al., 2018). Currently >400 lipids can be quantitatively accessed (Coman et al., 2016), while many lipid classes cannot be analyzed owing to impaired ionization and solubility, as well as low abundance. Recent publications demonstrated that the use of chemical tagging strategies lowered the detection limits of different lipid classes significantly (Züllig et al., 2020). At present one major obstacle within the field of brain lipidomics is to gain reproducible quantitative information about the spatial distribution of lipids as many lipids are present in different subcellular compartments. Thus, efforts to develop novel lipid quantification techniques tailored for the analysis of the synaptoneurolipidome will open up new avenues in synapse biology. Several lines of evidence suggest that the lipid composition of synapses is highly dynamic (Jurado et al., 2010; Martin et al., 2014a). Cholesterol is widely distributed in membranes and regulates the membrane fluidity. Removal of cholesterol from the hippocampus on the other hand results in a loss of LTP (Koudinov and Koudinova, 2001; Frank et al., 2008). Cholesterol has been shown to be recruited to the synapse upon glutamate stimulation (Dotti et al., 2014). In brain slices from aged mice adding cholesterol can restore the formation of LTP (Zhang and Liu, 2015). Sphingolipids have been shown to play a critical role in synapse formation and maintenance. Sphingomyelin (SM) has been shown to play an important role in the spine membrane-cytoskeleton crosstalk. SM mediates membrane binding and activity of main regulators of the actin cytoskeleton at synapses (Arroyo et al., 2014; Dotti et al., 2014). Sphingomyelinase KO for example results in a loss of F-actin (Arroyo et al., 2014). Another important synaptic sphingolipid is ceramide which influences membrane properties to favor receptor clustering and is involved in the transformation of filopodia into mature spines (Carrasco et al., 2012). It is also clear that lipids impact on cellular functions and it is therefore of fundamental importance to correlate lipid dynamics with proteins that are essential for the synthesis, modification and turnover of lipids. Another limitation that has to be overcome is that so far different biological building blocks i.e. proteins, lipids and

metabolites have largely been investigated independently. Thus, to date, studies targeting different molecular classes at once are cumbersome, rare and unique.

1.4 The endocannabinoid system is a prominent example for lipid signaling in the brain

Endocannabinoids were first discovered by studying the effects of tetrahydrocannabinol (THC) on the brain. While *Cannabis sativa* has been used for recreational and therapeutic purposes for millennia, THC was only identified as its active ingredient in 1964 (Gaoni and Mechoulam, 1964). The receptor to which THC binds was first identified in 1990 and named cannabinoid receptor 1 (CB1R) (Matsuda et al., 1990). Following this discovery, the two endogenous agonists of the endocannabinoid receptors, 2-Arachidonoylglycerol (2-AG) and N-arachidonylethanolamine (AEA) were identified.

The two endocannabinoid receptors CB1R and CB2R are expressed on various cell types throughout the body and are involved in a large variety of processes, including in the immune system as well as in the central and peripheral nervous system (Cartoon 1). The dominant endocannabinoid receptor in the central nervous system is the CB1R, which is expressed by neurons, as well as astrocytes and microglia (Kano, 2014). In hippocampal neurons the CB1R receptor is found in inhibitory synapses and in a subset of excitatory synapses. CB1R can couple to a large number of G proteins, depending on cell type and subcellular localization. CB1R can therefore trigger a wide variety of signal cascades. Additionally, the amount of CB1R that is expressed does not directly relate to the amount of endocannabinoid-related signaling (Breivogel et al, 1997). Inhibitory neurons in the hippocampus express more CB1R than excitatory neurons, but KO studies showed that excitatory neurons accounted for approximately 50% of endocannabinoid-dependent signaling in the hippocampus (Steindel et al., 2013).

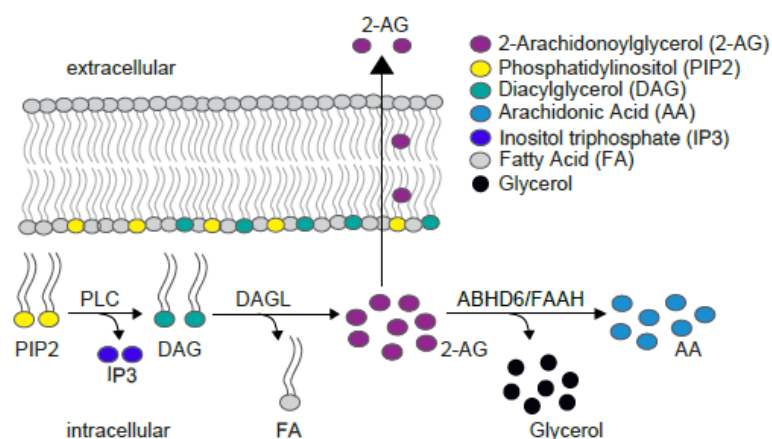


Cartoon 1. CB1R in the hippocampus

CB1R localizes to both inhibitory and excitatory presynaptic boutons in hippocampal neurons. All interneurons express CB1R and it is found in all inhibitory synapses. In contrast, only subsets of excitatory synapses in the Schaffer collateral projection contain CB1R. Release of ECs from the postsynaptic cell can therefore modulate both excitation (green) and inhibition (red) through activation of the CB1R.

While the main direction of signaling in neuronal communication is directed from the sending axon terminal via neurotransmitter release to the receptor-containing postsynaptic membrane also retrograde signaling mechanisms have been identified. One retrograde signaling

mechanism by which the postsynaptic receiving compartment sends feedback to the presynapse is the endocannabinoid system (Kano, 2014). Endocannabinoids (ECs) are non-charged lipids that following synthesis upon calcium influx readily pass the dendritic plasma membrane and largely act on a presynaptic CB1R (Castillo et al., 2012; Kano, 2014). Endocannabinoid signaling is probably best known for its role in short-term plasticity (Diana and Marty, 2004). The activation of CB1R can then lead to depolarization-induced suppression of inhibition (DSI) at inhibitory boutons and depolarization-induced suppression of excitation (DSE) at excitatory presynaptic terminals in order to match transmitter release to postsynaptic excitability and hereby locally modulate neurotransmission and modify excitation/inhibition (E/I) balance (Diana and Marty, 2004). In molecular terms this is caused by CB1R-dependent inhibition of presynaptic calcium channels which in turn reduces neurotransmitter release from the presynapse (Castillo et al., 2012). The dependence of both DSI and DSE on 2-AG-dependent activation was demonstrated by KO of diacylglycerol lipase (DAGL), which completely lacked retrograde endocannabinoid signaling (Gao et al., 2010; Tanimura et al., 2010; Yoshino et al., 2011). DAGLalpha is the dominant diacylglycerol lipase in the brain. Its constitutive KO was shown to result in an 80% reduction of 2-AG in the brain.

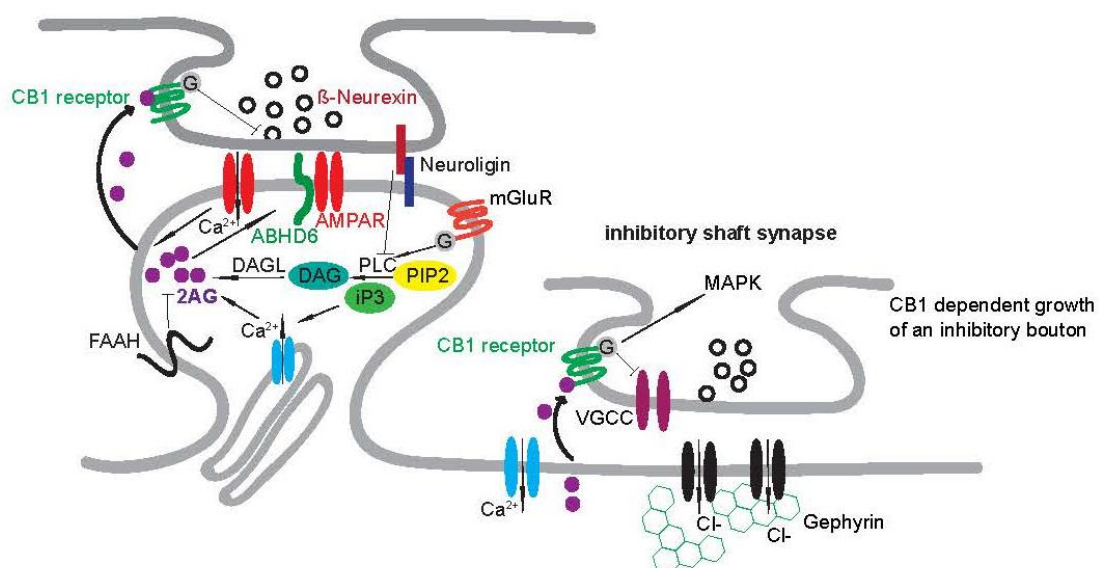


Cartoon 2. Synthesis and degradation of 2-AG

2-AG is synthesized from lipid precursors in the postsynaptic neuron. Diacylglycerol (DAG) is synthesized from Phosphatidylinositol by Phospholipase C (PLC). The second product of this reaction is inositol triphosphate (IP3), which can induce calcium release from intracellular calcium stores, by activation of the IP3-receptor (IP3R). 2-AG is synthesized from DAG by Diacylglycerol lipase (DAGL). Upon calcium influx, 2-AG exits the postsynaptic neuron and can bind CBRs. In the postsynaptic cell 2-AG can be degraded to Arachidonic Acid (AA) and Glycerol by either ABHD6 or FAAH.

The primary endogenous agonists of CB1R are 2-AG and AEA, with 2-AG being dominant in the hippocampus. 2-AG can be synthesized from diacylglycerol (DAG) by DAGL (Cartoon 2). DAGL has been found to localize to spines throughout the CA1 region of the hippocampus. (Katona et al., 2006) DAGL is localized perisynaptically within the spine head and mostly absent from the PSD, as was demonstrated by Katona et al. using immunogold electron microscopy (Katona et al., 2006). DAG in turn is synthesized from Phosphatidylinositol (PIP2) by Phospholipase C-β (PLCβ). PLCβ is activated by G protein subunit alpha q (Gq) following activation of G protein coupled receptors such as metabotropic

glutamate receptors (mGluRs), additionally PLC β requires an increase in calcium levels. PLC β is therefore considered to be a coincidence detector for combined mGluR activation and calcium influx (Hashimoto et al., 2005). Inositol trisphosphate (IP $_3$) activates the IP $_3$ receptor (IP $_3$ R) which is located on the ER and the spine apparatus and triggers release of calcium from these intracellular calcium stores. Shonesy et al. showed that postsynaptic calcium influx is required for the release of 2-AG (Shonesy et al., 2015). The main enzyme for the degradation of 2-AG on the presynaptic side is monoacylglycerol lipase (MAGL), which is responsible for the degradation of 85% of 2-AG in the brain (Savinainen et al., 2012). In the postsynaptic compartment alpha/beta-Hydrolase domain containing 6 (ABHD6) and fatty acid amide hydrolase (FAAH) are involved in the catabolism of 2-AG (Cartoon 3). However, FAAH is considered to be the main enzyme for the degradation of AEA but might under certain conditions also catabolize 2-AG (Di Marzo and Maccarrone, 2008). Thus, the degradation of endogenous cannabinoids might occur in a highly localized manner. Previous work has shown that both enzymes are found in apposition to a subset of CB $_1$ R-containing excitatory terminals (Schwenk et al., 2019), which account for 30% of all glutamatergic boutons on hippocampal CA1 pyramidal neurons (Marrs et al., 2010; Zimmermann et al., 2019). This is of interest because retrograde endocannabinoid signaling (ECS) has been shown to be not only involved in short-term plasticity but also in the regulation of longer lasting forms of plasticity. Of note in this regard, in addition to its role in the regulation of postsynaptic 2-AG, ABHD6 also acts as an accessory subunit of AMPARs. ABHD6 interacts with AMPARs during assembly in the ER and regulates forward trafficking to the synapse (Wei et al., 2017; Schwenk et al., 2019). Conclusive evidence was provided that ABHD6 is also an auxiliary subunit of AMPAR that negatively regulates surface expression (Henley and Wilkinson, 2016). It is currently unknown whether both functions are coupled but it is tempting to speculate that 2-AG levels and ECS are linked to secretory trafficking of both transmembrane proteins.



Cartoon 3. CB $_1$ R-containing synapses

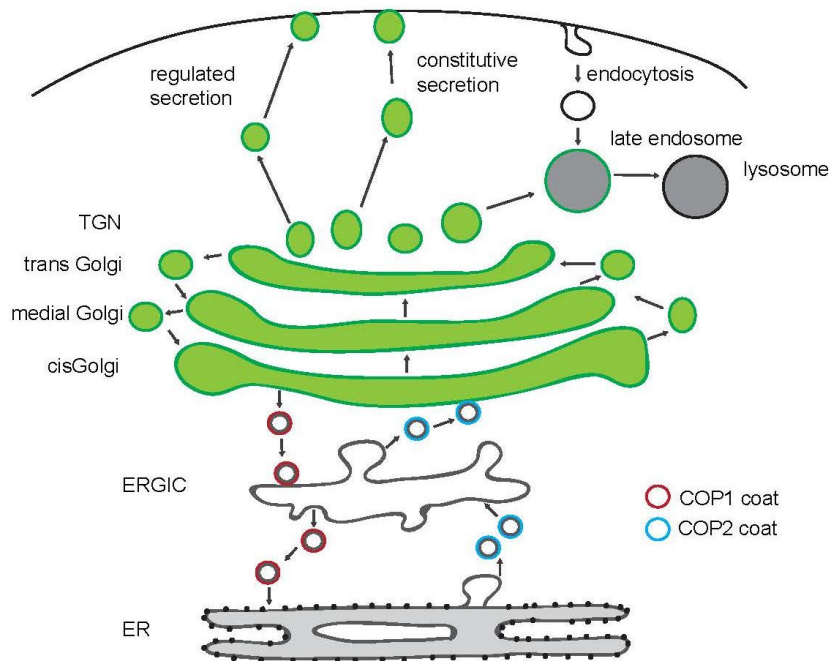
CB $_1$ R is located on presynaptic boutons of inhibitory and excitatory synapses. Inhibitory synapses localize to the dendritic shaft or the soma and contain the matrix protein Gephyrin

(green). 2-AG (purple) is released from the ER upon Ca^{2+} from extracellular or intracellular stores. Upon activation by 2-AG, the CB1R can inhibit neurotransmitter release and activate multiple downstream signaling cascades including mitogen-activated protein kinase (MAPK) signaling. 2-AG is synthesized in the postsynapse. The postsynaptic degradatory enzymes of 2-AG, FAAH and ABHD6 are located in the postsynapse.

1.5 Secretory trafficking of synaptic transmembrane proteins

AMPA receptors are heteromeric receptors that are assembled in varying combinations from four different subunits called GluA1, GluA2, GluA3 and GluA4 (Park, 2018). AMPARs are mediators of the majority of excitatory neurotransmission in the mammalian CNS. AMPAR trafficking is highly regulated and a key factor in neuroplasticity (Henley and Wilkinson, 2016). AMPARs are anchored to the postsynaptic density by PSD95. Interestingly, during the induction of LTP additional AMPARs are inserted into the postsynaptic membrane (Herring and Nicoll, 2016), whereas the opposite has been reported following the induction of LTD (Henley and Wilkinson, 2016). Secretory trafficking prior to their insertion into the synaptic membrane has been studied extensively and it was shown that AMPARs have to undergo a complex chain of quality controls and posttranslational modifications (Henley and Wilkinson, 2016). Specific glycosylation patterns are key to their assembly, turnover and function (Tucholski et al., 2013; Takeuchi et al., 2015; Kandel et al., 2018; Morise et al., 2020). This holds true for a large number of synaptic proteins, making proper functioning of secretory trafficking critical for neuronal function. Canonically, proteins that traffic to the cell membrane undergo the following stepwise processes: Following translation at the endoplasmic reticulum (ER), proteins are transported through the ER-Golgi intermediate compartment (ERGIC) (H. Lodish, 2013) (Cartoon 4). This transport is carried out through coat protein complex II (COP2) coated vesicles. These vesicles are formed by recruiting of COP2 and the secretion-associated Ras-related GTPase 1A (Sar1) from the cytosol. The disassembly of the COP2 coat is initiated by guanosine-5'-triphosphate (GTP) hydrolysis to guanosine diphosphate (GDP). Retrieval of membranes from the ERGIC occurs through COP1 coated vesicles. COP1 is associated with the GTPase ADP-ribosylation factor (ARF) and the disassembly is regulated in a similar manner. ER proteins contain specific signal sequences including the KDEL motif mediating their retrieval from the ERGIC to the ER (Capitani and Salles, 2009). The *cis*-Golgi lumen has a pH of 6; under these conditions the KDEL-receptor binds the KDEL motif with high affinity. Upon binding the receptor is sorted to vesicles and returns to the ER. In the higher pH environment of the ER lumen the affinity of the KDEL receptor for the KDEL-motif is reduced and the protein returns to the ER membrane, while the KDEL receptor is recycled back to the *cis*-Golgi. From the ER, proteins are exported to the *cis*-face of the Golgi Apparatus (GA); they are transported through the medial Golgi and are exported through the *trans*-Golgi network (TGN). The *cis*-Golgi is identified by the Golgi matrix protein 130 (GM130). The enzymes responsible for modification in the GA are sorted in the order of their activation. In the *cis*-Golgi the first phase of Golgi-modifications takes place. Mannose residues are removed from N-glycans allowing for complex modifications at a later stage. The second phase of modification takes place in the medial Golgi, where highly complex glycans are generated. In the *trans*-Golgi

and the TGN proteins are sorted depending on their final destination. In addition, specialized modifications such as polysialylation and fucosylation takes place here.



Cartoon 4. The secretory system in eukaryotic cells

Proteins are synthesized on ribosomes (black) at the rough endoplasmic reticulum (ER) (grey). Proteins are trafficked to the ER-Golgi intermediate compartment (ERGIC) in COP2 coated vesicles (blue). Retrograde trafficking takes place in COP1 coated vesicles (red). Cargo enters the Golgi Apparatus (GA) (green) on the *cis*-face and exits at the *trans*-face. From: <https://www.cureffi.org/2013/02/24/cell-biology-04-the-secretory-pathway/>

From here, surface proteins are transported to the cell membrane. The transport through the GA is bidirectional. Retrograde transport through the GA is mediated by the endosome-to-Golgi-retrieval pathway (Seaman et al., 1997; Seaman, 2009). A central part of this pathway is the retromer complex (Chen et al., 2019). It contains a trimeric subcomplex of vacuolar protein sorting-associated proteins (VPS) 26, 29 and 35 (Zhang et al., 2018). The VPS complex interacts with a wide variety of cargo adaptors, which are key for the recognition of specific cargoes. These cargoes can either be retrieved to the Golgi or transported out to the cell membrane.

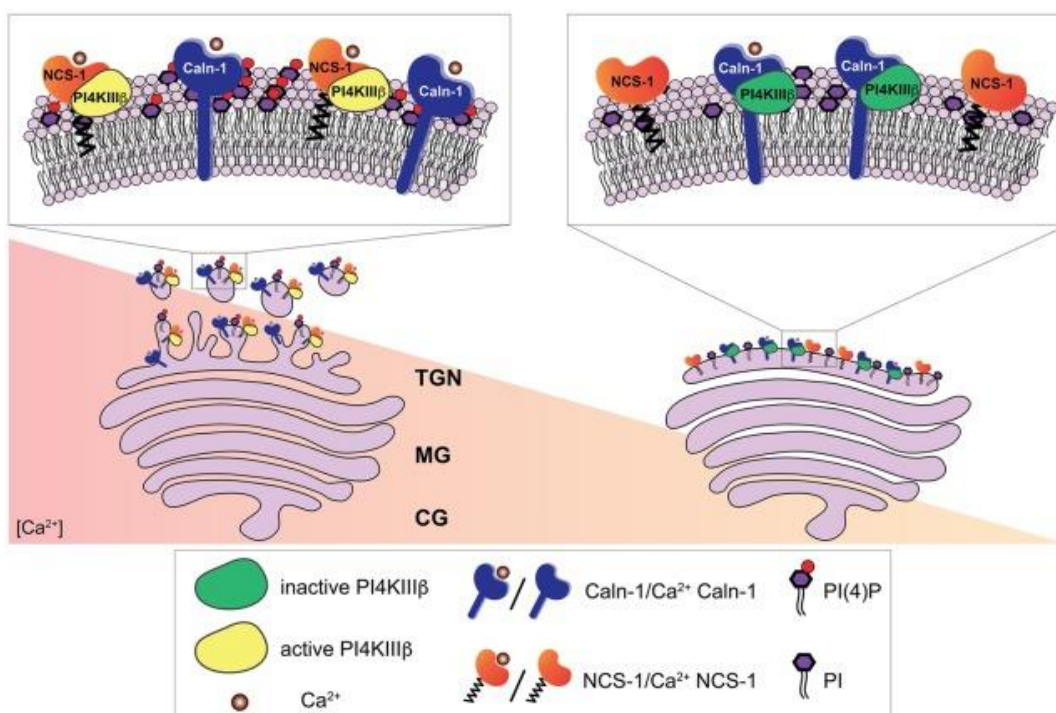
1.6 Polysialylation of the neuronal cell adhesion molecule (NCAM)

A specific type of glycosylation with many crucial functions in the central nervous system is polysialylation (PolySia). PolySia is a linear homopolymer of sialic acid; its length varies between 8 and 400 monomers. In vertebrates, PolySia is most abundant in the developing brain, but is also found at lower levels in the adult brain (Gascon et al., 2007; Rutishauser, 2008). The main carrier of PolySia is NCAM. The abundance of polysialylated NCAM is highly regulated. The two main responsible enzymes for the polysialylation of NCAM are alpha-2,8-sialyltransferase 8B (St8Sia2) and CMP-N-acetylneuraminase-poly-alpha-2,8-sialyltransferase (St8Sia4). St8Sia2 is the dominant enzyme during embryonal and early development (Kröcher et al., 2013). At this stage, polysialylation is crucial for cell migration, dendritic branching and axon growth and guidance (Mühlenhoff et al., 1996). All these

processes require membranes of neighboring cells to disassociate to move freely. This is achieved by accumulating negatively charged PolySia in the cell membrane. The negative charges repel each other and the PolySia chains take up a large volume, resulting in a widening of the intercellular space and inhibiting cell adhesion. During the early development, St8Sia2 is downregulated and replaced by St8Sia4 (Kröcher et al., 2013). Double KO of both enzymes results in severe morphological abnormalities in the mouse brain (Weinhold et al., 2005). Overall PolySia levels are low in the adult brain, with only adult stem cell niches such as the subgranular zone (SGZ) retaining high levels of PolySia throughout development. While the total abundance of polysialylated neuronal cell adhesion Molecule (PSA-NCAM) is low in the adult brain the process of polysialylation is crucial for the formation of both LTP and LTD (Muller et al., 1996), the reasons for the dependence of plasticity on polysialylation are biochemical and biophysical in nature. As is the case for cell migration plastic changes of synapses also require flexibility of the membrane which is achieved by reduction of cell adhesion (Gascon et al., 2007; Guan et al., 2015; Monzo et al., 2017). Additionally, NCAM directly and indirectly regulates a number of signaling pathways. Most notably, PSA-NCAM regulates Ca^{2+} channels (Kochlamazashvili et al., 2010). GluN2B-mediated Ca^{2+} transients are inhibited by PSA-NCAM only at low micromolar concentrations of glutamate, suggesting that the inhibition takes place at extrasynaptic GluN2B-containing NMDA receptors (Kochlamazashvili et al., 2010). PolySia can also prolong the opening time of AMPA receptors, but does not modulate the channel conductance (Vaithianathan et al., 2004). Modifications such as polysialylation take place on proteins all over the cell surface not just near the soma. This raises the question if all these processes can be carried out by the somatic GA. Additionally; some proteins are synthesized locally and are never transported through the soma. To this point it is unclear what percentage of proteins are synthesized in the soma compared to the neurites. Based on the relatively sparse distribution of large polyribosomes with more than three ribosomes it is being assumed that the vast majority of proteins are synthesized in the soma (Ostroff et al., 2018). This estimate has recently been challenged by the discovery of a large number of active monoribosomes in the neurites (Biever et al., 2020). It is however clear that the essential components of the secretory pathway are present in the entire dendritic arbor. The rough ER is continuous throughout the dendrites, ERGIC and retromer are also found all over the dendrites (Mikhaylova et al., 2016). Even though all other key components of the secretory system are present in the dendrites the presence of Golgi membranes was debated for a long time. Horton and Ehlers (2003) demonstrated for the first time the presence of Golgi membranes called Golgi outposts in the apical dendrite of hippocampal neurons (Horton and Ehlers, 2003). In pyramidal neurons the somatic GA can extend into the apical dendrite. In a subset of only 10% of the apical dendrites disconnected Golgi outposts were also found. This was in contrast to all other components which were present throughout all dendrites of all neurons. The labeling of Golgi membranes was mostly conducted using antibodies against proteins involved in the cisternae organization from *cis*- to *trans*- face, as a result smaller dendritic membranes that did not contain multiple cisternae were missed (Mikhaylova et al., 2016).

1.7 The discovery of Golgi-satellites

Mikhaylova et al. (2016) solved this problem by studying the protein family of Calneurons. Calneurons are prominently localized to the TGN and play an important role in the regulation of membrane export (Cartoon 5). Interestingly, Calneuron 1 and 2 are not only found in the soma, but also throughout the dendrites, suggesting a role in local secretory trafficking in dendrites. Calneurons are anchored to the TGN by their transmembrane domain. The transmembrane domain alone is sufficient for the Golgi localization of the full protein, due to its interaction with transmembrane domain recognition complex/ATPase (TRC40/Asna1) (Hradsky et al., 2011). At the TGN Calneurons interact with Phosphatidylinositol 4-kinase III beta (PI4KIII β) at low calcium levels and inhibits its activity. At higher calcium levels the Neuronal Calcium Sensor 1 (NCS1) binds calcium and replaces Calneuron 1 activating PI4K β (Taverna et al., 2002).

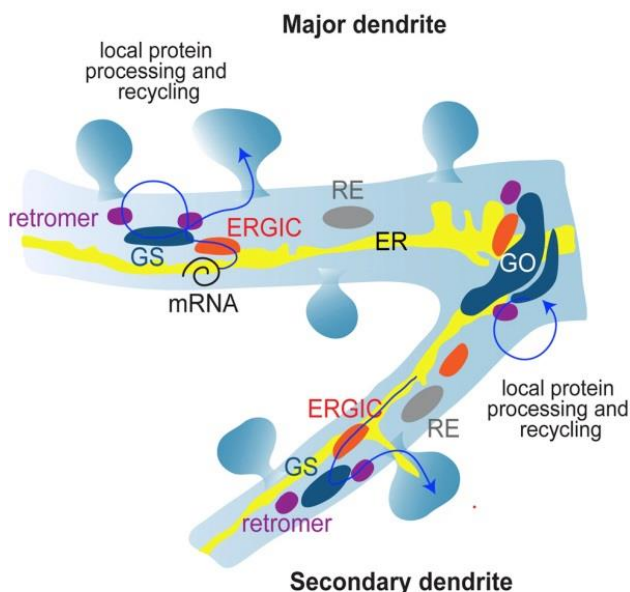


Cartoon 5. Calneuron 1

The GA consists of *cis*-Golgi, medial Golgi and *trans*-Golgi. Calcium-dependent regulation of the phosphatidylinositol 4-kinase III β (PI4KIII β) by Calneuron 1 and NCS-1 at the *trans*-Golgi network (TGN). The PI4KIII β -catalyzed synthesis of phosphatidylinositol 4-phosphate (PI(4)P) from phosphatidylinositol (PI) at the TGN membrane is a key step in the process of vesicle budding for TGN to plasma membrane trafficking. Ca²⁺-bound Calneuron 1 inhibits the activity of PI4KIII β at basal intracellular calcium concentrations, [Ca²⁺], (right). Middle and high calcium concentration (left) can lead to a fully Ca²⁺-bound NCS-1 protein, which then can replace Calneuron 1 from PI4KIII β thus leading to a strong increase in the production of PI(4)P and vesicle membrane budding (cartoon from Mundhenk et al., 2019).

Activation of PI4KIII β is necessary for the release of vesicles from the TGN. Integration of PI4P in the outer TGN membrane increases the membranes curvature promoting vesicle formation. Additionally, PI4P is indirectly responsible for the recruitment of cholesterol and Sphingomyelin to the TGN, by interacting with lipid transporter proteins. Reduction of Calneuron 1 levels can lead to an uncontrolled release of membrane from the TGN

(Mikhaylova et al., 2009). Overexpression of Calneuron 1 on the other hand leads to a replacement of NCS1 at higher calcium levels resulting in membrane retention and an expansion of the TGN. In addition to their function at the TGN, the NCS 1/Calneuron 1 switch can also regulate the signaling of G protein coupled receptors such as muscarinic acetylcholine receptor M1 (M1R) and CB1R (Angelats et al., 2018). The localization of Calneuron 2 on the other hand is more restricted to Golgi membranes. In contrast to Calneuron 1, Calneuron 2 expression in the brain is mostly restricted to the thalamus (Mikhaylova et al., 2006). Making use of the specific TGN localization of Calneuron 2 a probe was generated based on the transmembrane domain of Calneuron 2 coupled to an ER export signal and the fluorophore mCherry, called pGolt-mCherry (Bera et al., 2016). The probe labels the somatic GA in both neurons and non-neuronal cells, but in neurons it additionally labels small Golgi structures called Golgi-Satellites (GS) throughout the dendrite (Cartoon 6) (Mikhaylova et al., 2016). While Golgi marker proteins involved in the cisternal organization of the GA are missing from GS, Golgi enzymes such as the Lactosylceramide alpha-2,3-sialyltransferase (ST3Gal5) and Mannosidase 2 (Man2) are frequently found in GS (Mikhaylova et al., 2016). GS can be visualized using *Aleuria aurantia* lectin (AAL) which labels fucosylated glycans and PSA-NCAM is accumulated in GS. Collectively this data suggests that different components of the glycosylation machinery are present in GS. Additionally, GS are frequently localized in close proximity to the ERGIC, thus the GS might receive newly synthesized proteins from the ER (Cartoon 6). Additionally, GS are closely associated with the retromer complex raising the possibility that GS might also receive retrograde traffic of synaptic receptors (Mikhaylova et al., 2016). This suggests that GS are able to receive cargo from both the ER and the plasma membrane.

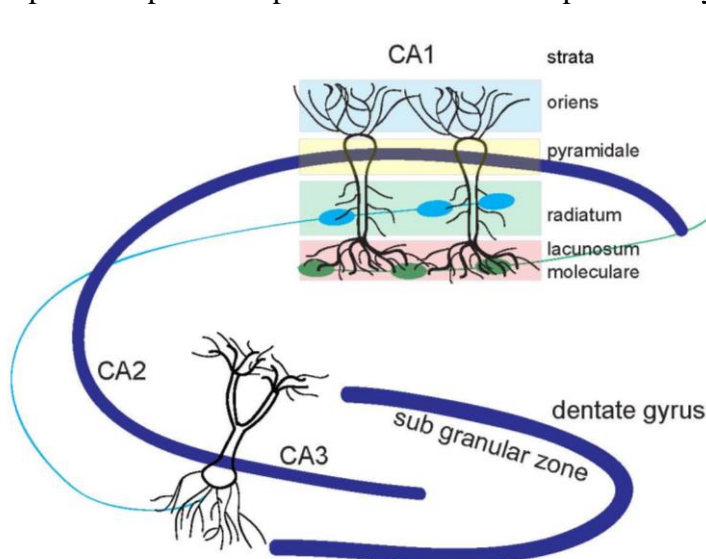


Cartoon 6. Golgi satellites inbetween ERGIC and Retromer

In contrast to Golgi outposts (GO), Golgi satellites (GS) are present throughout basal and apical dendrites of all pyramidal neurons. The GS system contains glycosylation machinery and is localized between ERGIC (red) and retromer (violet). GS receive cargo from the ER (yellow) which is continuous throughout the dendrite and from the cell membrane. Cartoon from Mikhaylova et al., 2016.

1.8 The hippocampus plays a crucial role in learning and memory and has been studied widely in the context of the cell biology of pyramidal neurons

Structure and function of the hippocampus show many similarities between humans and mice and all the main strata and projections are found in both species (Bergmann et al., 2016). Mice are therefore a popular model in learning and memory research and many standardized tests have been established to test their cognitive abilities (Vorhees and Williams, 2014). The hippocampus is also a key structure in the study of learning and memory (Knierim, 2015). Key processes of synaptic plasticity such as LTP and LTD were originally studied in the hippocampus (Knierim, 2015). As a matter of fact the Schaffer collateral projection from the CA3 to the CA1 region is one of the best studied projections of the brain. The hippocampus is divided into four main regions (Cartoon 7). The dentate gyrus (DG) constitutes a separate structure and is mainly made up of granule cells. It contains the SGZ, which is one of only two regions in the adult brain that contains neuronal stem cells. From the DG mossy fibers project on the CA3 regions (Cartoon 7). Schaeffer collaterals project from the CA3 region to the CA1 and CA2 regions. The CA1 pyramidal neurons project out of the hippocampus to the entorhinal cortex and the subiculum. The CA1 region is separated into four main regions (Cartoon 7). The stratum oriens contains the basal dendrites of the pyramidal neurons; they receive their main excitatory input from the CA3 region and the contralateral hippocampus. The somata of interneurons, including inhibitory basket cells are also localized in the stratum oriens (Kochlamazashvili et al., 2010). The stratum pyramidale contains the soma of the pyramidal neurons. The somata contain the highest density of inhibitory synapses in and receive input from interneurons from the other strata. Some of the somata of interneurons are also localized in the cell layer. The stratum radiatum contains the apical main dendrites of the pyramidal neurons. It receives the main input from the CA3 region (P. Andersen et al. 2007). The most distal dendrites are located in the stratum lacunosum moleculare (Lacaille and Schwartzkroin, 1988). When the apical main dendrites reach the stratum lacunosum moleculare, they rapidly branch into smaller dendrites. The lacunosum moleculare receives input from perforant path fibers from the superficial layers of the entorhinal cortex.



Cartoon 7. Schematic representation of the hippocampus

Cell layers are shown in dark blue. The strata of the CA1 region are shown: Stratum oriens (blue), pyramidale (yellow), radiatum (green), lacunosum moleculare (pink). The Schaffer collateral projection to the CA1-region is shown in blue, the perforant path from the cortex is shown in green.

1.9 Aims

To understand how the brain reacts to internal or external stimuli is still subject to many investigations. This study aims to test the utility of a novel multiomics approach, allowing for an in depth analysis of multiple components of the synapse. This approach will be tested using a mild stimulation protocol called environmental enrichment, to demonstrate its utility in the detection of plasticity induced changes of the molecular composition of the synapse. I further aim to use the data generated by this approach to formulate hypotheses regarding synaptic signaling pathways that depend on proteins and lipids and test those using a variety of independent methods.

Crucially, changes in synaptic protein composition as detected by the multiomics approach require secretory trafficking, local protein synthesis and protein modification in dendrites. Therefore, my second aim was to get a deeper insight into these processes. I concentrate on the function of Calneuron for dendritic trafficking and on the role of Golgi-satellites for local protein modification. To this end, I want to develop tools to study the function of GS *in vivo*, by generating and characterizing a transgenic mouse line expressing a molecular marker for GS. Further, I aim to study the role of Calneuron 1 in secretory trafficking *in vivo* and *in vitro*, with a focus on its role in the membrane of GS. To this end, I will generate and characterize a Calneuron 1 KO mouse line.

2 Materials and Methods

2.1 Materials and reagents

2.1.1 Table 1 Drugs

| Drug | Source | Solvent/final concentration |
|----------------------------|------------------------|--|
| Tetrodotoxin citrate (TTX) | Alomone labs T-550 | solvent: H ₂ O final concentration: 1 μ M |
| Bicuculline | Tocris bioscience 2503 | solvent: DMSO final concentration: 50 μ M |
| Am251 | Cayman chemicals 71670 | solvent: DMSO final concentration: 10 μ M |
| Rimonabant | Sigma-Aldrich | solvent: DMSO final concentration: 1 μ M |
| D-AP5 | Tocris bioscience 0106 | solvent: H ₂ O final concentration: 50 μ M |
| CNQX | Tocris bioscience 0190 | Solvent: DMSO final concentration: 10 μ M |

2.1.2 Table 2 Antibodies

| Antibody | Source | Identifier and dilution |
|-------------------------|--|--|
| rabbit anti-ABHD6 | Ken Mackie; Indiana University Bloomington | N/A |
| guinea pig anti-Shank3 | Synaptic Systems | Cat# 162304; RRID:AB_2619863 IHC 1:300 ICC 1:1000 |
| Rabbit anti-MAP2 | Millipore | AB5622 |
| mouse anti-MAP2 | Sigma-Aldrich | Cat# M440; RRID:AB_477193 IHC 1:500 |
| guinea pig anti-MAP2 | Synaptic Systems | Cat# 188 004; RRID:AB_2138181 IHC 1:500 |
| guinea pig anti-Bassoon | Synaptic Systems | Cat# 141004; RRID:AB_2290619 IHC 1:500 |
| mouse anti-Gephyrin | Synaptic systems | Cat# 147011; RRID:AB_887719 IHC 1:500 |
| mouse anti-PSD 95 | UC Davis/NIH, NeuroMab | Cat# 75-028; RRID:AB_2307331 WB 1:1000 |
| mouse anti-CB1R | Synaptic Systems | Cat# 258 003; IHC, ICC 1:500 |
| rabbit anti-GluA1 | Merck Millipore | Cat# ABN241 Surface staining 1:500 |
| rabbit anti-GluA1 | Cell Signaling Technology | Cat# D4N9V IHC 1:500 |
| rabbit anti-FAAH | Cayman Chemicals | Cat# 101600 ICC, IHC 1:200 |
| mouse anti-FAAH | Abcam | Cat# ab54615 WB 1:1000 |
| rabbit anti-MAGL | Abcam | Cat# ab24701 ICC 1:500 |

| | | |
|---|-------------------------|---|
| mouse anti-Synaptophysin1 | Synaptic Systems | Cat# 101 011 ICC, IHC 1:500 |
| mouse anti beta Tubulin | Sigma-Aldrich | Cat# T8660; RRID:AB_477590 WB 1:1000 |
| mouse anti-Synaptopodin | Origene | Cat#BM5086; Clone G1D4 |
| rabbit anti-Calneuron 1, 8921,8929,8930 serum / purified Ab | Kreutz laboratory | N/A |
| rabbit anti-Phospho-CREB (ser133) (87G3) | Cell Signaling | 9198 |
| mouse anti-GM130 | Abcam | ab52649 |
| guinea pig anti-Giantin | Synaptic Systems | 263 005 |
| rabbit anti-RFP | Rockland | 600-401-379 |
| rabbit anti-Syntaxin 6 | Synaptic Systems | 110 062 |
| mouse anti-Syntaxin 6 | BD Biosciences | 610635 |
| mouse anti-Polysialic Acid- NCAM (PSA-NCAM) | Millipore | MAB5324 |
| rat monoclonal anti-HA | Roche | 11867423001 |
| mouse anti-NCAM1 (RNL-1) | Abcam | ab9018 |
| anti-mouse-AlexaFluor 488 | ThermoFisher Scientific | Cat# A-11001, RRID:AB 2534069, IF- 1:500 |
| anti-guinea pig-AlexaFluor 488 | ThermoFisher Scientific | Cat# A-11073; RRID:AB_2534117 IF- 1:500 |
| anti-mouse-AlexaFluor 568 | ThermoFisher Scientific | Cat# A-11004; RRID:AB_2534072 IF- 1:500 |
| anti-Rabbit IgG–Abberior STAR 635P | Abberior | Cat# 2-0012-007-2 IHC/ICC 1:500 |
| anti-guinea pig-AlexaFluor 568 | ThermoFisher Scientific | Cat# A-11075; RRID:AB_2534119 IF- 1:500 |
| anti-rabbit-IgG-HRP | Dianova | Cat# 111-035-114 1:20000 |
| anti-mouse-IgG-HRP | Dianova | Cat# 115-035-146 1:20000 |
| GFP-Booster Atto488 | Nanotag | Cat# N0304-At488-L 1:250 |
| RFP-Booster Atto580 | Nanotag | Cat# N0401-Ab580-L 1:250 |
| anti-rabbit-ATTO 647N | Sigma-Aldrich | Cat# 40839 1:250 |
| AbberiorStar 580 guinea pig | Abberior | Cat# 2-0012-005-7 1:250 |
| AbberiorStar 580 mouse | Abberior | Cat# 2-0012-005-1 1:250 |

2.1.3 Table 3 Lectins

| Lectins | Source | Identifier and dilution |
|---|-------------------------|--|
| ConA-biotin (Concanavalin A biotinylated, from <i>Canavalia ensiformis</i> (Jack bean)) | Sigma-Aldrich | C2272 ICC: 0.33 µg/ml IHC: 0.66 µg/ml |
| WGA-biotin (Lectin from <i>Triticum vulgare</i>) | Sigma-Aldrich | L5142 ICC: 0.4 µg/ml |
| HPL-biotin (Lectin from <i>Helix pomatia</i>) | Sigma-Aldrich | L6512 ICC: 0.9 µg/ml |
| Streptavidin conjugated with Alexa Fluor® 647 | ThermoFisher Scientific | S21374 |

2.1.4 Table 4 Constructs

| Construct | Promoter | Source |
|--------------------------------------|----------|--|
| EGFP-C1 | CMV | Addgene (discontinued) |
| EGFP-N1 | CMV | Addgene 6085-1 |
| m-Kate C | Syn | T. Oertner (ZMNH Institut für Synaptische Physiologie) |
| m-Kate N | Syn | T. Oertner (ZMNH Institut für Synaptische Physiologie) |
| MARCKS-GFP | CMV | M. Sperveslage (ZMNH, Dendritische Organellen und synaptische Funktion) |
| pGolt-mCherry (cell line expression) | CMV | Bera et al.2016 |
| pGolt-mCherry (neuronal expression) | Syn | Mikhaylova et al. 2016 |
| Man2-GFP-RUSH | CMV | Addgene 65258 |
| RUSH-ER-hook-only | CMV | Addgene 65306 |
| NCAM180-GFP-RUSH | CMV | This study |
| FKBP | CMV | Jason Casler (University of Chicago; Glick lab, department of Molecular Genetics and Cell Biology) |
| NCAM180-FKBP | CMV | This study |
| panCalneuron KD | CMV | J. Hradsky (LIN Magdeburg, Nplast) |
| Scrambled control | CMV | J. Hradsky (LIN Magdeburg, Nplast) |
| ABHD6 KD | CMV | This study |
| FAAH KD | CMV | This study |
| Tfr1-GFP | CMV | Guido Hermey (ZMNH Institut für Molekulare und Zelluläre Kognition) |
| Tfr1-GFP-Syn | Syn | This study |

| | | |
|----------|-----|------------|
| St8SiaII | Syn | This study |
|----------|-----|------------|

2.1.5 Table 5 Software

| Software | Source | link |
|----------------------|---|---|
| SynGo 1.0 | SynGo consortium | https://syngoportal.org/index.html |
| OpenView Version 1.5 | DOI:10.1371/journal.pbio.0040271 | N/A |
| Fiji/ImageJ | https://doi.org/10.1038/nmeth.2019 | http://fiji.sc/ RRID:SCR_002285 |
| GraphPad Prism 8 | GraphPad | https://www.graphpad.com/scientificsoftware/prism/ |
| SerialCloner | serialbasics | http://serialbasics.free.fr/Serial_Cloner.html |

2.1.6 Table 6 Solutions and Kits

| Chemical | Company | Identifier |
|---|-------------------------|------------|
| Roti-Histofix 10% (PFA) | Carl Roth | A146.6 |
| Roti-Cell 10x PBS | Carl Roth | 9150.1 |
| NucleoBond Xtra Midi EF | Macherey-Nagel | 740420 |
| PCR Elution kit | Macherey-Nagel | 740609 |
| Endogenous Biotin blocking kit | ThermoFisher Scientific | E21390 |
| MEM | Sigma-Aldrich | M7278 |
| Dulbecco's Modified Eagle Medium (DMEM) | Gibco | 41966-029 |
| Brainphys | Stemcell Technologies | 05790 |
| Neurobasal A | Gibco | 12349-015 |
| Poly-L-lysine | Sigma-Aldrich | P2636 |
| HBSS | Gibco | 24020 |
| Tissue-Tek | Sakura | 4583 |
| Random prime kit | Amersham | RPN1607 |
| Lipofectamine 2000 | ThermoFisher Scientific | 11668-019 |
| 0.25% Trypsin-EDTA | Gibco | 25200-056 |
| Penicillin Streptomycin (PenStrep) | Gibco | 15140-122 |
| Mowiol | Carl Roth | 0713 |

2.1.7 Table 7 Buffers and Media

| Name | Composition | Application |
|------------------------------|--|--|
| Poly-L-lysine-solution (PLL) | 100 mg/l L-PLL (Sigma-Aldrich) in 100 mM boric acid pH 8.4 | Coating of coverslips |
| mouse culture medium | Neurobasal A without phenol red (Gibco), 1x B27, Glutamax 4 mM, Sodium Pyruvate 1 mM | Culturing of primary hippocampal mouse neurons, P0-1 |
| BrainPhys+/+ | BrainPhys medium + SM1 supplement 1x (Stem cell)+ Glutamine 0.5 mM | Culturing of Hippocampal rat primary neurons E18-19 |

| | | |
|----------------------------------|--|--|
| DMEM+/+ (full medium) | DMEM + 10% (v/v) FCS + 2 mM glutamine + 1x Pen/Strep | Plating of primary neurons and culturing of cell lines |
| slice culture medium | Heat-inactivated horse serum, 200 mM L-glutamine, Insulin 0.01 mg/mL, NaCl 14.5 mM, MgSO ₄ 2 mM, CaCl ₂ 1.44 mM, ascorbic acid 0.00125%, D-glucose 13 mM | Culturing of organotypic slices |
| Blocking buffer 1 | Horse Serum, 0.1% (v/v) Triton-X100 in PBS | Blocking of unspecific binding sites in ICC |
| Blocking buffer 2 | 2% (v/v) glycine, 2% (v/w) BSA, 0.2% (v/w) gelatine and 50 mM NH ₄ Cl in PBS | Blocking of unspecific binding sites in ICC |
| Blocking buffer IHC | 10% (v/v) NGS, 0.3% (v/v) Triton X-100 in PBS. | Blocking of unspecific binding sites in IHC |
| Blocking buffer 3 | 10% (v/v) HS; 5% (w/v) BSA; 0.1% (v/v) Triton X-100 in PBS | Blocking solution for staining with HPL |
| 20x SSPE | NaH ₂ PO ₄ xH ₂ O 0.2 M, EDTA 0.02 M | Southern blotting |
| 20x SSC | 3 M NaCl, 0.3 M Na ₃ Citrate-dihydrate | Southern blotting |
| Speed Hyb II | 7% (w/v) SDS, 10% (w/v) Polyethylenglykol 6000, 1,5x SSPE (20x) | Southern blotting |
| 4xSDS sample buffer | 250 mM Tris/HCl, pH 6.8, 1% (w/v) SDS, 40% (v/v) Glycerol, 20% (v/v) β-mercaptoethanol, 0,004% (v/v) Bromophenol Blue | SDS-page |
| Tail lysis buffer | 25 mM NaOH, 0.2 mM EDTA in H ₂ O | Genotyping |
| Tail lysis neutralization buffer | Tris/HCl, pH 5.5 | Genotyping |
| Electrophoresis buffer | 192 mM glycine, 0.1% (w/v) SDS, 25 mM Tris-base, pH 8.3 | SDS-PAGE |
| Blotting buffer | 192 mM Glycine, 0.2% (w/v) SDS, 20% (v/v) Methanol, 25 mM Tris-base, pH 8.3 | Western blotting (wet blot) |
| Ponceau red | 0.5% (w/v) Ponceau S in 3% (v/v) acetic acid solution | Verification of transfer efficiency |
| Homogenisation buffer (buffer A) | 0.32 M sucrose, 5 mM HEPES, pH 7.4 | Homogenisation of tissue for synaptic preparations (P2, synaptosomes, synaptic junction) |
| Homogenisation buffer (buffer B) | 0.32 M sucrose, 5 mM Tris/HCl, pH 8.1 | Rehomogenisation of P2 fractions for further synaptic enrichment |
| Annealing buffer | 150 mM NaCl, in TE buffer | Annealing of DNA oligonucleotides |
| 50x TAE buffer | 40 mM Tris; 20 mM acetic acid; 1 mM EDTA | Preparation and running of agarose gels |
| LB-Medium (Carl Roth) | 20 g LB-powder in 1l H ₂ O | Culturing of <i>E. coli</i> |

| | | |
|--------------------------------|---|--|
| LB-Agar (Carl Roth) | 40 g LB-Agar in 1l H ₂ O | Plating of bacteria |
| SOC-Medium | 20 mM Glucose in SOB Medium | Culturing of bacteria after transformation |
| Transformation buffer 1 (TfB1) | RbCl 100 mM, MnCl ₂ 50 mM, potassium acetate 30 mM, CaCl ₂ 10 mM, Glycerol 15% (v/v) (pH 5.8 with CH ₃ COOH) | Chemical competent cells |
| Transformation buffer 2 (TfB2) | MOPS 10 mM, RbCl 10 mM, CaCl ₂ 75 mM, Glycerol 15% (v/v) (pH 6.8 with KOH) | Chemical competent cells |
| P1 buffer | 50 mM Tris/HCl pH 8.0 10 mM EDTA | Mini preparation |
| P2 buffer (lysis) | 200 mM NaOH 1% (w/v) SDS | Mini preparation |
| P3 buffer (neutralization) | 3.0 M Potassium acetate (pH 5,5 with HCl) | Mini preparation |

2.1.8 Table 8 Molecular cloning reagents

| Reagent | Company |
|--|-----------------------------------|
| Polymerase X - Hybrid DNA Polymerase | Roboklon |
| Deoxynucleotide Triphosphate set (dNTPs) | ThermoFisher Scientific |
| T4 DNA Ligase + buffer | ThermoFisher Scientific / Promega |
| Roti®-GelStain | Carl Roth |
| 1 kb DNA Ladder | NEB |
| GeneRuler Low Range DNA Ladder | ThermoFisher Scientific |
| DNA loading dye purple 6x | NEB |

2.2 Methods

2.2.1 Bacterial culture and molecular cloning

For the amplification of plasmid DNA *E. coli* strain XL10-Gold® was used for plasmid preparation for transfection and midi preparations. The DNA adenine methylase (Dam-methylase) negative strain GM2163 (NEB) was used to prepare plasmids for restriction assays with enzymes inhibited by dam-methylation. Bacteria were cultured in LB medium at 37 °C under 200 rpm shaking.

2.2.2 Competent bacteria

To allow transformation with plasmids bacteria were made chemo-competent according to published protocols (Hanahan, 1983). Cells were grown in LB medium until an optical density OD₆₀₀ of 0.6. The cells were put on ice for 15 min and then pelleted by centrifugation at 4000 rcf. The pellet was resuspended in transformation buffer 1 (TfB I), pelleted at 4000 rcf. The pellet was resuspended in transformation buffer 2 (TfB II). The cells were rapidly shock frozen in liquid nitrogen (-195.79 °C) and stored at -80 °C.

2.2.3 Transformation

Chemical competent cells were transformed by heat shock. The cells were thawed on ice, mixed with the plasmid (10 ng) and subsequently heat shocked at 42 °C for 45 sec. The bacteria were kept on ice for 2 min to recover and subsequently cultured in SOC medium at 37 °C for 60 min and then plated on antibiotic supplemented agar plates, to select the transformed bacteria. Bacterial plates were incubated overnight at 37 °C.

2.2.4 Plasmid preparation

Plasmids were isolated on a Midi (200 ml LB-medium) or Mini scale (2 ml LB Medium). Midis were prepared using the NucleoBond® Xtra EF Kit according to the manufacturer's instructions. The DNA was precipitated using Isopropanol. The DNA pellets were washed in 70 % ethanol (v/v), air dried and resuspended in H₂O. Minis were prepared using alkaline lysis. Overnight bacteria cultures were centrifuged for 15 min at 5000 g at 4 °C. The pellet was resuspended in 200 µl ice cold buffer P1 containing RNase. Lysis was carried out by adding 200 µl of buffer P2. After 5 min the lysis was stopped by adding 150 µl of neutralization buffer, leading to protein coagulation. The probes were centrifuged for 15 min at 4 °C. The DNA was precipitated from the supernatant using Isopropanol. DNA pellets were washed with 70% (v/v) ethanol, air dried and resuspended in H₂O.

2.2.5 Molecular cloning

Constructs were designed using the serial cloner software (Table 4). Small fragments were ordered as individual oligo-nucleotides. 20 µl (10 pmol/µl) of each oligo-nucleotide was mixed with annealing buffer, heated to 95 °C and then slowly cooled down to RT.

Larger fragments were generated by PCR. The target backbone was opened using the appropriate restriction enzymes. The PCR products were inserted following digestion with the corresponding restriction enzymes and subsequent ligation with T4 DNA ligase for 60 min at room temperature. Alternatively, the PCR-primers were designed with 3' and 5' overhangs homologous to the target vector and integrated by homologous integration. DNA strands were

separated by gel electrophoresis in agarose gels. The DNA was labeled by ROTI®GelStain or ethidium bromide. The bands were isolated on an UV plate and eluted using Nucleo Spin PCR and Gel clean-up kit (Machery-Nagel), according to the manufacturer's instructions.

2.2.6 Cell culture

2.2.6.1 Coating of coverslips

Coverslips were incubated in 65% HNO₃ under agitation for at least 12 h, followed by two washes in H₂O then air dried and baked for 4 h at 200 °C.

Coverslips were coated for both neuronal primary and cell line culture placing them on a drop of Polylysine (0.1 mg/ml PLL in 0.15 M borate buffer) and incubated at 37 °C, 5% CO₂ for 4 h. They were inverted and washed four times in H₂O. The coverslips were kept in HBSS at 37 °C until use.

2.2.6.2 Cell lines

Human embryonic kidney 293 cells (HEK cells) and Medical Research Council cell strain 5 (MRC5) cells were used. Cell lines were passaged by D. Hacker and Dr. A. Konietzny. The cells were cultured in full medium, on either coated coverslip for imaging applications, or in petri dishes. The cells were split regularly to prevent overgrowth of the culture. The medium was removed; the cells were dissociated using Trypsin-EDTA 0.05% for 5 min at 37 °C. Trypsination was stopped by adding full medium (Table 7). The cells were diluted 1:10 and added to the coverslips in 6 well plates.

2.2.6.3 Transfection of cell lines

Cells were transfected at 50-60% confluence typically 24 h after plating. The full medium was removed and DMEM without additions (DMEM (-/-)) was added. The plasmid was diluted in 100 µl of DMEM per well. The amount of DNA used per well was adjusted depending on the construct, typically 1 µg DNA per 1 ml culture medium was used. PEI was diluted in 100 µl of DMEM per well, 3 µl of PEI were used for 1 µg of DNA. After 5 min of incubation PEI and DNA solutions were mixed and incubated for 20 min at RT. The mixture was added to the cells dropwise and the cells were placed in the incubator at 37 °C and 5% CO₂. After 4 h the medium was changed to fresh full medium.

2.2.6.4 Hippocampal rat primary culture

Primary rat hippocampal cultures were prepared from Wistar rats (E18), as described by Karpova et al., 2013. The preparation was carried out by various colleagues including M. Andres-Alonso, J. Bär and M. Marunde. The rats were decapitated and hippocampi dissected. After treatment with trypsin at 37 °C for 15 min and subsequent mechanical dissociation, cells were plated on 18 mm glass coverslips coated with poly-D-lysine at a density of 10.000 - 30.000 cells per well in DMEM medium (Gibco) supplemented with 10% (v/v) fetal bovine serum (FBS), 0.5 mM Glutamax (Gibco). After 1 h, media was exchanged to BrainPhys (+/+); (Table 7). Cells were kept at 37 °C, 5% CO₂ and 95% humidity until use. Cells were feed once a week by removing 100 µl of old medium and adding 200 µl fresh BrainPhys (+/+).

2.2.6.5 Mouse hippocampal primary cultures

Tissue and cell preparation was carried out under the license number Org886. Hippocampal mouse cultures were prepared from mice at postnatal day 0 or 1. The mice were decapitated and the dissected hippocampi were collected in 450 μ l HBSS. 50 μ l Trypsin (0.25% Trypsin-EDTA) was added followed by incubation for 15 min at 37 °C. After two washes with HBSS the HBSS was removed and the hippocampi were taken up in full medium. The hippocampi were mechanically triturated using different sized cannula from 0.9 to 0.45 gauge (Braun) until no chunks of tissue remained. 15 μ l of the cell suspension were taken up in 15 μ l of Trypan blue. Cells were counted in a Neubauer counting chamber after adding 15 μ l Trypan blue to 15 μ l of cell suspension. 40000 cells were added to each well for a 12-well plate in a volume of 1 ml full medium. The coverslips were prepared as described above. After the cells were attached about 1 h after plating the medium was exchanged for Neurobasal A (+/+) (Table 7). Cells were fed once a week by removing 100 μ l of medium and adding 200 μ l of fresh Neurobasal A (+/+).

2.2.6.6 Transfection of hippocampal primary neurons

The medium was removed from the wells and stored at 37 °C and 5% CO₂. The medium was replaced by 1 ml/well BrainPhys Neuronal Medium (BrainPhys (-/-)) (Table 7) and the cells were returned to the incubator. The DNA was diluted in 100 μ l of BrainPhys (-/-) per well. The amount of DNA used was adjusted depending on the individual construct; typically 0.3-1 μ g of DNA per 1 ml of culture medium was used. In parallel 2 μ l of Lipofectamine 2000 for 1 μ g of DNA was diluted in 100 μ l Brainphys (-/-) per well. The solutions were incubated at RT for 5 min, mixed and incubated at RT for 20 min. 200 μ l of the mixture was added dropwise to every well. The cells were returned to the incubator for 45 min. The medium was removed and replaced by the conditioned medium that was collected in the first step. The expression time was adjusted for the individual constructs. KD-constructs were typically expressed for 5 days while fast expressing constructs were expressed for 12 h.

2.2.6.7 Treatments

All treatments were conducted in culture medium at 37 °C, 5% CO₂ and 95% humidity. For synaptic stimulation the cells were first silenced with 1 μ M TTX for 1 h (Table 1). TTX was washed out in the stimulated group while the control group was left silenced. 50 μ M bicuculline and 2.5 mM 4-aminopyridine (4AP) was added to the coverslips for 30 min before fixation. For long-term silencing the cells were treated with TTX for 48 h. To control the effects of the stimulation protocol, cells were stained with an antibody for pCREB and with DAPI. Inhibition of the CB1R was carried out by treating the cells with 10 μ M AM-251 for 48 h.

2.2.6.8 Release systems

Retention using selective hooks (RUSH) system (Boncompain et al., 2012): To study the forward trafficking of NCAM, NCAM was fused to a streptavidin binding peptide (SBP) and hooked in the ER by expressing streptavidin coupled to the ER-retention signal KDEL and the transmembrane domain of the ER localized protein STIM1 (Table 4). NCAM was released by adding 40 μ M biotin to the cells.

FKBP-System: NCAM retained in the ER by self-crosslinking FK506 binding protein domain (FKBP). The version of FKBP used in this study was a gift from Jason Casler; it is mutated in multiple spots to improve its release properties. C22V reduces crosslinking with other proteins in the ER. F36L increases the affinity of ligand binding. I90V accelerates ligand-induced dissociation of the dimers. The dissociation of the FKBP-domains was induced by adding 10 μ M synthetic ligand of FKBP (SLF) to the medium. SLF was used instead of the FK506, since FK506 inhibits Calcineurin (Dumont, 2012).

2.2.6.9 Organotypic slice preparation

Organotypic slices were prepared according to Gee et al., 2017 (Table 7). The hippocampus was removed from mice age 5-8 days and cut into 400 μ m slices using a tissue chopper and transferred into dissection solution. The slices were carefully transferred on culture membranes. The membranes were placed into 6-well plates filled with slice culture medium (Table 7). It was made sure that the slices are in contact with the medium through the membrane, but were not submerged. The slices were fed every 2-3 days with fresh medium.

2.2.6.10 AAV production and transduction

AAV production was carried out by the UKE vector facility. AAV transduction of organotypic slices was carried out according to Wiegert et al., 2017. AAV injection was carried out using custom-pulled injection glass pipettes. The tip was broken off to create a \sim 10 μ m opening. The AAV solution was filled into the pipette and the pipette was connected to a Picospritzer device. The membrane was transferred into the microscope chamber filled with transduction medium, pH 7.4. The AAV solution was injected into the target cell layer.

2.2.7 Cell culture stainings

2.2.7.1 Immunocytochemistry (ICC)

Cells were fixed by incubation in 4% (m/v) PFA and 4% (m/v) sucrose in PBS 3 times for 15 min and washed 3 times in PBS. They were permeabilized in 0.2% Triton-X100 (v/v) for 10 min. Unspecific binding sites were blocked by incubating the cells with a blocking buffer for a minimum of 1 h at RT. The cells were incubated with the primary antibody (Table 2) in the appropriate blocking buffer for at least 12 h at 4 $^{\circ}$ C. Cells were washed 3 times in PBS for at least 5 min. The secondary antibody was diluted in the blocking buffer and briefly centrifuged to remove aggregates. Cells were incubated with the secondary antibodies in blocking buffer for 1 h at RT, followed by 3 washes in PBS for at least 5 min each and mounted in Mowiol. For surface labeling the cells were incubated with the primary antibody in culture medium before fixation in PFA before proceeding as described above.

2.2.7.2 Lectin staining

The protocols for lectin stainings were established by Kim Klein. For staining with lectins fixation and permeabilization were carried out identical to regular ICC and both can be carried out on the same coverslips in parallel (Table 3). Lectins are coupled to biotin and are labeled using streptavidin, therefore endogenous biotin from the cells was blocked using the endogenous biotin blocking kit (ThermoFisher, E21390) according to the manufacturer's instructions, followed by 3 washes in PBS. The staining was carried out with the same steps

as the ICC described above always using blocking buffer 2, to avoid unspecific interactions with serum components. For staining of *Helix pomatia* agglutinin (HPL) blocking buffer 3 was used (Table 7). The lectins were labeled with fluorophore coupled streptavidin in parallel to secondary antibody staining.

2.2.8 Immunohistochemistry (IHC)

2.2.8.1 Perfusion

Mice were deeply anesthetized by intraperitoneal injection of an overdose of Ketamin/Xylazin (160 mg/kg/BW, 16 mg/kg/BW). A small incision was made through the integument and abdominal wall beneath the rib cage. The diaphragm was cut and the ribcage was opened up to the collar bone. The sternum was lifted and any tissue connecting it to the heart was cut.

A small incision was made in the posterior end of the left ventricle, to insert the injection needle. To create an outlet a small insertion was made in the left atrium. The perfusion was started with PBS until the blood was visibly removed from the liver and the lung. The mouse was perfused with 4% (m/v) PFA in PBS. The brain was removed and post-fixed in 4% (m/v) PFA in PBS overnight at 4 °C. To protect the tissue from crystallization during shock freezing, the brains were incubated in 0.5 M Sucrose/ PBS until they sank to the bottom of the tube. The procedure was repeated with 1 M Sucrose. The brains were then shock frozen at -50 °C in liquid methyl butane for 30 sec and stored at -80 °C until use. Before sectioning the brains were transferred to -20 °C.

2.2.8.2 Immunostaining of cryosections

To prepare hippocampal sections, the frontal cortex and the cerebellum were removed. The brains were mounted in Tissue-Tek mounting medium and frozen through at -20 °C.

Cryosections of 20-40 µm thickness were prepared in a cryostat (Zeiss, HYRAX C 60) with MX35Ultra microtome blades. The temperature of the blade and the sample were individually adjusted between -15 and -25 °C, to avoid ripping or curling of the slices. The slices were washed 3 times in PBS and incubated in blocking solution for a minimum of 2 h. They were incubated with the primary antibody at 4 °C for 48 h in blocking buffer under slight shaking rinsed in PBS, washed in PBS for 1 h and incubated with 0.2% (m/v) BSA in PBS for 1 h followed by incubation with the secondary antibodies for 2 h in blocking buffer and 3 washes for 15 min each in PBS before they were treated with DAPI (1:10000) in PBS for 10 min, rinsed in PBS and mounted with Mowiol.

2.2.8.3 Lectin staining of cryosections

For labeling with lectins, the sections were treated with the endogenous biotin blocking kit according to the manufacturer's instructions. The blocking buffer 2 with 0.3% (v/v) Triton was used. The slices were incubated with the lectin in blocking buffer 2 for a minimum of 48 h. They were rinsed in PBS, washed in PBS for 1h and then in 0.2% (v/v) BSA in PBS. They were labeled with fluorophores coupled to streptavidin for 2 h in blocking buffer at RT.

2.2.9 Histology and electron microscopy

2.2.9.1 Nissl staining

Cryosections were acidified in 0.05 M sodium acetate buffer, pH 4.0-4.2 (adjusted with acetic acid) and subsequently stained in 0.5% (v/v) cresylviolet for 5-10 min. Dehydration was by incubation in 0.05 M sodium acetate buffer for 3 min, 50% ethanol, 70% ethanol and 96% ethanol (v/v) for 2 min each. To clear the sections, they were incubated with 2/3 ethanol and 1/3 isopropanol twice for 5 min before they were subjected to 3 washes in xylol for 5 min each and mounted in Mowiol.

2.2.9.2 Section preparation for transmission electron microscopy

Probes for electron microscopy (EM) imaging were prepared by the staff of the EM-facility of the ZMNH: Mice were deeply anaesthetized and transcardially perfused with a mixture of 4% PFA and 1% glutaraldehyde (GA) in 0.1 M phosphate buffer (PB) at pH 7.4, as described above. 100 µm thick vibratome sections mouse brains were cut with a Vibratome VT 1000S (Leica Biosystems Nussloch, Germany). The sections were rinsed three times in 0.1 M sodium cacodylate buffer (pH 7.2–7.4) and osmicated using 1% (m/v) OsO₄ in cacodylate buffer. Following osmication, the sections were dehydrated using ascending ethyl alcohol concentration steps, followed by two rinses in propylene oxide. Infiltration of the embedding medium was performed by immersing the pieces in a 1:1 mixture of propylene oxide and glycidether 100 (Epon) (Carl Roth Karlsruhe, Germany) and finally in neat Epon and hardened at 60 °C. Semithin sections (0.5 µm thick) from the hippocampus were cut with a diamond knife (Diatome, Nidau, Switzerland) using an EM UC7 Ultramicrotome (Leica Microsystems, Wetzlar, Germany) and mounted on glass slides for light microscopy after being stained for 1 min with 1% (m/v) toluidine blue.

2.2.10 Subcellular fractionation experiments

Subcellular fractionation was carried out with support from C. Borutzki. Hippocampi were homogenized in 10 ml/g buffer A (0.32 M sucrose, 5 mM HEPES, pH 7.4) including protease inhibitor cocktail (PI) and phosphatase inhibitor (PhosSTOP) and centrifuged at 1000 g for 10 min. The pellet was re-homogenized and centrifuged in buffer A (Table 7). The resulting pellet 1 containing nuclei and cell debris was discarded and the supernatants were combined. They were centrifuged at 12000 g for 20 min and the supernatant (S2) was collected (Sorvall RC6, F13-14 x 50cy rotor). The pellet P2 was re-homogenized in buffer A and centrifuged again 12000 g for 20 min. The supernatant (S2') was collected and combined with supernatant S2. The resulting pellet was collected as crude membrane fraction P2. One eighth of the P2 fraction was collected, washed in PBS and centrifuged at 12000 g for 20 min (Sorvall RC6, F13-14xcy-rotor). Pellets were resuspended in PBS, snap-frozen in liquid nitrogen and stored at -80 °C. For further purification, the remaining P2-fraction was re-homogenized in buffer B (0.32 M sucrose, 5 mM Tris/HCl, pH 8.1). The homogenate was loaded on a 0.85 M/1.0 M/1.2 M sucrose step gradient and centrifuged at 85000 g for 2 h (Beckmann XPN-80 centrifuge, SW32 Ti rotor). The synaptosomes were collected from the 1.0 M/1.2 M sucrose interphase. 40% of the solution was washed in PBS with PI and PhosSTOP and centrifuged at 90000 g for 1 h (Beckmann XPN-80, SW32 Ti rotor). The pellets were resuspended and centrifuged at 90000 g for 1 h (TLA-55). Next, the pellets were frozen in liquid nitrogen and

stored at -80 °C. To isolate the synaptic junctions, the synaptosomes were opened by hypoosmotic shock. Hence, the synaptosomes were mixed for 30 min at 4 °C in 1 mM Tris/HCl, pH 8.1 with PI and PhosSTOP. The samples were then centrifuged at 3200 g for 30 min (Sorvall RC6, SS-34 rotor). The Pellet P3 was resuspended in 1.5 ml/g 5 mM Tris/HCl pH 8.1 with PI and PhosSTOP and loaded on a 1.0 M/1.2 M sucrose step gradient and centrifuged at 85000 g for 2 h (Beckmann XPN-80 centrifuge, SW32 Ti rotor). The synaptic junctions were collected from the 1.0 M/1.2 M sucrose interphase and stored on ice overnight. The synaptic junctions were resuspended in 10 mM PBS, pH 7.4 with PI and PhosSTOP. The resulting solution was centrifuged at 120000 g for 1 h (Beckman Optima XPN-80, SW32 Ti rotor). The pellet was resuspended in 10 mM PBS and centrifuged at 120000 g for 1 h. The pelleted synaptic junctions were shock frozen in liquid nitrogen.

2.2.11. SDS-PAGE and western blot

2.2.11.1 Protein measurement

Protein concentrations were measured using amido black. A standard curve was established using defined concentrations of bovine serum albumin (BSA). Amido black was added to the protein samples and the controls and incubated for 20 min at RT in a 96 well plate. The wells were washed 3x in methanol-acetic acid solution. The wells were air dried and dissolved in 300 µl of methanol-acetic acid solution by shaking for 30 min. The optic density was measured at 620 nm with Fluoro Star Optima Flurimeter (BMG Labtechnologies, Offenburg, Germany). The protein concentrations were calculated based on the BSA standard curve.

2.2.11.2 SDS-PAGE

SDS-PAGE and western blot was conducted according to Seidenbecher et al., 2004. SDS-PAGE was performed on 5% to 20% gradient gels. The probes were dissolved in SDS sample buffer. The gel run was run at 12 mA per gel at 4 °C.

2.2.11.3 Immunoblotting

Immunoblotting was at 200 mA for 2 h (minimum of 60 V), on nitrocellulose or PVDF membranes. Efficiency of the transfer was controlled by staining the membrane with Ponceau solution for 5 min. The membranes were blocked with 5% (m/v) milk powder or BSA in TBS-T. The blocking buffer was adjusted to each individual primary antibody for minimal unspecific binding. The membranes were incubated with the primary antibody in TBS-A overnight at 4 °C under light shaking. They were washed 10 min in TBS, 10 min in TBS-T, 5 min TBS-T and 5 min TBS followed by incubation with the HRP-coupled secondary antibody in the blocking buffer. Washes were performed for 10 min in TBS and in TBS-T, and for 5 min TBS-T and 5 min TBS. To develop the signal, ECL solution (Pierce, Rockford, USA) was used and the image was acquired with Intas ECL chemocam imager (Licor, Cambridge, UK). The bands were analyzed using the blots function of Fiji. The intensity of the bands of the protein of interest was normalized to a loading control. Tubulin or Actin was used for normalization. For synaptic fractions PSD95 was used.

2.2.12 Southern blot

Southern blotting was performed with the alkaline methods using Hybond-N membranes. Probes were prepared by restriction digest with subsequent gel elution. For labeling the Random Prime Labeling Kit (Amersham) with ^{32}P -ATP as radiolabeled nucleotide was used. For hybridization for at least 18 h at 65 °C Speed Hyb II hybridization buffer with 200 mg/ml sonicated fish DNA and 5×10^5 cpm/ml were added to the hybridization tube. Washes were performed at 65 °C with descending salt concentration until no radioactivity could be detected in the discarded buffer. The Speed Hyb II buffer was heated to 68 °C in a water bath. The target DNA-probe and the herring sperm DNA were denatured at 100 °C for 5 min. The denatured DNA was kept on ice to block the forming of double strands. The hybridization tube was filled with 29 ml Speed hybrid 2 with 200 µg/ml denatured herring sperm DNA. The membrane was blocked at 68 °C in the rotation oven. The denatured DNA probe (25 ng) was labeled with α ^{32}P dATP using the Random Primed DNA Labeling Kit according to the manufacturer's instructions. The membrane was incubated with the hybridization mix overnight at 68 °C in the rotation oven. The liquid was removed and stored in the freezer. The membrane was washed twice with wash buffer in the rotation oven for 20 min. Washing was continued until the now radioactivity was measurable in the discarded washing buffer. The membrane was exposed on a phosphor-imager plate overnight which was scanned in the BAS-reader using the TINA0209 program.

2.2.12 Mutant and transgenic mouse breeding

Animals were housed at 22 °C on a 12 h light/12 h dark cycle with *ad libitum* access to food and water in the breeding barriers of the Forschungstierhaltung of the University Medical Center Hamburg-Eppendorf. All experiments were approved by the local authorities of the State of Hamburg (Org 886; Nr.125/17). C57BL6J /UKE mice were used for matings and backcrossings. For the mGolt mouse line 4 founders were tested for sufficient expression of the probe and 1 founder was used for the establishment of the line which was classified as “unbelasted”. For the Calneuron 1 KO line founders were backcrossed to C57BL6/J/UKE to avoid mosaicism and offspring exhibiting the correct genotype was then used to establish the KO line. This line was also classified as “unbelasted”.

2.2.12.1 Pronucleus injection

To obtain the DNA-fragment for pronucleus injection DNA has to be isolated with special care. To ensure optimal DNA quality a Midi preparation was made from a low density bacterial culture. 30 µg of DNA digested with specific restriction enzymes under optimal buffer conditions in a volume of 200 µl and loaded on an agarose gel without ethidium bromide and run at max 60 V. The sides of the gel were cut off and stained with ethidium bromide. The gel was reassembled; the bands on the left and right side of the gel were used to locate the unlabeled bands. The unlabeled central bands were cut and eluted using the Machery and Nagel kit with the modification that 400 µl NT1 were used for 100 mg of gel. The DNA was eluted in 10 µl of ultrapure water.

To control the purity of the eluate 2, 4, 6 and 8 µl were loaded on a control gel to assess purity and concentration.

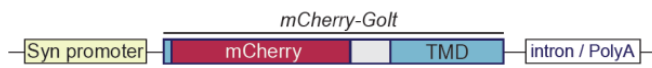
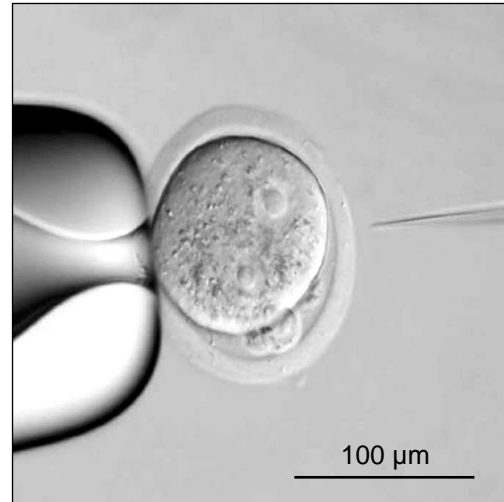


Figure 1. Pronucleus injection procedure

C57BxCBA (= F1) or B6, 3-4 weeks old were superovulated by hormone injection. The holding pipette (left) holds the embryo. The DNA solution is injected through the injection pipette (right).



Superovulated donor mice were sacrificed, by cervical dislocation, disinfected with Braunoderm before the abdominal cavity was opened. The ovaries were located and gripped at the fatpad with a tweezer. The ovaries were dissected by cutting above the ovary and then below the oviduct. Embryos were released from the ampulla of the oviduct in drops of KSOM/HEPES containing 0.3 mg/ml hyaluronidase to remove the cumulus cells. Using a fine capillary they were pipetted up and down to get rid of the cumulus cells and then thoroughly washed in KSOM/HEPES. Before they were incubated at 5% CO₂, 37 °C until both pronuclei were clearly visible. Injection was performed using 2 ng/μl of isolated fragment diluted in 10 mM Tris, pH 7.4, 0.1 mM EDTA with the help of a Femtojet and micromanipulators (Eppendorf) using DIC optics of an Olympus microscope (Figure 1). These steps were performed with support of the transgenic mouse facility of the UKE.

2.2.12.2 Implantation

Implantation in pseudopregnant foster mothers was performed by the staff of the Transgenic Core Unit of the ZMNH. The surgery area was thoroughly disinfected. The foster mother was sedated with 4% isoflurane. After reaching deep sedation the isoflurane concentration was reduced to 2%. As analgesic Burprenorphin (0.05 mg/kg BW) was injected subcutaneously 30 min before start of the surgery and carprofen (5 mg/kg BW) was injected at the end of the surgery. To keep the body temperature stable the foster mother was placed stomach down on a 37 °C heating plate. To keep the eyes hydrated eye drops were applied. The hair was shaved clean of the back and the skin was disinfected. The ovary was gripped at the fat pad with a curved dull tweezer. The bursa was opened above the infundibulum. The embryos were injected into the infundibulum and the wound was closed.

2.2.12.3 Single cell embryo electroporation

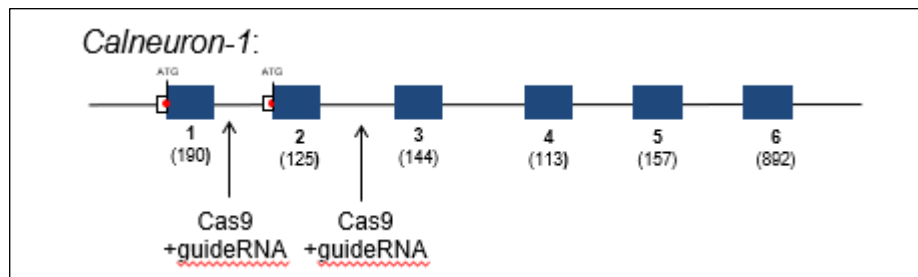


Figure 2. Map of the CALN1 gene

The CALN1 gene consists of 6 exons (blue boxes) and has two alternative start codons (red dots) on exon1 and 2, resulting in two isoforms. For generation of the Calneuron 1 KO, 2 sgRNAs 5' and 3' of the second exon were designed.

For the generation of KO and KI mice the CRISPR-Cas9 system was used. Single guide RNAs (sgRNAs) were designed to specifically bind the genome upstream and downstream of the second exon of the CALN1 gene (Figure 2).

The sgRNA sequences targeting exon 2 of the murine CALN1 gene were designed using the CRISPOR Program (Haeussler et al., 2016). The template for transcription was derived by annealing of two oligonucleotides followed by a fill-in reaction using Q5-Polymerase (Biolabs). Transcription was performed using the HiScribeT7 kit (Biolabs, E20140S) with subsequent purification of the transcript with the MEGAClear kit (Fisher Scientific, AM1908), both according to the manufacturer's instructions.

The single cell embryos were isolated as described above. The zygotes were taken up in KSOM; zygotes with clearly visible pronuclei were selected. The selected zygotes were washed in OptiMEM at 4 °C. sgRNAs (600 ng/μl) and Cas9 protein (IDT) were diluted in OptiMEM. 5 μl of the solution was pipetted in the electroporation chamber. The electroporation was carried out with an NEPA21-electroporator (Nepagene). The zygotes were aligned between the electrodes (Figure 3). The impedance was controlled to be between 120 and 180 Ω, if the impedance was correct, the electroporation was started. The electroporation was carried out in two steps, the poring pulse and the transfer pulse. The poring pulse opens pores in the cell membrane; the transfer pulse is an alternating current (+/-) that channels sgRNA and the Cas9 protein into the zygotes. Surviving zygotes were implanted into pseudo pregnant foster mothers as described above.

| Pulse | Voltage | Duration (msec) | Interval (msec) | Decay | Current | Repetitions |
|----------|---------|-----------------|-----------------|-------|---------|-------------|
| poring | 40 | 3.5 | 50 | 10% | + | 4x |
| transfer | 5 | 50 | 50 | 40% | +/- | 5x |

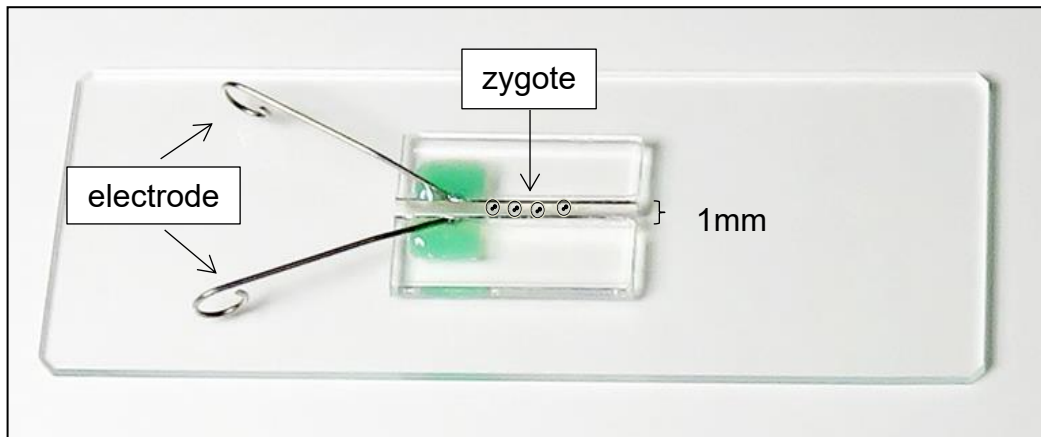


Figure 3. Embryo electroporation

Pulse settings and electrode setup, zygotes are placed in between the two electrodes. The cell membrane is opened by a poring pulse. RNA and protein in the solution are transported into the cell by the transfer pulse (modified from <http://www.xceltis.de/equipment?ix=2x3x2>).

2.2.12.4 Environmental enrichment

A total of 168 male C57BL/6J mice (Charles River, country), 4 weeks old were used. Upon arrival, the animals were housed in a light-dark cycle of 12 h (lights on at 7:00 am) (4 per cage) with free access to food and water. After one week of adaption period to the experimental room, the animals were randomly assigned to either control or enriched environment (EE) group. In order to cover the most important aspects of EE, each cage (60 cm x 35 cm x 20 cm) had one running wheel, plastic house cups, acrylic tubes, bedding material (Nestlets, Ancare) and other objects with different textures and sizes, made of plastic, wood, rope and glass (Figure 4). The cage also had a rope or wooden bridge attached to the grid, providing a fully three-dimensional exploration space. The control group cage consisted of a regular IVC cage. Animals were assigned either to EE or the control group and kept in these conditions for 6 weeks. Cages and objects were cleaned once a week. At the end of this period the animals were euthanized and the hippocampi were dissected for immediate synaptic junction preparation.

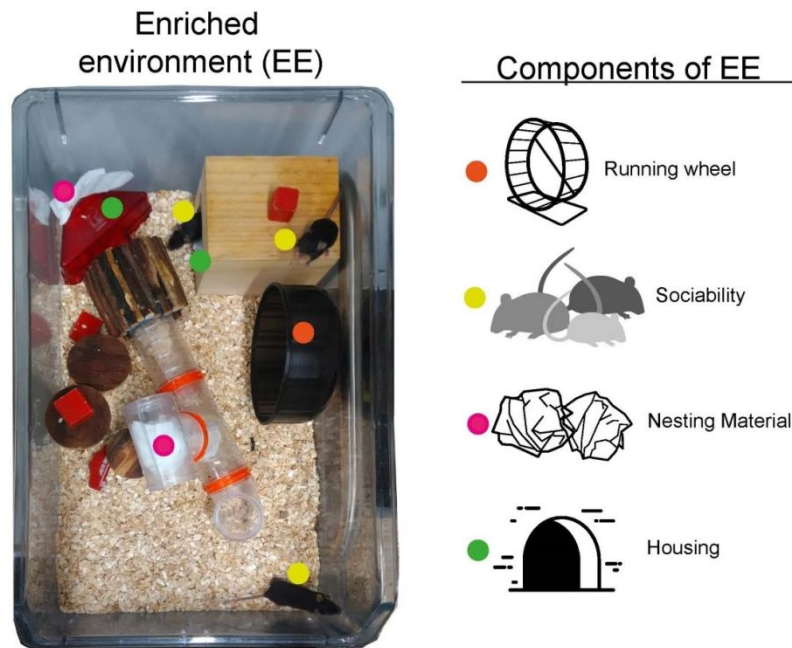


Figure 4. Enriched environment housing

Representative picture of a typical EE cage is shown. Mice were housed in a large cage containing a running wheel (orange), nesting material (magenta) and housing (green)

2.2.12.5 Genotyping

For genotyping pups were toe- tattooed and ~ 2 mm of the tail tip was cut. The DNA was isolated by heating the tail tips for 1 h at 98 °C in tail lysis buffer. The lysis was stopped by adding 75 µl of neutralization buffer. The genotype was determined by PCR using the following primers.

Calneuron 1 genotyping

| | |
|-----------|---|
| Caln1 fwd | CCC TAA AAT CAA TTA GGA GTT ATT CAA GTG ATG G |
| Caln1 rev | CAC ACC TAG TCC TAG CTA ATC AAC GCT C |

mGolt genotyping

| | |
|-----------|-------------------------------------|
| mGolt fwd | GGC GAG TTC ATC TAC AAG GTG AAG CTG |
| mGolt rev | GAC ACT GAT GAT GAA GGC GAT GGC GA |

2.2.13 Acute hippocampal slice preparation and electrophysiology

Hippocampi from mice kept under standard or enriched environment housing conditions were dissected into 350 µm thick slices using a vibratome (LeicaVT1000S, Nussloch, Germany). Hippocampal slices were pre-incubated for 2 h in carbogenated (95% O₂ ~ 5% CO₂) ACSF (110 mM NaCl; 2.5 mM KCl; 2.5 mM CaCl₂; 1.5 mM MgSO₄; 10 mM glucose; 27.4 mM NaHCO₃ in H₂O at pH 7.3) at RT. Once slice at a time was transferred into a slice recording chamber (Scientific systems Inc.) and allowed to recover for at least 30 min. Field excitatory

postsynaptic potentials (fEPSPs) were evoked by stimulation of CA1 Schaffer collateral with 0.9% NaCl filled glass capillary microelectrodes (3-5 M Ω). fEPSPs were recorded and amplified by an Extracellular Amplifier (EXT-02B, npi, Germany) and digitized at a sample frequency of 20 kHz by AD/DA converter (POWER 1401mkII, CED, England). The stimulation strength was adjusted to 30 - 40% of the maximum fEPSP-slope values. For basal recording a single biphasic stimulus (half-pulse width: 100 μ s) was applied every 60 s and the resulting signals were offline averaged over 5 min. After a stable baseline recording, long term potentiation (LTP) was induced by either 100 Hz trains or theta-bursts. Following tetanization sequences were applied: Weak theta-burst stimulation consisted of five bursts with four stimuli (100 Hz) every 200 ms; or 8 theta-burst sequences every 30 s that had 10 bursts of five stimuli; or single 100 Hz tetanization that consisted of a 1 s 100 Hz train (100 stimuli, half-pulse width: 100 μ s); or three repeated 1 s 100 Hz trains every 10 min (half-pulse width: 200 μ s).

2.2.14 Imaging

2.2.14.1 Confocal imaging

Images of fixed samples were acquired using a Leica SP8 microscope (Wetzlar, Germany), or alternatively using an Olympus confocal microscope. If not indicated otherwise high resolution images were acquired using a 60x oil objective and the following parameters, frames of 512 x 512 pixels (36.89 μ m x 36.89 μ m) were acquired, with a z-step size of 0.3 μ m.

2.2.14.2 STED imaging

Gated STED images were acquired with a Leica TCS SP8 STED 3X equipped with pulsed White Light Laser (WLL) and diode 405 nm lasers for excitation and pulsed depletion with a 775 nm laser. A Leica HC APO CS2 \times 100/1.40 oil objective was used. Images were taken as a single plane of 1024 \times 1024 pixels and optical zoom of 5 with a pixel size of 18 nm.

2.2.14.3 Live cell imaging (TIRF, wide field)

Live imaging was conducted in a Ludin chamber, either in the culture medium or in imaging medium. Live imaging was performed using the Nikon Eclipse Ti-E microscope controlled by VisiView software (VisitronSystems). 488 nm, 561 nm, and 639 nm were used for excitation of the fluorophores. Total internal reflection fluorescence microscopy (TIRF) was applied for high resolution live imaging. TIRF illumination functions by illuminating a selected region with an evanescent wave allowing for the restricted imaging of cell surface areas. TIRF illumination was conducted with a spinning-TIRF system based on an iLas 2 platform (Gataca systems), using a 100x TIRF objective (Nikon, ApoTIRF 100x/1.49 oil).

2.2.14.4 Electron microscopy

EM images were acquired by the staff of the EM-facility of the ZMNH. Ultrathin sections (60 nm) were examined in a transmission electron microscope (TEM) EM902 (Zeiss, Oberkochen, Germany). Images were acquired with a MegaViewIII digital camera (A. Tröndle, Moorenweis, Germany) in the stratum radiatum of the hippocampal CA1 region and in the mossy fiber region of the hippocampal CA3 region. To maximize the number of

synapses analyzed, regions of interest (ROIs) were chosen in between the main dendrites. Synapses were identified by the following criteria: An electron dense zone is present at the postsynaptic membrane, small vesicles are present in the presynaptic compartment and both are in juxtaposition to each other. Perforated synapses were identified as previously described by Neuhoff et al. 1999 (Neuhoff et al., 1999). Mitochondria were defined as double membrane structures containing parallel membrane stacks.

2.2.14.5 Image analysis

Images were modified using the ImageJ software (Schindelin et al., 2012). For immunostainings the background signal was measured in multiple ROI and the average background was subtracted from all images. Punctuated stainings such as synaptic stainings were analysed using the Open View software (Tsurriel et al., 2006). To quantify synapses, intensity maxima were detected automatically, and boxes of equal size were centered on each maximum. The mean fluorescence intensity was measured for each box in the channel of interest. For colocalization analysis the boxes from the first channel were transferred to the second channel and the match set function was applied. For triple colocalization the boxes were transferred to the third channel and the match set function was applied again. Alternatively, the find maxima function and the time series analyser plugin of Fiji was used according to suppliers' instructions. Dendritic arborisation was measured using Sholl analysis (Sholl, 1953). In brief, a point was set in the middle of the soma. Circles increasing in diameter in equal steps were set around the middle point. Crossings of these circles with the dendrite of the target cell were counted automatically.

3 Results

3.1 A novel multiomics approach using mice raised in an enriched environment

In this thesis a novel multiomics approach was used that integrates data from the lipid metabolisms with the proteome of synaptic junctions (Coman et al., 2016). Although lipidomics and dual-omics was successfully applied to image different brain regions (Ellis et al., 2018; Lerner et al., 2018), the potential of multiomics has not been used before in neuroscience to study synaptic function with purified synaptic fractions. In addition, it was mandatory to demonstrate the heuristic value of the approach to generate hypotheses on alterations in synaptic function in response to environmental stimuli. Membrane lipids are important components of synaptic junctions. Compelling evidence suggests their participation in fundamental processes of synaptic neurotransmission. However, our knowledge about the exact lipid composition of synaptic membranes is still sparse. In collaboration with the laboratory of Robert Ahrends at the Leibniz Institute for Analytical Sciences in Dortmund, where all MS and bioinformatics analysis was done, we provide the first quantitative lipid inventory of mouse and rat synaptic junctions (Figure 6). This analysis is exhaustive; the lipidome analysis structurally characterized and identified 416 lipid species, covering 49 different lipid classes (Figure 6A) (Borgmeyer et al, under revision).

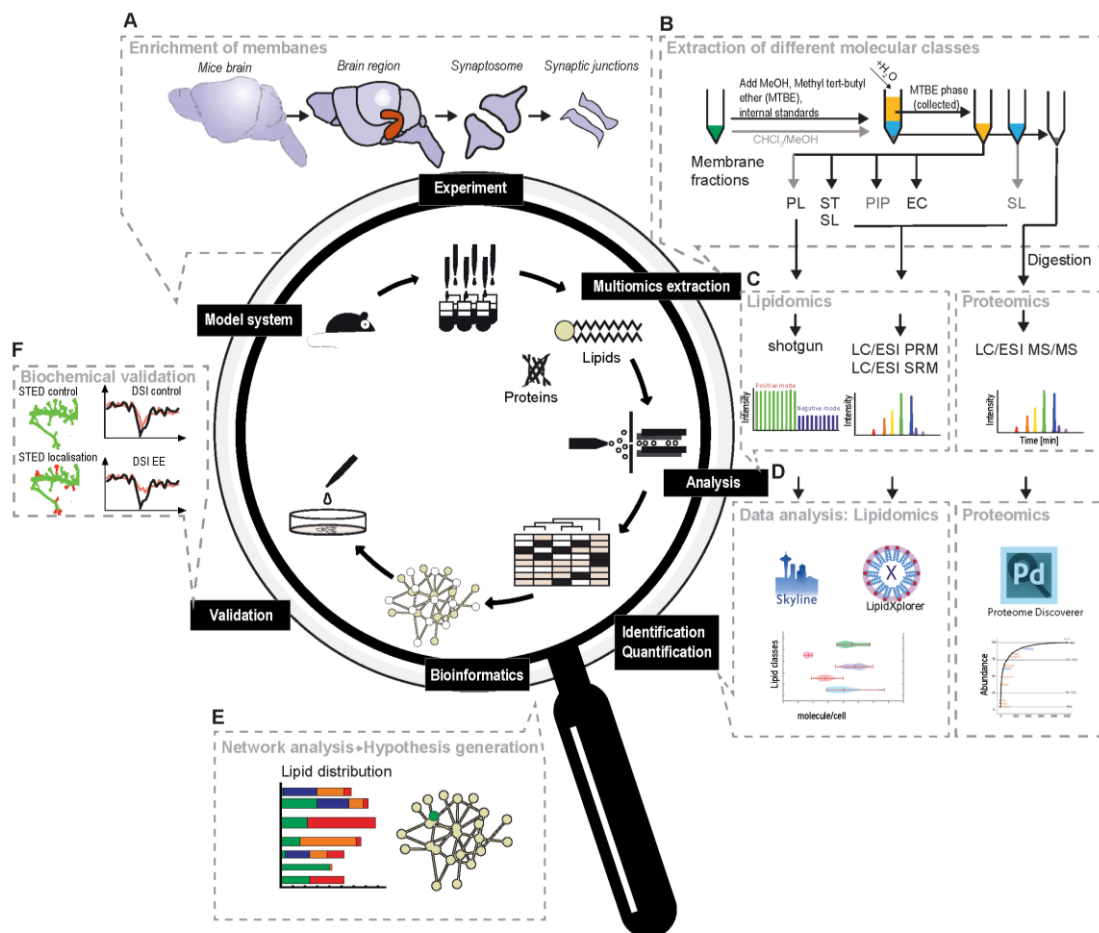


Figure 5. Comprehensive multiomics analysis of synapse compartments

- A:** Isolation and purification of organelles from rodent models.
- B:** Lipid extraction and internal standard addition applied to lipid-category tailored analysis. Proteins are hydrolyzed and subjected to tandem mass tag labeling.
- C:** Lipid and protein analysis by shotgun or targeted MS/MS analysis.
- D:** Lipidomics and proteomics data analysis. The structural characterization of lipids by LipidXplorer or Skyline, followed by absolute quantification of all detected lipid species. The proteins were identified with an FDR \leq 1% and quantified using Proteome Discoverer.
- E:** Establishment of a lipid-protein matrix to form a lipid network. Elucidation of EE specific differences identified from quantification of proteins and lipids.
- F:** Validation by additional *in-vitro* and *ex vivo* experiments, including functional assays.

MS analysis of the synaptic junction fractions reveals the enrichment and depletion of distinct lipid classes and species, with a number of surprising findings that we discuss in the corresponding manuscript. Interestingly, the lipid species cover a concentration range over seven orders of magnitude. We next established a novel multiomics workflow (Figure 5) that allowed for an assessment of over 5428 proteins of the proteome from the same sample (Figure 6A, B) (Borgmeyer et al., under revision). This analysis permitted a systematic assessment of the lipid metabolic network in synaptic junctions. Altogether, 527 molecules were identified in lipid metabolic networks comprising of glycerol-, glycerophospho-, sphingo-, mediator- and endocannabinoid-lipid metabolism by the group in Dortmund (Figure 6C). We next reasoned that the novel multiomics workflow that we developed in this study to execute lipidomics and proteomics from the same sample might be useful to generate and test novel hypotheses on synaptic plasticity. To this end, we compared the lipidome and proteome of synaptic junctions of mice raised in enriched or standard environment. Enriched environment improves cognition, learning and memory by yet unknown mechanisms in mice (Kempermann, 2019). We found that multiomics is suitable to generate hypotheses about novel mechanisms underlying complex changes in synaptic connectivity elicited by environmental stimuli. I should emphasize that I have only followed up on one hypothesis in my thesis work and other interesting and testable hypotheses might be delineated from the data set that was generated in Dortmund by the team of Robert Ahrends. The contribution of the thesis work was in generating and testing this hypothesis. Thus, this thesis focuses exclusively on this final stage of this workflow.

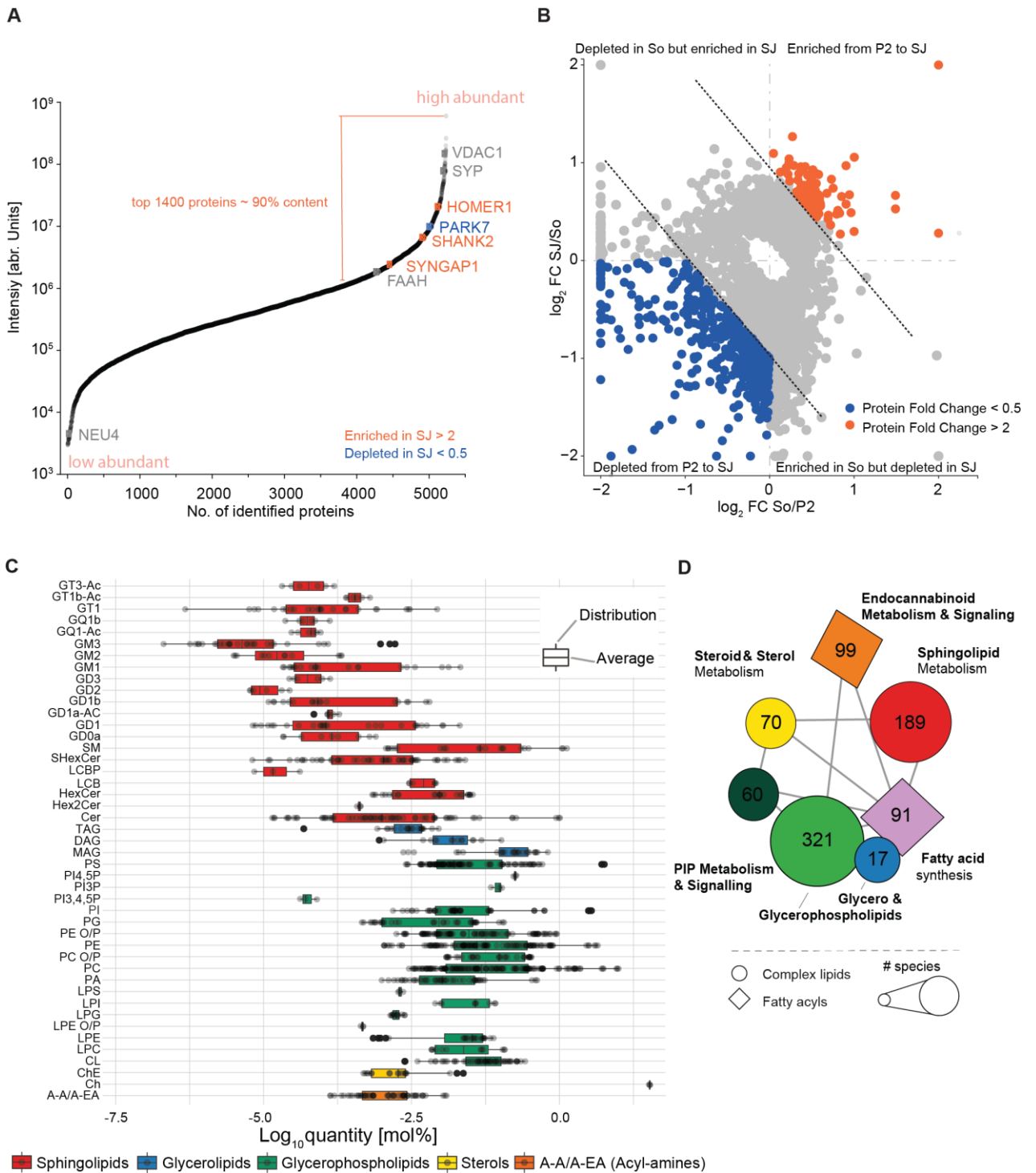


Figure 6. The global quantitative proteome of rat hippocampal synaptic junctions and quantitative inventory analysis of the synaptic junction lipid content

- A:** Based on TMT labeling global proteomics analysis, 5248 proteins were identified both in hippocampal membrane (P2), synaptosome (So) and synaptic junction (SJ) fractions. The dynamic range of these proteins were depicted according to cumulative protein abundance in percentage. Protein abundance percentages were classified as low, medium and high based on quartile. High abundance range is between max and 75% (TQ: third quartile); medium range is between 75% and 25% (FQ: first quartile); low range is between FQ and minimum abundance. The proteins which have statistical significance (p value < 0.05) were classified as enriched (orange) and depleted (blue) according to their abundance change from P2 to SJ. Some of these enriched in SJ (fold change > 2) and depleted in SJ (fold change < 0.5) proteins were indicated on the line plot.
- B:** Sector plot showing Log_2 fold change of 3580 statistically significant proteins (p -value ≤ 0.05) in hippocampal membrane, synaptosome and synaptic junction. Proteins are classified as depleted or enriched based on log_2 fold change threshold. The statistical significance was calculated based on one-way ANOVA test followed by Benjamini-Hochberg correction. Among significant proteins (grey), depleted proteins whose expressions are decreasing from P2 to SJ continuously are shown as blue, enriched proteins whose expressions are increasing from P2 to SJ are shown as orange.
- C:** Box plots displaying the dynamic range of the synaptic junction lipidome of hippocampal rat brain. Five lipid categories (glycerolipids, glycerophospholipids, sphingolipids, sterols and endocannabinoids) are shown containing in total 45 lipid classes and 416 lipid species. Distribution of the lipid classes in the synaptic junction fraction in molar percentage.
- D:** Lipid-related network mapping showing the significantly quantified lipid- related enzymes and significantly quantified lipids. The significantly enriched and depleted proteins were queried against KEGG databases and KEGG annotated enzymes were mapped to “Metabolism of lipid“related subpathways such as glycerophospholipid and glycerolipid metabolism pathways. The lipid species which are related to each mapped subpathway were compared against the quantified lipids. To overcome the nomenclature problem, KEGG annotated lipids and the quantified lipids in this study were converted to their upper classes. The upper class names were compared. Overall, all KEGG annotated lipid-related enzymes and lipids quantified in this study were represented in a network structure. The node shape represents the lipid complexity as circle referring complex lipids and diamond as fatty acyls. The number of overall mapped molecule numbers were indicated. The size of the nodes are proportional to the number of molecules. The empirical relationship between the metabolisms are indicated as edges.

These data were generated by Cristina Coman and Robert Ahrends from Leibniz Institute for Analytical Sciences in Dortmund.

3.1.1 Subcellular fractionation experiments

From the isolated hippocampi synaptic fractions of increasing purity were isolated, the heavy membrane fraction (P2), synaptosomes (So) and synaptic junctions (SJ). To ensure that the fractions were not contaminated by nuclear proteins, an antibody against the Histone binding protein 3 (H3) was used as a negative control. H3 was only found in the P2 fraction and was absent from synaptosomes and synaptic junctions (Figure 7A, E). The NMDA-receptor subunit *N*-methyl D-aspartate receptor subtype 2B (GluN2B, gene name: GRIN2B) was most abundant in postsynaptic membranes (Figure 7A, D). It was also clearly enriched in the synaptic junction fraction. The postsynaptic density protein 95 (PSD95) was also clearly enriched in synaptic junctions showing that the postsynaptic density was enriched along with

the postsynaptic membrane (Figure 7A, B). The synaptic vesicle protein 2B (SV2B) was enriched in synaptic vesicles and only transiently present in the synaptic membrane following vesicle fusion. SV2B was most abundant in synaptosomes and only present at low levels in synaptic junction and the P2 fraction (Figure 7A, C). Collectively, these data show that synaptic membranes were isolated, successfully allowing for an in-depth analysis of the samples.

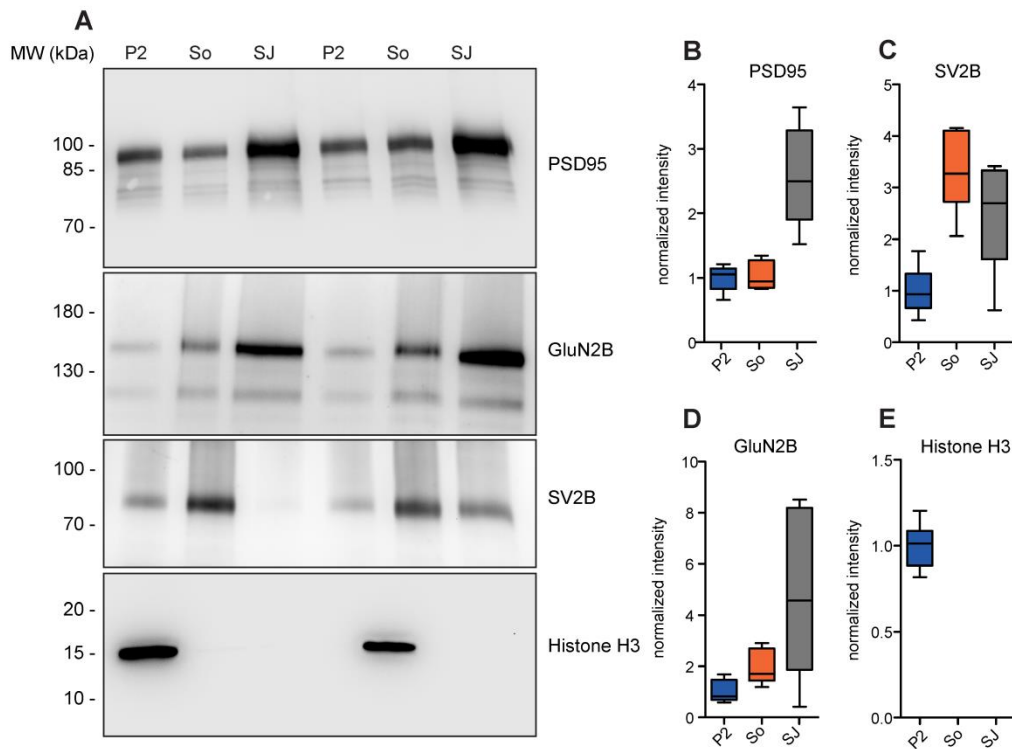


Figure 7. Purity control of synaptic fractions

A: Immunoblotting from 6 independent synaptic preparations (P2), synaptosome (So) and synaptic junction (SJ) (n=6).

B-E: Quantification for the postsynaptic marker PSD95 (B), the synaptic vesicle protein SV2B (C), GluN2B (D) and the nuclear marker Histone H3 (E).

Data information: In B-E data are presented as box plots with whiskers minimum to maximum value.

3.1.2 No gross structural alterations occur in synaptic connectivity in response to EE

To ensure that no gross morphological changes occur in response to EE in comparison to standard environment (SE) that might influence the results of the proteomics analysis, the ultrastructure of the synapses was analyzed in stratum oriens and stratum radiatum of the CA1 region (Figure 8A).

The number of synapses was unchanged following EE, in both stratum radiatum and oriens (Figure 8B, F). Synapses were identified by the presence of a PSD and associated presynapse containing synaptic vesicles. The average spine area was also unchanged following EE in stratum radiatum and oriens (Figure 8C, G). The length of PSDs was measured in both shaft and spine synapses and was unchanged in EE in both strata (Figure 8D, H). The number of

mitochondria was counted in the fields of both strata. Mitochondria were identified as organelles with a double membrane and internal membrane stacks and no degraded material. The density of mitochondria was unchanged in both strata following EE (Figure 8E, I).

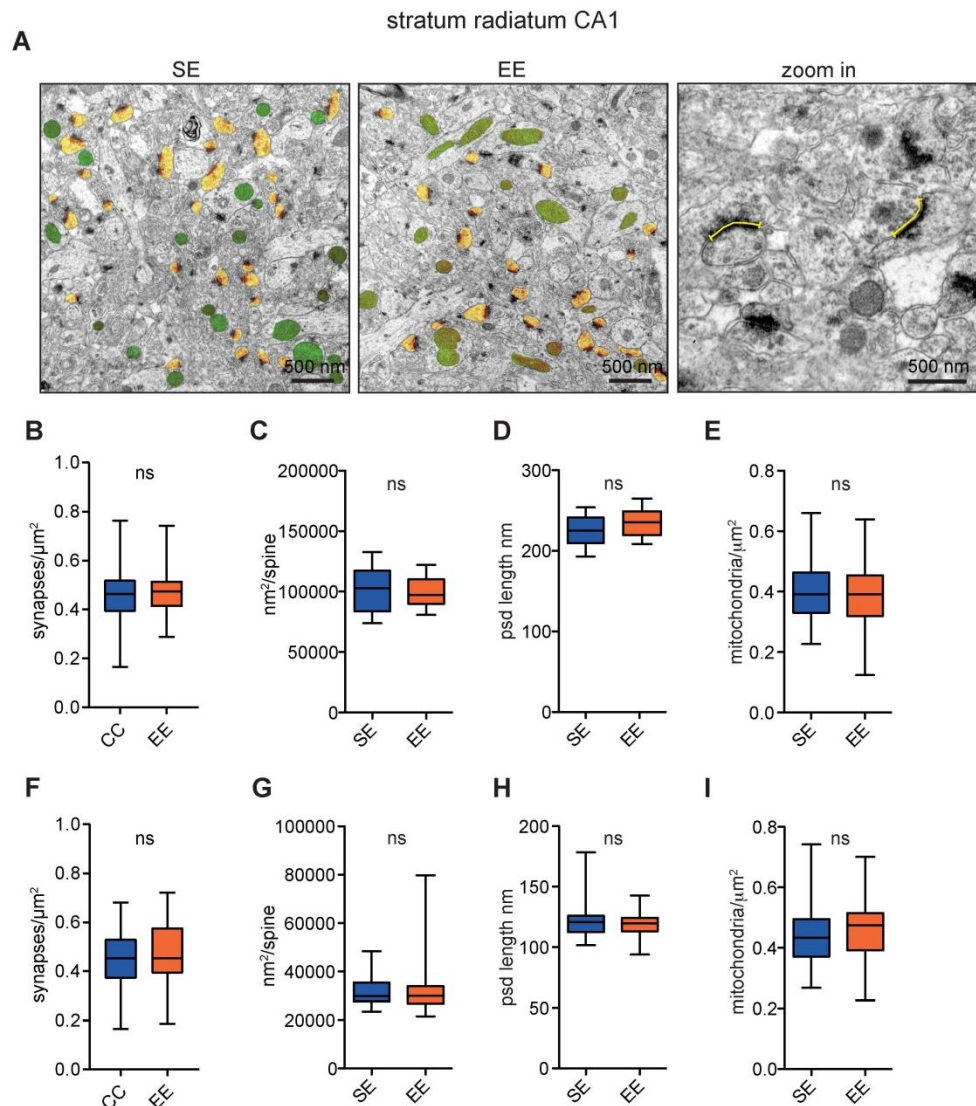


Figure 8. Ultrastructural characterization of EE and SE mice in the CA1 region

A: Sections were prepared from 4 standard environment (SE) and 4 enriched environment (EE) animals. Representative frames from the stratum radiatum of the CA1 region, mitochondria green, spines yellow, scale bar: 1 μm (A), example measurements of PSD length in CA1, scale bar: 500 nm (zoom in).

B-E: Average synapse density (B), spine area (C), average PSD length (D), number of mitochondria/ μm^2 (E), were measured in the CA1 region.

F-I: Average synapse density (F) spine area (G), average PSD length (H) and mitochondria/ μm^2 (I) were measured in the stratum oriens of the CA1 region. Data information: In B-H data are presented as box plots with whiskers minimum to maximum value.

In addition, the ultrastructure of the mossy fiber region in the CA3 region was analyzed (Figure 9A). Mossy fiber boutons are much larger and more complex than other hippocampal presynapses, the same is true for the thorny excrescences of the connected postsynapses. One thorny excrescence contains multiple PSDs and often appears as multiple spines in a two-

dimensional image. The complexity of these structures makes it impossible to count the synapses in two-dimensional images. As an approximation, the spine area (Figure 9B) and the number of PSDs (Figure 9C) were quantified, both were unchanged following EE. In the mossy fiber region mitochondria are present mostly localized to the presynapse. The number of synaptic mitochondria was unchanged following EE (Figure 9D).

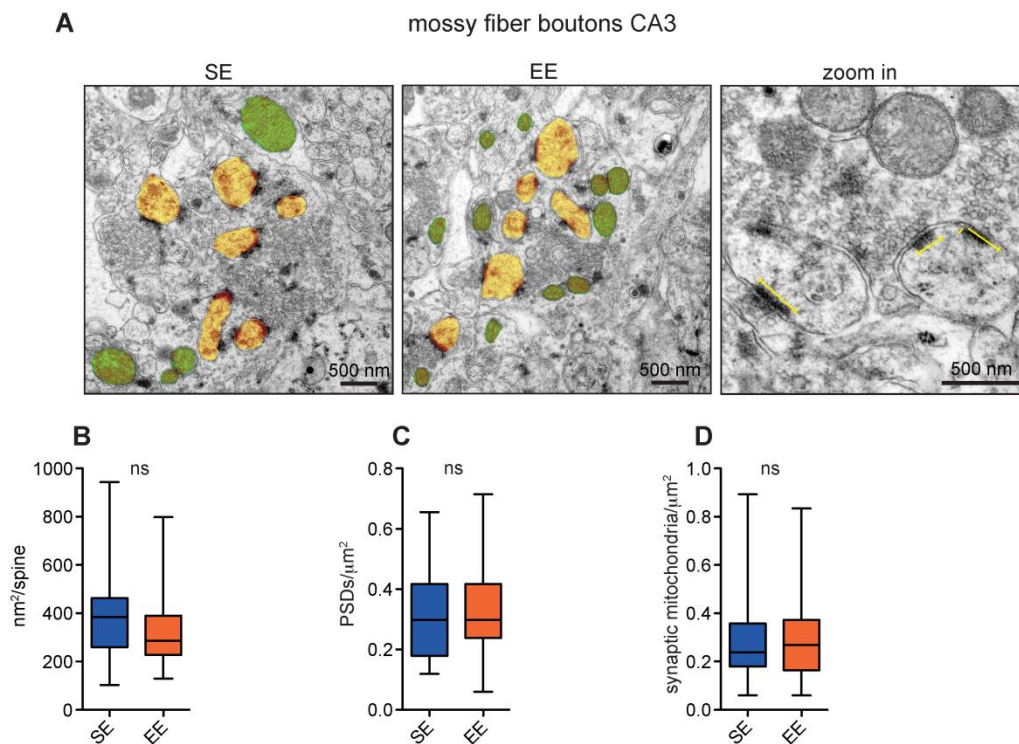


Figure 9. Ultrastructural characterization of EE and SE mice in the CA3 region

- A:** Representative frame from the CA3 region, mitochondria green, spines yellow, scale bar 500 nm.
- B-D:** Average PSD length per spine (B), PSDs per μm^2 (C) and the average number of synaptic mitochondria per μm^2 (D) were measured in the CA3 region.

3.1.3 Results of the multiomics screen

An unbiased protein ontology enrichment analysis revealed that 26 pathways related to synaptic plasticity are regulated differently following environmental enrichment including retrograde endocannabinoid signaling. To test the utility of the workflow we therefore focussed on the endocannabinoid pathway, since this pathway was affected on protein and lipid level. Two proteins involved in the retrograde endocannabinoid signaling were significantly regulated following EE: ABHD6 was significantly downregulated in the synapse following EE (Figure 10A, C). FAAH on the other hand was upregulated in the synapse following EE. Additionally, multiple G proteins were regulated, but it is unclear if this regulation is due to binding to the CB1R. Most importantly, we found differential regulation of the endocannabinoid 2-AG, which was significantly downregulated in the synaptic membrane following EE (Figure 10B).

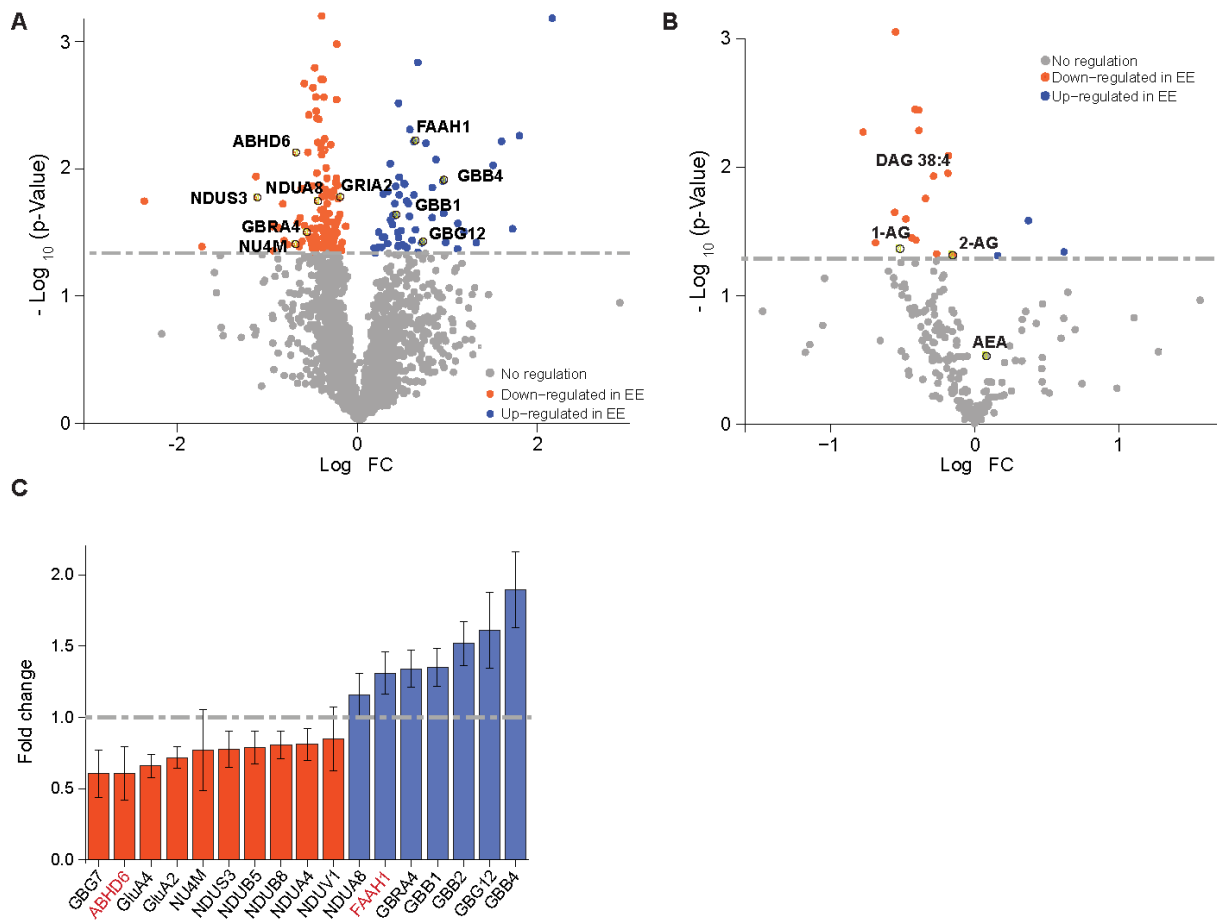


Figure 10. Multiomics analysis of EE and SE synaptic junctions

- A:** Volcano plot of log₂ fold changes of proteins in hippocampal synaptosome of the EE. Orange down regulated species, blue up-regulated species and grey non-regulated lipids. Global proteomics analysis identified 2164 proteins from which 57 and 121 proteins revealed a significant up and down regulation, respectively. Significant changes in the proteome were indicated by minimum log₂ fold change with a p-value ≤ 0.05 . Proteins of the retrograde endocannabinoid pathway were identified and individually labeled.
- B:** Volcano plot of log₂ fold changes of lipid species concentrations in hippocampal synaptosome of the mice housed in enriched environment. Global lipidomics analysis identified 23 regulated lipids. Red: down-regulated species, blue: up-regulated species and grey: non-regulated lipids. 2-AG, 2-arachodonyl glycerol and NAE, N-arachodonyl ethanolamide are indicated.
- C:** All significantly upregulated proteins are displayed in blue, all down-regulated proteins in red. All data are combined from 3 independent biological experiments, and mean values are shown; error bar presents standard error of the mean. These data were generated by Cristina Coman and Robert Ahrends from Leibniz Institute for Analytical Sciences in Dortmund.

3.1.4 Endocannabinoid-dependent plasticity is altered by EE

Endocannabinoids are synthesized and released upon demand in an activity-dependent manner (Castillo et al, 2012). Drugs known to prevent the activation of CB1R or to inhibit the synthesis of 2-AG, the predominant endocannabinoid in the hippocampus, cause enhanced long-term plasticity (LTP) that is induced by a weak- θ -burst stimulation, thus suggesting that

endocannabinoids regulate such form of LTP (Figure 11). We tested whether treatment with the CB1-antagonist rimonabant influences LTP formation following TBS. CB1R antagonist attenuated the fEPSP slope following TBS in slices from SE mice whereas the opposite was found in slices from EE mice (Figure 11).

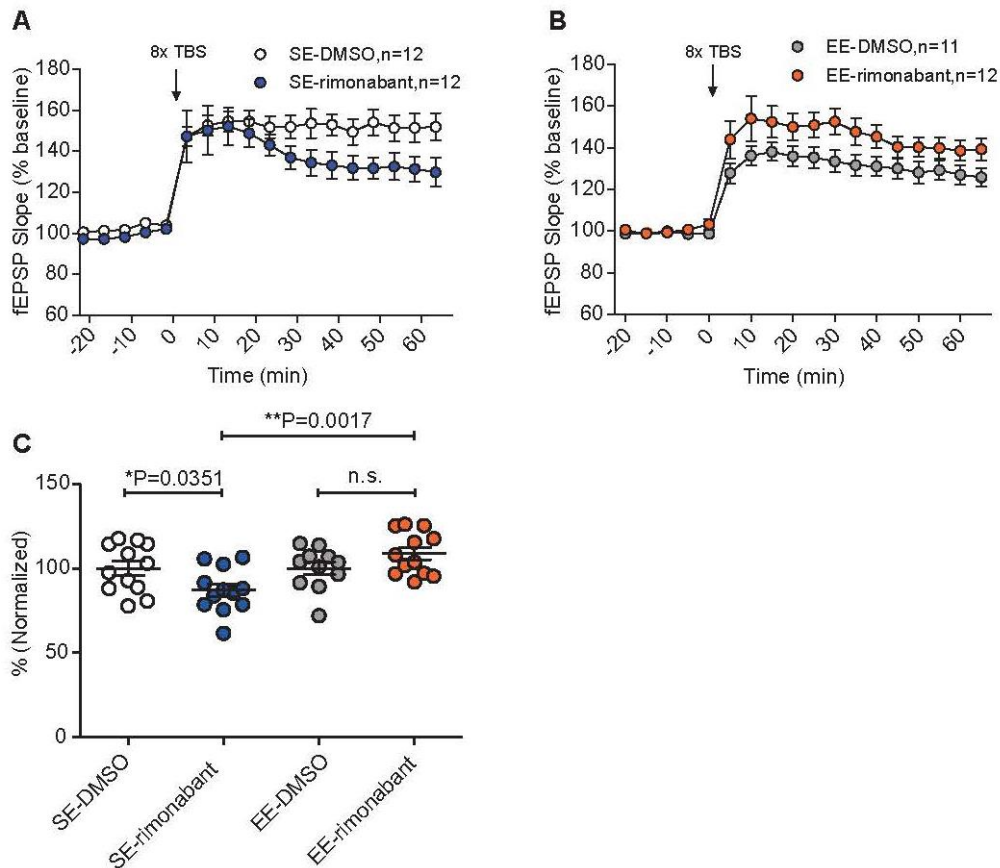


Figure 11. LTP induction in acute slices from mice raised in EE

A-C: Involvement of CB1 receptors in LTP formation induced by repeated theta-burst stimulation (TBS) sequences in SE and EE mice. Induction of LTP by 8 repeats of a TBS theta-burst sequence that consisted of 10 bursts of 5 stimuli every 30 s resulted in a stable potentiation under control condition (DMSO) (A, B). However, application of the CB1R antagonist rimonabant (1 μ M) over the whole recording period resulted in a declined potentiation in SE mice (A, C). These data were generated by PingAn Yuanxiang at the Leibniz Institute for Neurobiology (LIN) in Magdeburg.

3.1.5 Expression of catabolic enzymes of the endocannabinoid pathway are regulated following EE

The MS results were controlled by immunoblotting. To control not only for protein levels, but for the amount of postsynaptic membranes in each individual probe as well, PSD95 was used as a loading control. As shown in MS, synaptic ABHD6 levels were reduced in the synapse following EE (Figure 12A). In the supernatant ABHD6 levels remained unchanged (Figure 18C). FAAH levels on the other hand were increased following EE (Figure 18B). In the supernatant FAAH levels were unaffected by EE (Figure 18D).

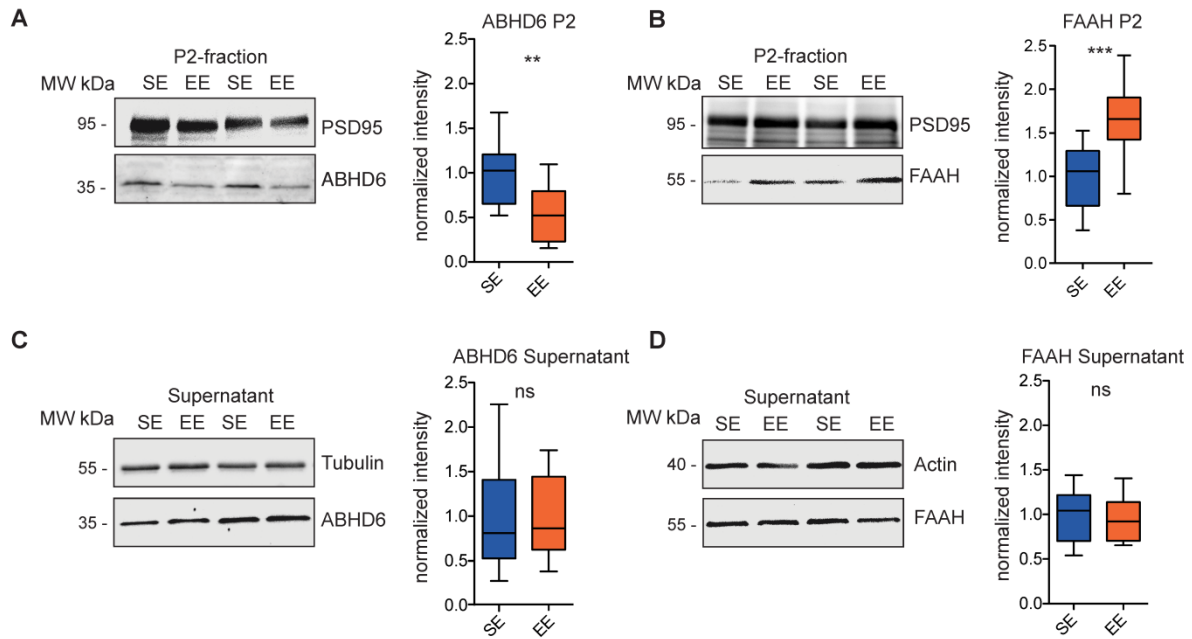


Figure 12. Immunoblots of FAAH and ABHD6

A-B: Blots of P2-fraction and supernatant of 14 EE and 14 SE animals. Blots of the P2-fraction were developed with antibodies against ABHD6 (A), FAAH (B) and PSD95 (A, B) as a loading control. ABHD6 and FAAH signals were normalized to PSD95.

C-D: Blots of the supernatant were developed with ABHD6 (C) and FAAH (D), beta-Tubulin and beta-Actin antibodies, respectively. ABHD6 signal was normalized to beta-Tubulin and FAAH signal to beta-Actin.

Data information: Data are presented as boxplots with whiskers from minimum to maximum. *** $p \leq 0.001$ (Student's t-test), ns $p > 0.05$.

To identify the synapse population in which these changes take place, we first tested inhibitory synapses since the vast majority of these synapses contain the CB1R. Hippocampal cryosections were stained for the inhibitory synapse marker Gephyrin and ABHD6 or FAAH, respectively. The colocalization of ABHD6 and FAAH was analyzed in the different strata of the hippocampal CA1 region (Figure 13A). The percentage of inhibitory synapses containing ABHD6 or FAAH was 10% or less in stratum oriens, radiatum and lacunosum moleculare of the CA1 region (Figure 13C, E)

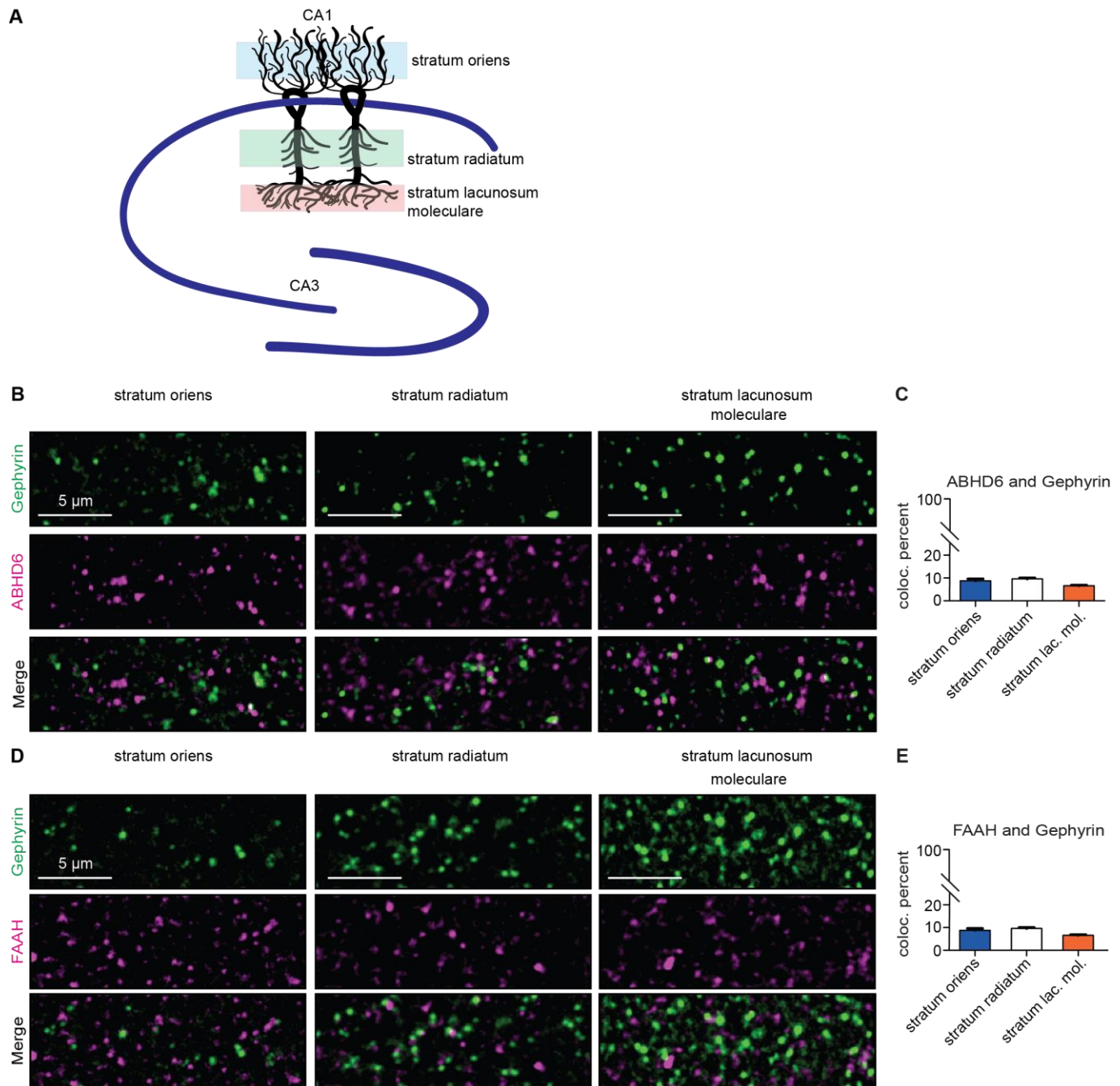


Figure 13. ABHD6 and FAAH are absent from inhibitory synapses

- A:** Representative scheme of the hippocampus, strata of the hippocampal CA1 region are highlighted
- B, C:** Cryosections from two mice housed in SE were stained with antibodies for ABHD6 and the inhibitory synapse marker protein Gephyrin. Colocalization of ABHD6 with Gephyrin was analysed in the stratum oriens, radiatum and lacunosum moleculare of the hippocampal CA1 region (C). Scale bar: 5 μ m
- D, E:** Cryosections from two mice housed in SE were stained with antibodies for FAAH and Gephyrin (D). Colocalization of Gephyrin with FAAH was analyzed in the stratum oriens, radiatum and lacunosum moleculare of the hippocampal CA1 region (E).
Data information: In (C, E), data are presented as mean + SEM. Scale bar: 5 μ m

Cryosections were then stained for the excitatory synapse marker Shank3 combined with FAAH or ABDH6 (Figure 14A, E). The staining revealed that 30% of excitatory synapses in

the stratum radiatum contained ABHD6 (Figure 14B). To pinpoint the region of the hippocampus where the regulation of FAAH and ABHD6 takes place, cryosections from EE and SE animals were analyzed. ABHD6 levels were reduced in stratum oriens (Figure 14C) and radiatum (Figure 14B), but not in the stratum lacunosum moleculare (Figure 14D), which receives no input from the Schaffer collateral projections. In parallel, FAAH levels were increased in the stratum oriens (Figure 14G) and radiatum (Figure 14F), while no significant change was observed in the stratum lacunosum moleculare (Figure 14H).

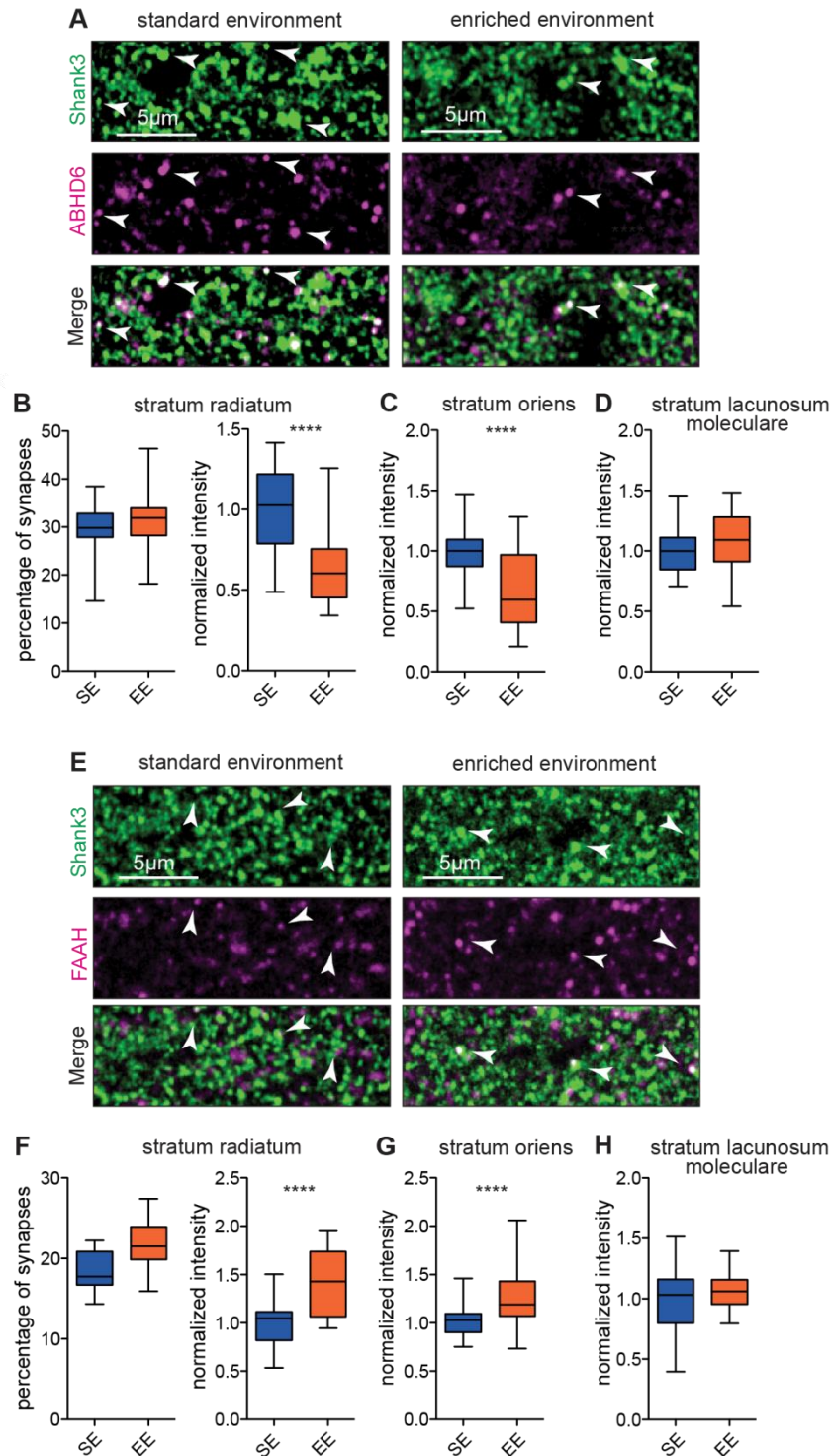


Figure 14. FAAH and ABHD6 levels in the stratum radiatum of EE and SE mice

A-D: Cryosections from 4 SE animals and 4 EE animals were stained against ABHD6 and Shank3 (A). Images were acquired in the stratum radiatum (A, B), stratum oriens (C) and stratum lacunosum moleculare (D), scale bar: 5 μ m. Intensity of the ABHD6 staining was measured for ABHD6 puncta colocalizing with the synaptic marker Shank3. Colocalization is indicated by arrowheads.

E-H: Cryosections from 4 SE animals and 4 EE animals were stained for FAAH and Shank3 (E). Images were acquired in the stratum radiatum (F), stratum oriens (G) and stratum lacunosum moleculare (H), scale bar: 5 μ m. Intensity of the FAAH staining where measured for Shank3 puncta positive for FAAH. Colocalization is indicated by arrowheads.

Data information: Data are presented as boxplots with whiskers from minimum to maximum. **** $p \leq 0.0001$ (Student's t-test), ns $p > 0.05$.

To control the distribution and expression of CB1R cryosections were cut from EE and SE animals and stained for the postsynaptic marker Shank3, the presynaptic marker Synaptophysin and for CB1R (Figure 15A). Only synapses labeled by the pre- and postsynaptic marker were analyzed. The number of CB1R positive presynapses and the intensity of the synaptic CB1R staining was quantified in stratum oriens, stratum radiatum and stratum lacunosum moleculare (Figure 15B-D). The number of CB1R positive presynapses and the intensity of the staining were unchanged by EE in the stratum oriens, stratum radiatum and stratum lacunosum moleculare. In all three strata around 20% of excitatory synapses were immunopositive for CB1R.

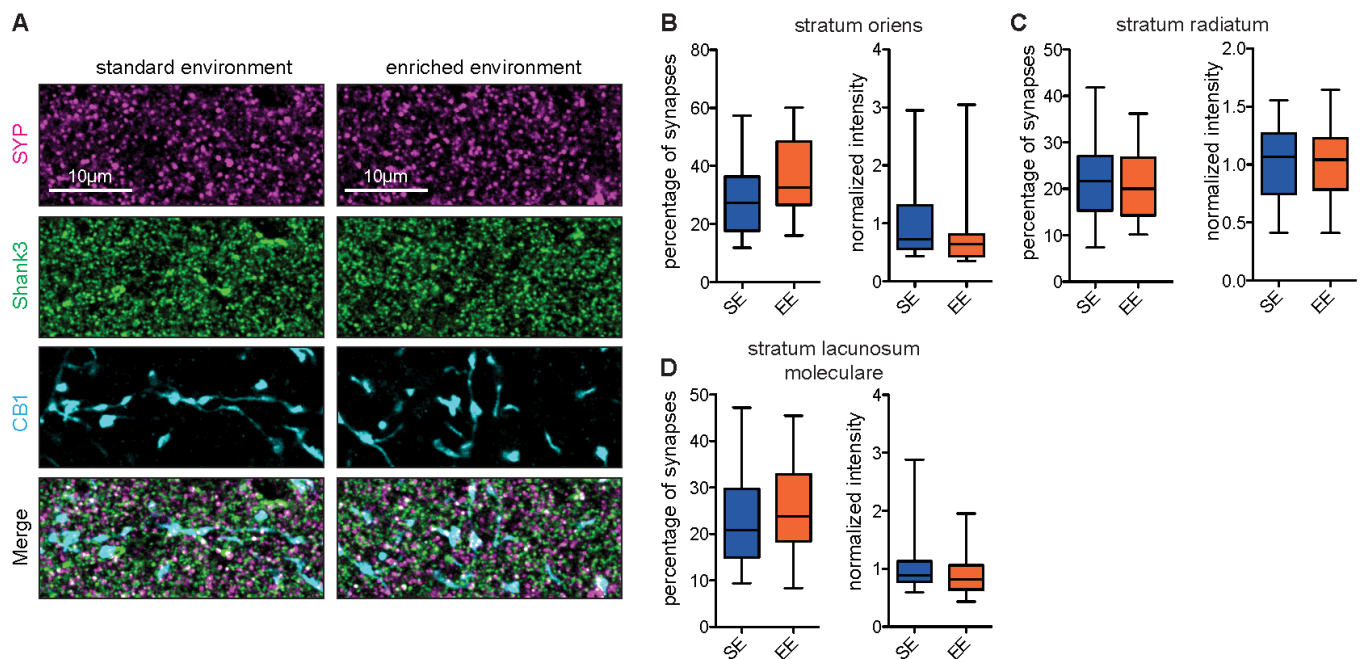


Figure 15. Distribution of the CB1R in the CA1 region of EE and SE mice

A: Cryosections from 4 SE animals and 4 EE animals were stained for Synatophysin (SYP), Shank3 and CB1R.

B-D: The percentage of SYP labeled presynaptic boutons localizing with CB1R and the excitatory postsynaptic marker Shank3 was measured in stratum oriens (B) stratum radiatum (C) and stratum lacunosum moleculare (D). The intensity of CB1R staining was measured in presynaptic boutons localizing with Shank3 in stratum oriens (B), stratum radiatum (C) and stratum lacunosum moleculare.

Data information: Data are presented as boxplots with whiskers from minimum to maximum.

3.1.6 Localization and regulation of catabolic enzymes of the endocannabinoid pathway

In the next set of experiments mature primary hippocampal neurons were used to study the distribution and regulation of ABHD6 and FAAH in greater detail. To this end the specificity of the antibodies was tested using shRNA mediated KD of both enzymes. Cells were transfected with the ABHD6 KD construct or a scrambled control at DIV 9. To check for transfection of the cells EGFP was coexpressed from the same plasmid. The cells were fixed at DIV 14 and immunostained for ABHD6 (Figure 16A). The ABHD6 signal was measured in the dendrites of transfected cells using the EGFP signal as a mask. The ABHD6 signal was significantly reduced following KD suggesting that the antibody is specific for the target sequence. Cells were transfected with the FAAH KD construct or a scrambled control at DIV 9. To control for transfection of the cells EGFP was coexpressed from the same plasmid. The cells were fixed at DIV 14 and immunostained for ABHD6 (Figure 16A). The FAAH signal was measured in the dendrites of transfected cells using the EGFP signal as a mask. The FAAH signal was significantly reduced following KD suggesting that the antibody is specific for the target. Since both ABDH6 and FAAH are involved in the degradation of CB1R agonists, it is plausible that they might localize in close proximity to CB1R-containing presynapses. Presynaptic boutons were labeled using the synaptic vesicle protein Synaptophysin (SYP). To label dendrites and spines postsynaptic cells were filled with EGFP as a volume marker and stained for ABHD6 or FAAH (Figure 16E, F). The percentage of spines contacting a SYP-labeled presynapse containing ABHD6 and the percentage of those spines contacting a CB1R-containing presynapse was counted. 40% of all spines contained ABHD6; of those spines 80% contacted a CB1R positive bouton (Figure 16F). The percentage of spines contacting a SYP-labeled presynapse containing FAAH and the percentage of those spines contacting a CB1R containing presynapse was counted. 40% of all spines contained ABHD6; of those spines 80% contacted a CB1R positive bouton (Figure 16H).

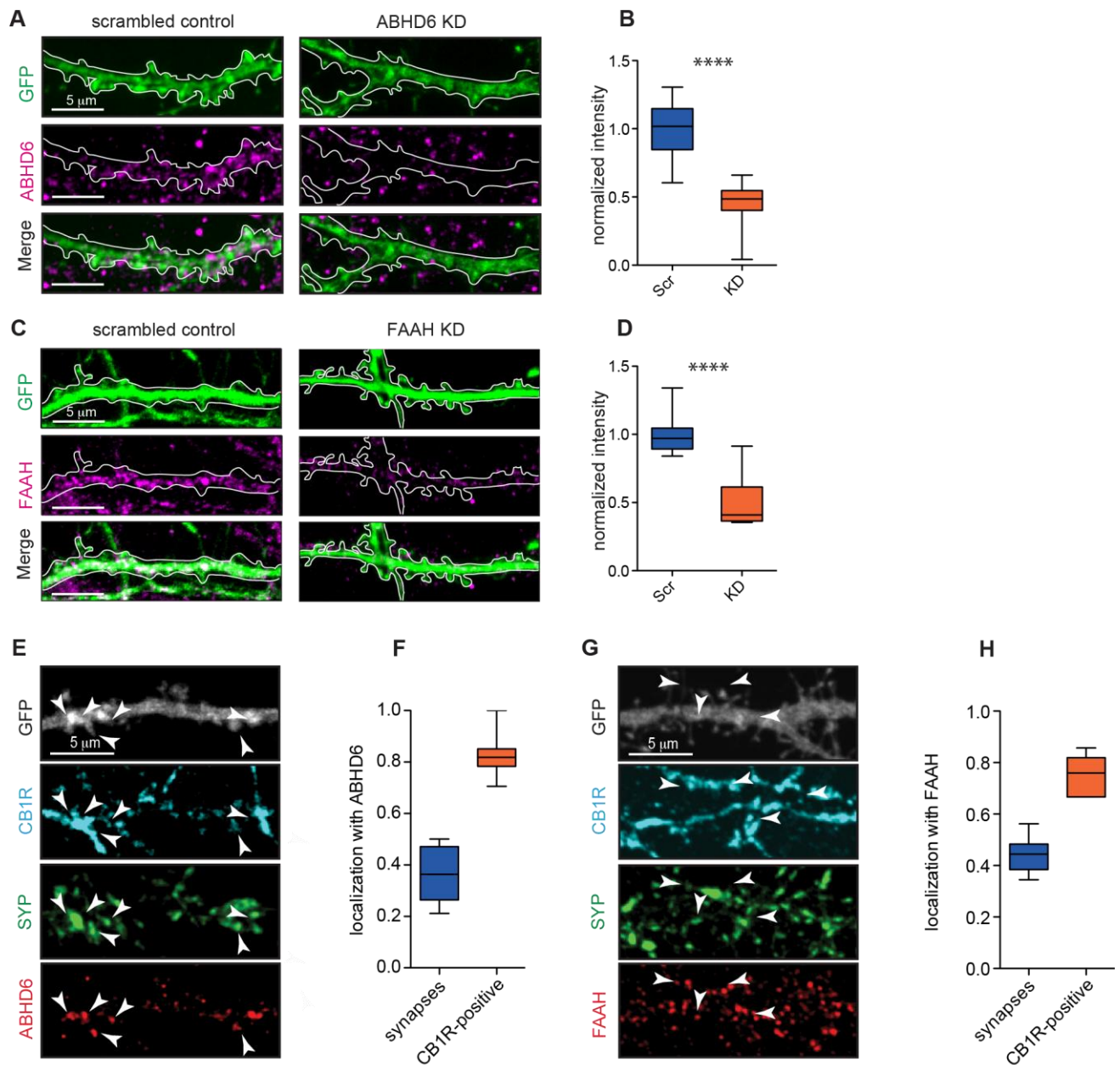


Figure 16. ABHD6 and FAAH localization and KD verification

A-B: ABHD6 intensities were measured in cells transfected with ABHD6 KD (n=16) or scrambled control (n=17). Scale bar: 5 μ m

C-D: FAAH intensities were measured in cells transfected with FAAH KD (n=8) or scrambled control (n=8). Scale bar: 5 μ m

E-H: Hippocampal primary neurons were transfected at DIV 20 with GFP-N1 and fixed after 24 h at DIV 21. The cells were stained for CB1R, SYP and ABHD6 (n=8) (E). Total localization of ABHD6 with the synaptic marker SYP and with synapses labeled by both SYP and CB1R were analyzed (F). GFP transfected cells were stained for CB1R, SYP and FAAH (n=10) (G). Total localization of FAAH with the synaptic marker SYP and with synapses labeled by both SYP and CB1R were analyzed (H). Scale bar: 5 μ m

Data information: Data are presented as boxplots whiskers minimum to maximum.

**** $p < 0.0001$ (Student's t-test).

We then studied how the synaptic levels of FAAH and ABHD6 are regulated using primary hippocampal neurons. To analyze the levels of both proteins, synapses were immunolabeled

for the excitatory synapse marker Shank3 (Figure 17A, C, E, G). Since EE results in an increase in synaptic activity (Ohline and Abraham, 2019b), the effect of synaptic silencing on the synaptic localization of FAAH and ABHD6 was studied, by bath application of TTX in the culture medium for 48 h (Figure 17A-D). Synaptic ABHD6 levels were not affected by synaptic silencing (Figure 17B); the synaptic expression of FAAH on the other hand was reduced following synaptic silencing (Figure 17D). It was previously shown that a positive feedback loop exists between presynaptic CB1R activation and postsynaptic 2-AG synthesis (Anderson et al., 2015). To explore the effect of CB1R signaling on the synaptic localization of ABHD6 and FAAH, the cells were treated with the CB1R-antagonist AM-251 (Figure 17E-H). Inhibition of CB1R signaling resulted in a reduction of synaptic ABHD6 levels (Figure 17F), but did not affect the synaptic levels of FAAH (Figure 17G). This suggests that synaptic localization of ABHD6 is dependent on synaptic 2-AG production.

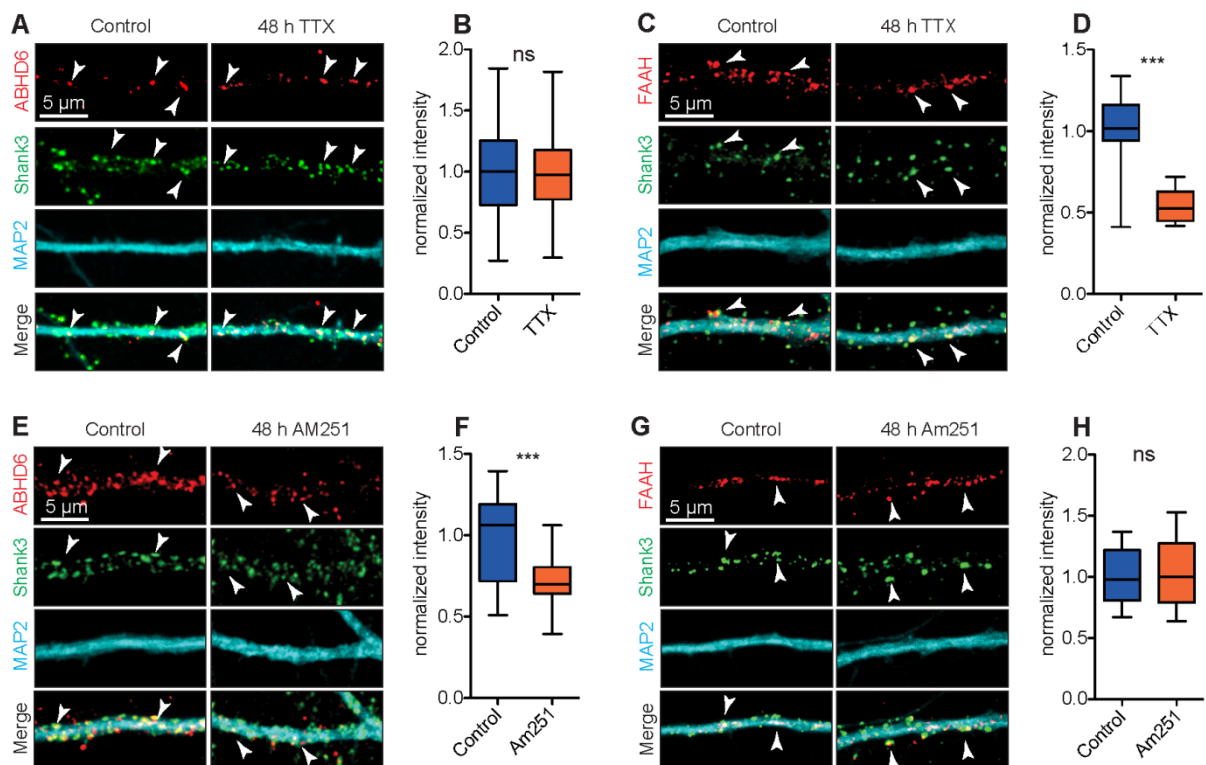


Figure 17. Regulation of ABHD6 and FAAH levels in hippocampal primary neurons

A-D: Hippocampal neurons were silenced by 1 μM TTX for 48 h (A, D). The cells were stained for MAP2, Shank3 and ABHD6 (n=28) (G) or FAAH (n=9) (H) at DIV 21. The levels of ABHD6 (G) and FAAH (H) were measured in Shank3 labeled synapses.

E-H: Hippocampal neurons were treated for 48 h with the CB1R antagonist AM-251 for 48 h (E, G). The cells were stained for MAP2, Shank3 and ABHD6 (n=18) (F) or FAAH (n=23) (H) at DIV 21. The levels of ABHD6 (F) and FAAH (H) were measured in Shank3 labeled synapses.

Data information: Data are presented as boxplots whiskers minimum to maximum.

*** $p \leq 0.001$ (Student's t-test).

We then aimed to get a more detailed understanding of the subcellular localization of ABHD6. Mature hippocampal rat neurons (DIV 21) were transfected with a MARCKS-GFP

expressing construct, labeling the cell membrane. The cells were stained with antibodies against ABHD6 and Shank3 (Figure 18A). Imaging at STED-resolution revealed clusters of ABHD6 associated with the postsynaptic density (PSD), in a subset of spines (Figure 18A 1, 2), with some spines lacking ABHD6 (Figure 18A, 3). ABHD6 is known as both a postsynaptic and an ER protein; it was therefore tested if ABHD6 is localized to spines containing a type of ER membrane known as the spine apparatus. Mature hippocampal rat neurons were stained for the spine apparatus marker Synaptopodin, Shank3 and ABHD6. 20% of Shank3 labeled synapses contained Synaptopodin, of these synapses 80% also contained ABHD6, while only 36% of Shank3 labeled synapses contained ABHD6 (Figure 18C, D). This suggests that the presence of the spine apparatus is not necessary for the localization of ABHD6 in spines, but that spines containing a spine apparatus are highly likely to contain ABHD6.

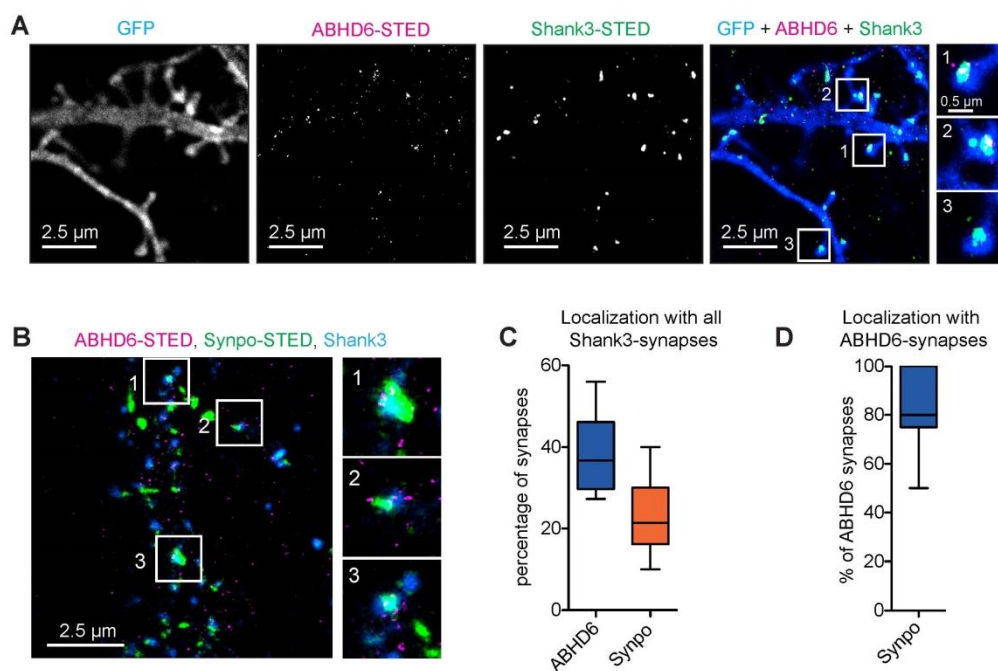


Figure 18. Synaptic distribution of ABHD6

- A:** Cells were transfected with MARCKS-GFP on DIV 15 and fixed on DIV 16. Cells were stained against Shank3 and ABHD6. Individual spines with ABHD6 (1, 2) and without ABHD6 (3) are shown.
- B:** Cells DIV 16 were stained for ABHD6, Synaptopodin and Shank3 (n=15).
- C-D:** Colocalization of ABHD6 and Synaptopodin with Shank3 and the colocalization of Synaptopodin and Shank3 positive synapses with ABHD6.
Data information: Data are presented as boxplots whiskers minimum to maximum.

ABHD6 is an ER-resident enzyme and most interestingly its reduced postsynaptic localization following blockage of CB1R came along with a displacement of the Synaptopodin-positive spine apparatus (Figure 19). To analyze if the regulation of synaptic ABHD6 levels might be dependent on the spine apparatus, hippocampal primary neurons were again treated with AM-251 for 48 h. corresponding to the effect on synaptic ABHD6 the number of spines containing

Synaptopodin was also reduced following inhibition of CB1R signaling (Figure 19). Thus, most likely a retraction of ER membranes from spines of CB1R bearing synapses underlies the removal of ABHD6 from synapses in response to reduced ECS.

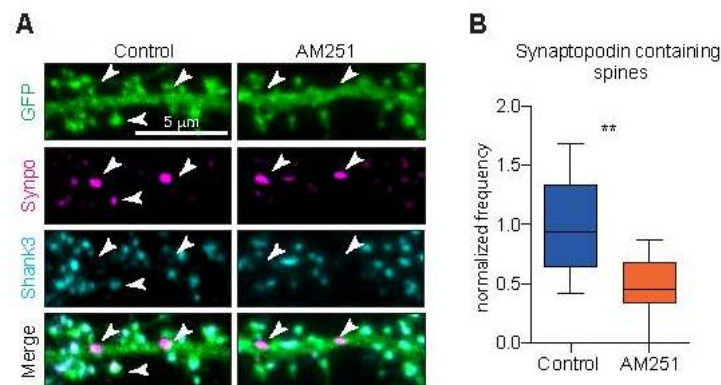


Figure 19. Inhibition of CB1R decreases the number of spine apparatus containing synapses

A, B: Cells were treated with AM-251 for 48 h and stained for Shank3 and Synaptopodin (SynPo) (A) (n=11), Scale bar: 5 μm. Co-staining of Synaptopodin containing spines after blockage of CB1R with AM-251 reveals a displacement of the Synaptopodin-positive spine apparatus (B). Data information: Data are presented as boxplots with whiskers from minimum to maximum value. **p≤0.01 (Student's t-test).

The major 2-AG degrading enzyme is Monoacylglycerol lipase (MAGL). Several studies point to a predominant role of MAGL in the catabolism of 2-AG also at hippocampal synapses (Horváth et al., 2014; Guggenhuber et al., 2016; Wang et al., 2017). However, in contrast to FAAH and ABHD6 the levels of MAGL were not changed in mice subjected to EE in the proteomic analysis (Figure 10). Importantly, MAGL is a membrane-associated, but not a transmembrane protein and is thought to predominantly localize to presynapses (Hashimoto et al., 2007). Further analysis of the mechanisms of altered ECS following EE therefore required substantiating these findings in primary neurons. Hippocampal primary neurons (DIV 21) were stained for MAGL, CB1R and the presynaptic marker SYP. MAGL indeed localized mainly to CB1R positive presynapses (Figure 20A), but not to CB1R negative synapses or extrasynaptic CB1Rs. To further prove that MAGL is indeed specifically localized to presynapses and not to dendrites and spines, hippocampal neurons were transfected with GFP as a cell fill and stained for MAGL (Figure 20B). It turned out that MAGL is predominantly localized outside of dendrites, excluding a major function in control of postsynaptic 2-AG catabolism.

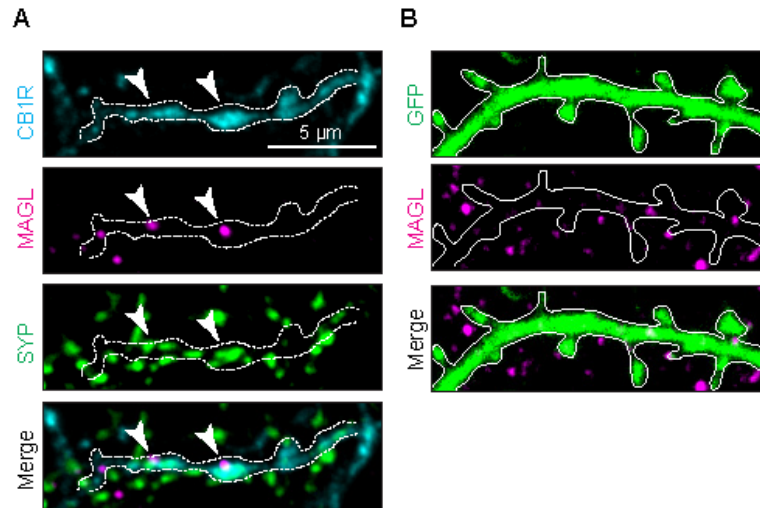


Figure 20. Synaptic localization of MAGL

- A:** Hippocampal primary neurons stained for CB1R (blue), MAGL (magenta) and SYP (green) at DIV21
- B:** Hippocampal neurons filled with GFP stained for MAGL at DIV 21

3.1.7 ABHD6 regulates the surface expression of AMPARs

Collectively, these findings open up an interesting scenario. ABHD6 has a second cellular function as an auxiliary subunit of AMPARs that negatively controls surface expression of GluA1 (Figure 7) (Wei et al., 2017). We therefore wondered whether downregulation of ABHD6 at the postsynapse might go along with increased surface expression of AMPARs. To test this hypothesis hippocampal primary neurons were transfected with the ABHD6 KD construct or a scrambled control at DIV 9 and processed for immunofluorescence staining at DIV 14 (Figure 21A). Live cells were first live stained with an antibody directed against an extracellular epitope of GluA1. Following fixation, the cells were also stained with antibodies raised against CB1R and SYP. The surface expression of GluA1 was measured in CB1R positive and negative dendritic spines in cells transfected with the ABHD6 KD or the scrambled control. There was no difference in GluA1 surface expression between CB1R positive and negative synapses in cells transfected with the scrambled control (Figure 21B). The KD of ABHD6 in hippocampal primary neurons resulted in increased surface expression of GluA1 at CB1R positive synapses (Figure 21B). The effect was absent at CB1R negative synapses (Figure 21B).

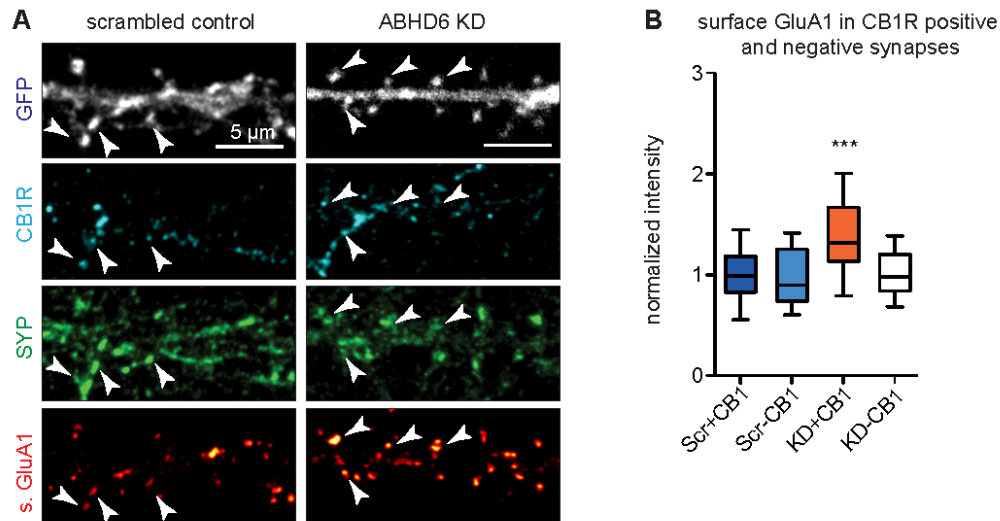


Figure 21. ABHD6 KD increases GluA1 surface expression in CB1R positive synapses

A-B: Hippocampal primary neurons were transfected with an ABHD6 KD, or scrambled control for 5 days from DIV 9 to 14 and live stained for GluA1. Post fixation cells were stained for SYP and CB1R (A). Synaptic GluA1 levels were measured in CB1R positive and negative synapses in control (n=48) and KD (n=48) (B). Data are presented as boxplots with whiskers from minimum to maximum value. Scale bar: 5 µm

Data information: Data are presented as boxplots with whiskers from 10 to 90 percent. *** $p \leq 0.001$ (Student's t-test).

In a parallel approach, hippocampal primary neurons were treated with the CB1R antagonist AM-251 for 48 h. Control cells and AM-251 treated cells were silenced with TTX for 1 h. For stimulation the TTX was washed out and the cells were kept with 50 µM bicuculline (BIC) and 2.5 mM 4-Aminopyridine (4-AP) for 30 min. Bicuculline is an inhibitor of GABA-receptors resulting in a reduction of inhibitory signaling; 4-AP inhibits voltage-activated K^+ channels, resulting in prolonged depolarization of neurons. Live cells were live stained with the surface GluA1 antibody during the last 15 min of treatment. They were then fixed and immunostained for Shank3 and CB1R (Figure 22A). The surface expression of GluA1 was analyzed in CB1R positive and negative synapses. Stimulation with BIC/4-AP resulted in an overall increase in synaptic surface expression of GluA1. In CB1R negative synapses treatment with the CB1R inhibitor AM-251 treatment had no effect on the surface expression of GluA1 (Figure 22C). In non-stimulated cells there was no significant difference between CB1R positive and negative synapses, while treatment with AM-251 prior to stimulation resulted in an additional increase in surface expression of GluA1 (Figure 22B).

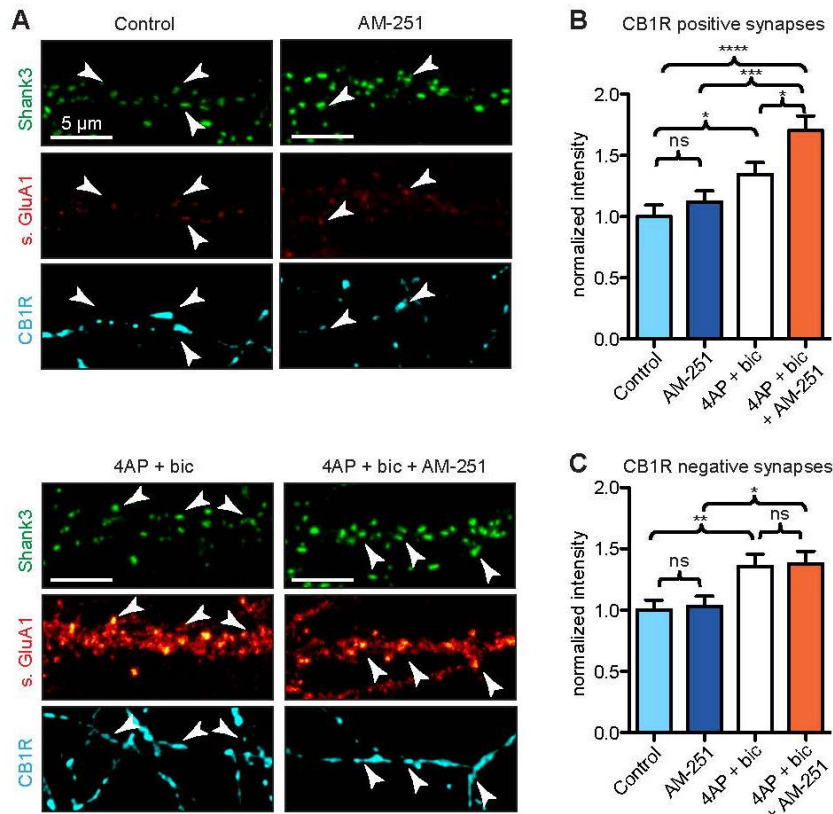


Figure 22. CB1R-dependent regulation of surface GluA1

A: Cells DIV15 surface stained for GluA1 (Control (n=32); 10 μ M AM-251 (48 h) n=25); 50 μ M Bicuculline, 2 mM 4-AP (30 min) (n=32), 50 μ M Bicuculline, 2mM 4-AP (30 min) and 10 μ M AM-251 (48 h) (n=29) (C, D). Cells were stained post fixation for CB1R and Shank3. Scale bar: 5 μ m

B-C: Surface in GluA1 intensity was quantified in synapses positive for Shank3 and CB1R (B) and synapses positive for Shank3 and negative for CB1R (C).

Data information: Data are presented as mean + SEM. * $p \leq 0.05$ (Student's t-test).

We now aimed to analyze the effect of EE on the expression of GluA1 in CB1R positive and negative synapses. Cryosections of EE and SE animals were stained with antibodies directed against GluA1, Shank3 and CB1R (Figure 23A). The intensity of GluA1 was analyzed in Shank3 positive synapses, positive or negative for CB1R (Figure 23B-D). In EE animals, the amount of GluA1 was slightly increased in CB1R positive synapses, in strata oriens and radiatum. In SE animals no difference between CB1R positive and negative synapses was detected in the strata radiatum and oriens. In stratum lacunosum moleculare there were no differences in GluA1 levels between CB1R positive and negative synapses in both EE and SE (Figure 23D).

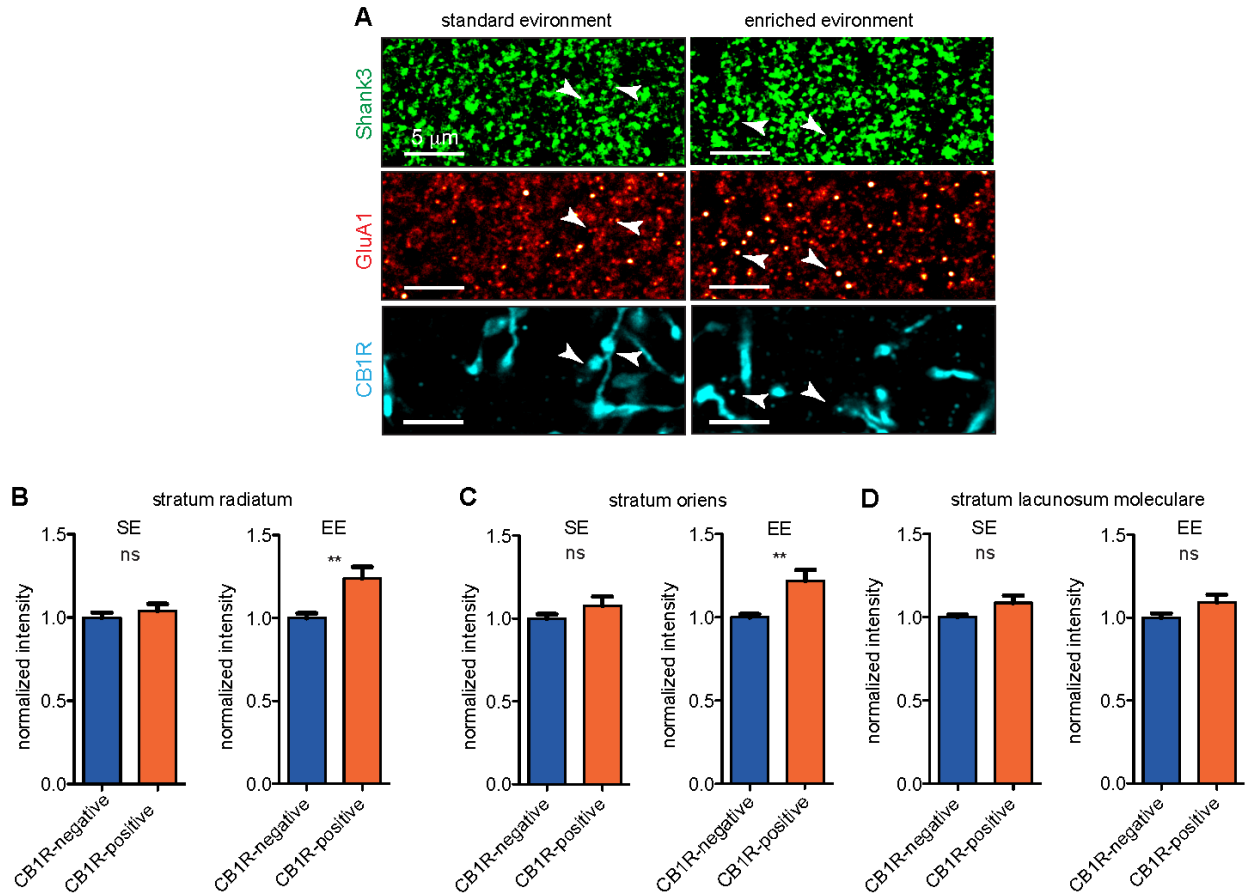


Figure 23. GluA1 levels in CB1R positive and negative synapses of EE and SE mice

A: Cryosections from EE and SE animals were stained for Shank3, GluA1 and CB1R. Scale bar 5 μm : arrowheads show CB1R positive synapses

B-D: The intensity of the GluA1 staining was quantified in CB1R positive and CB1R negative synapses of the stratum radiatum (B), the stratum oriens (C) and stratum lacunosum moleculare (D).

Data information: data are presented as mean + SEM. ** $p \leq 0.01$ (Student's t-test).

ABHD6 and FAAH are both transmembrane proteins that reach the cell surface through the secretory pathway. The reduction of Synaptopodin-positive ER structures in spines, following blockage of presynaptic CB1R, point to an interesting scenario. It might be that the retraction of the ER results in reduced spine localization of ABHD6 or alternatively ABHD6 might traffic retrogradely to a Golgi compartment, a common pathway of membrane proteins for recycling and potentially re-glycosylation. At present only a role of ABHD6 in the ER for assembly of AMPA-receptors has been described (Schwenk et al., 2019) and not much is known about secretory trafficking of the protein. To provide the basis for future studies and to better understand ABHD6 trafficking in dendrites, pGolt-mCherry was expressed to label Golgi Satellites (GS) and the cells were stained for ABHD6. Around 50% of GS contained ABHD6 (Figure 24) suggesting that ABHD6 is transported through dendritic Golgi compartments and might be glycosylated there.

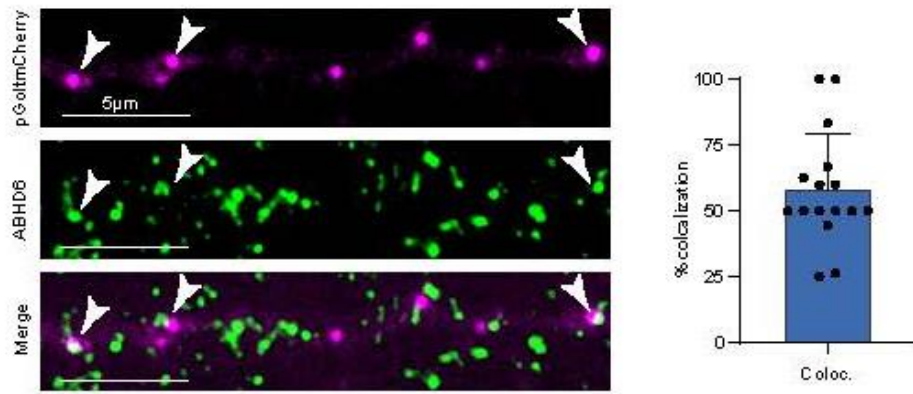


Figure 24. Colocalization of ABHD6 with GS

Colocalization of ABHD6 with pGolt-mCherry was analyzed in primary hippocampal neurons DIV 16

3.2 A functional characterization of Golgi satellites

The second part of this thesis is concerned with the trafficking and posttranslational modification of proteins in neuronal dendrites, it aims to better understand the pathway that synaptic proteins have to undergo, to function correctly. Transmembrane proteins such as synaptic receptors and cell adhesion molecules have to undergo a complex series of quality controls and posttranslational modifications. One such modification is the addition of sugars in the ER and the Golgi known as glycosylation. Complex glycosylations typically take place in the somatic Golgi Apparatus (GA), but neurons with their highly arborized cytoarchitecture additionally contain Golgi Satellites (GS) throughout their dendritic arbor, as shown by Mikhaylova et al. 2016 in hippocampal primary neurons. This thesis aims to further characterize distribution and function of GS in the mouse brain.

3.2.1 A GoltmCherry expressing mouse line, to label GS *in vivo*

To ease further studies and to label Golgi satellites within the brain a transgenic mouse line was generated by pronucleus injection. The line expresses the GoltmCherry probe under the neuron-specific Synapsin promoter (Figure 31A). Using a transgenic line has multiple advantages compared to vector-based overexpression. Transfection or transduction through viral infection is not necessary and thus results are more reproducible; it allows studying the probe in every cell at more evenly distributed expression levels, since all cells of one genotype contain the same copy number. Most importantly it allows studying the transgene *in vivo* without a need for surgery and AAV injection. Pronuclear injection results in random integration in the genome. Therefore, multiple founders were generated of which one passed on the construct and expressed the probe at a sufficient level for detection. The transgene was passed on in a Mendelian ratio, with ~50% of the offspring inheriting the allele from a heterozygous parent. The weight of the animals at birth was unaltered compared to the wildtype (WT). The ratio of male to female was 1 to 1 over all matings. Transgenic animals gained weight at similar rates as their WT littermates. The transgenic animals showed no obvious physical abnormalities nor increased mortality, accordingly the line was registered as unburdened (unbelastet), as defined by German animal welfare legislation. It is even possible to maintain the line with homozygous genotype without any problems. Genotyping of the mice was performed by PCR (Figure 30B) with primers specific for the integrated probe. Integration into the mouse genome was characterized by Southern blot (Figure 31C). The expression was controlled on protein level by immunoblotting with an antibody specific for RFP and mCherry in brain lysates from hippocampi and cerebella. The *cis*-Golgi-marker GM130 was used as a loading control. The mGolt probe was detected at the expected size of 35 kDa and no signal was detected in the WT controls (Figure 31D). To assure that the expression of the mGolt transgene did not affect the structure of the somatic Golgi, EM-images of the GA were acquired in transgenic animals and WT controls. Expression of the mGolt probe did not result in obvious changes of the ultrastructure of the GA (Figure 30E).

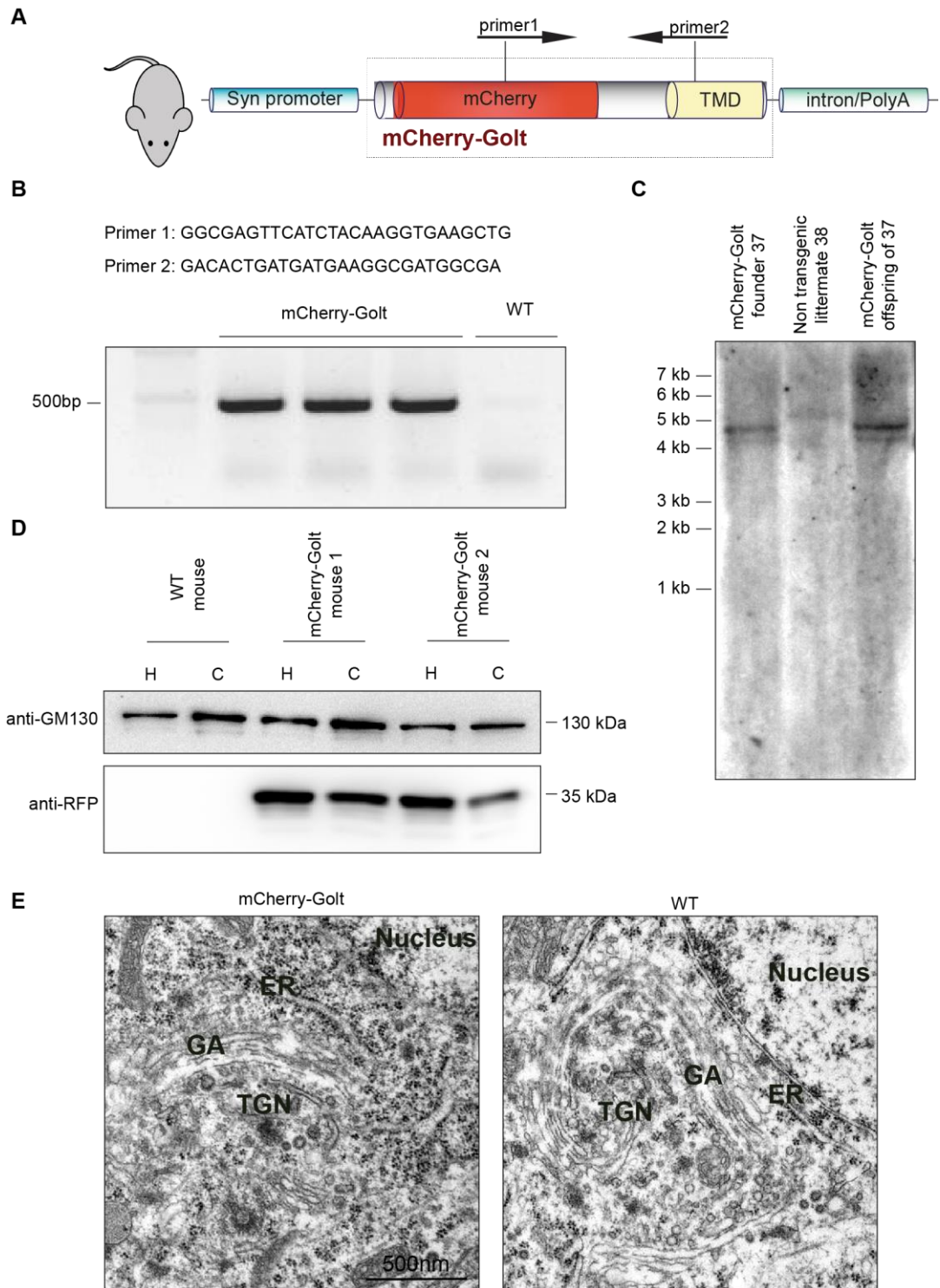


Figure 25. Generation of the mGolt mouse line

- A:** The mGolt mouse line was generated by random integration of the depicted construct.
B: The DNA was extracted from tail tips. The genotyping was performed by PCR.
C: The integration of the sequence into the genome was confirmed by Southern blot.
D: The expression of the protein was confirmed by WB. GM130 was used as a loading control.
E: EM images from mGolt animals and WT controls show no major differences. Scale bar 500 nm

The question whether glycosylation is taking place in GS was addressed further by staining with lectins (Figure 26). Before entering the Golgi, proteins are glycosylated in the ER. This short chain attachment of glycans is called core glycosylation. These core glycosylated

proteins then traffic through ERGIC to the GA where they accumulate and obtain further modifications. Additionally, it is possible for core glycosylated proteins to bypass the Golgi and to integrate into the membrane and recycle to the GA (Lodish 2013). To test if core glycosylated proteins also accumulated in GS, hippocampal primary neurons were transfected with pGolt-mCherry and stained for the core-glycan specific concanavalin A (ConA). ConA showed extensive colocalization with GS in the dendrites of transfected neurons (Figure 26A, B). Staining of cryosections from the transgenic mGolt line confirmed high colocalization of mGolt with ConA (Figure 26C, D). This indicates that core-glycosylated proteins in dendrites traffic through the GS. The two main forms of complex glycans are N- and O-glycans added to the corresponding termini of proteins. Labeling with the N-glycan marker wheat germ agglutinin (WGA) again showed extensive colocalization with GS (Figure 26A, B). Labeling with the O-glycosylation marker *Helix pomatia* lectin (HPL) resulted in a mixed pattern with an average colocalization of 60%. Individual neurons showed extensive colocalization of HPL with pGolt-mCherry, whereas others showed less than 50% colocalization, indicating that O-glycosylation does not occur in all GS at the same time. The specificity of lectin labeling was controlled in hippocampal primary culture. Cells were treated with tunicamycin, which inhibits the initiation of N-linked glycosylation. Tunicamycin treatment resulted in a dramatic reduction in ConA labeling (Figure 26E, F).

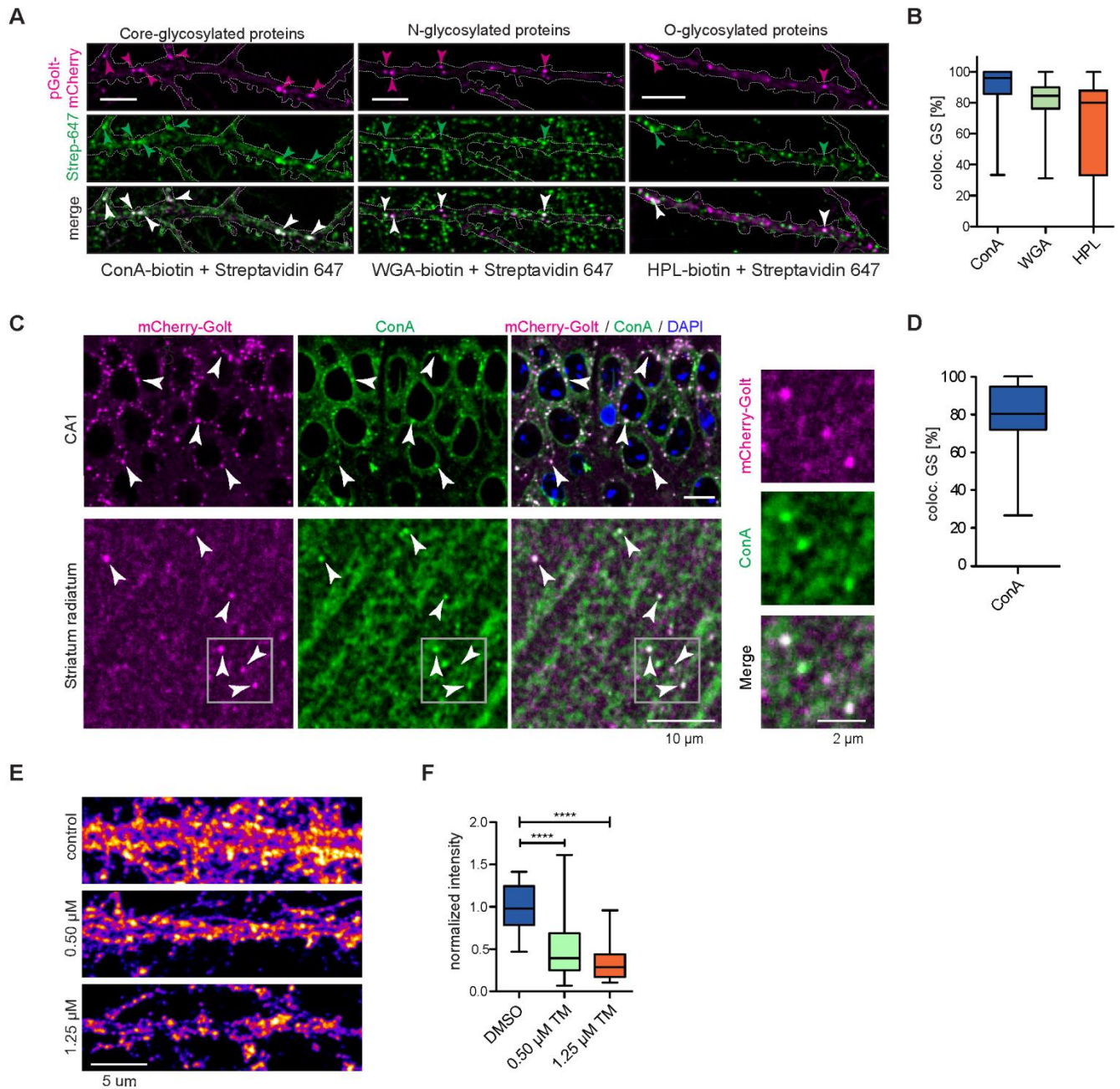


Figure 26. Lectin labeling shows co-localization with GS and evidence for glycosylation

- A:** Specific labeling of: core-glycosylated proteins with biotinylated ConA and Streptavidin647, N-glycosylated proteins with biotinylated WGA and Streptavidin647 and O-glycosylated proteins with biotinylated HPL and Streptavidin647. Scale bar: 5 μ m.
- B:** Quantification. Percentage of lectins (ConA, WGA, HPL) co-localizing with GS.
- C:** 4 cryosections from two male 10 week old mice, expressing mCherryGolt under the Synapsin promoter. Cryosections were stained for ConA and labeled with Alexa 647 bound to Streptavidin.
- D:** Quantification. Percentage of GS colocalizing with ConA (n = 2 animals, 4 sections).
- E:** Testing specificity of ConA after tunicamycin treatment for 3 days (0.5 μ M, 1.25 μ M) and DMSO control. Scale bar: 5 μ m.
- F:** Quantification of measured intensity. Statistics by one-way Anova (Bonferroni's multiple comparison test) **** < 0.0001 . Scale bar: 5 μ m
Data information: Data are presented as box plots with whiskers from min to max.

In the next set of experiments, the localization of the probe and the distribution of GS in the hippocampus was analyzed by IHC and EM. IHC of cryosections with the somato-dendritic neuronal marker MAP2 showed that all hippocampal neurons expressed the probe, the mGolt expression was absent from MAP2 negative cells (Figure 27E). Since there is an abundance of well-established Golgi markers for the somatic Golgi, the Golgi localization of the probe was first tested in the soma (Figure 27A). The sections were stained for the *cis*-Golgi marker GM130. Only minor colocalization was detected but the somatic mGolt was consistently localized in close proximity to *cis*-Golgi membranes. Staining with the TGN-marker Syntaxin 6 revealed extensive somatic colocalization with mCherry-Golt (Figure 27A). Sections from the mGolt mice were labeled with 3,3'-Diaminobenzidine (DAB) and EM images of the somatic Golgi were acquired (Figure 27B). In the soma the mGolt probe labels the *trans*-Golgi and the TGN.

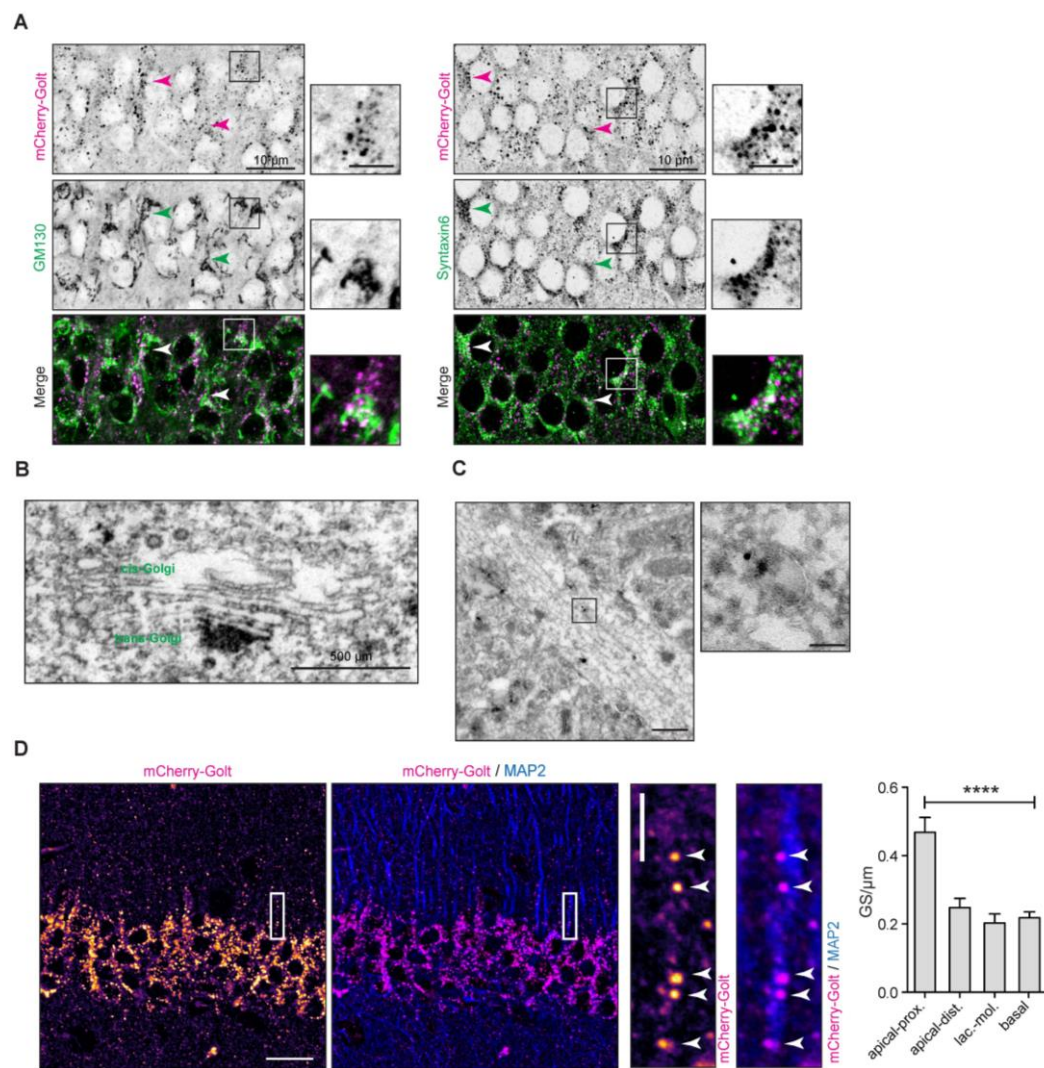


Figure 27. Characterization of the mGolt mouse line

- A:** mCherryGolt localizes with *cis*-Golgi marker GM130 and *trans*-Golgi marker Syntaxin 6 in 8 week old mice. Scale bar 5 μm.
B: DAB staining of mGolt at the somatic Golgi
C: Immunogold images of mCherryGolt-labeled structures in apical dendrites of the hippocampal CA1 region. Scale bars 500 and 100 nm.

D: GS are found in apical and basal dendrites of the hippocampal CA1 region, being most abundant in the proximal apical dendrite 10 to 50 μm from the soma (right panel). Scale bars 10 (left panel) and 5 μm (right panel).
Data information: Data are presented as mean + SEM. **** $p \leq 0.0001$ (Student's t-test).

To characterize the ultrastructure of GS, immunogold-EM was performed (Figure 33C). Ultrathin sections were labeled with a primary antibody against mCherry, which was in turn labeled by a secondary antibody coupled to a small gold particle. The gold particle appears as a black dot in the EM. GS were shown to be above 200 μm in size and shaped irregularly, with no perfectly round GS found (Figure 33C). This observation matches results obtained by STED imaging *in vitro* by Mikaylova et al. 2016. The distribution of GS was further analyzed in the dendritic arbor of CA1 pyramidal neurons of the dorsal hippocampus. In proximal apical dendrites of the stratum pyramidale one GS was found on average every 2 μm (Figure 33D). In basal dendrites of the stratum oriens in distal apical dendrites of the stratum radiatum and lacunosum moleculare one GS was found on average every 5 μm (Figure 33D).

3.2.2 What is the role of Calneuron 1 in the assembly, maintenance and function of GS?

GS are relatively small and exhibit high dynamics of vesicle trafficking. Thus, mechanisms must be in place for assembly and stabilization of this organelle. One possible mechanism for the stabilization of GS is membrane retention through Calneurons. Calneurons are tail-anchored proteins that interact with TRC40/Asn1 with their minimal Golgi-targeting sequence, which assists their membrane insertion (Hradsky et al., 2011). They are post-translationally inserted into the ER and then transported to the TGN where they regulate Golgi-to-plasma membrane trafficking through an interaction with phosphatidylinositol 4-OH kinase III β (PI-4K β), one of the key enzymes for production of phosphatidylinositol 4-phosphate at the TGN (Mikhaylova et al., 2009; Hradsky et al., 2011). Calneuron 1 and 2 inhibit PI-4K β profoundly at resting and low calcium levels, and negatively interfere with Golgi-to-plasma membrane trafficking. At high calcium levels this inhibition is released and PI-4K β is activated. Knockdown of both Calneuron 1 and 2 (panCalneuron KD) in early development from DIV 3 to 8 resulted in a reduction of dendritic arbor complexity (Figure 28A, B). Sholl analysis revealed that cells transfected with the panCalneuron KD construct developed the same number of primary dendrites, but showed reduced branching (Figure 28B). At a distance of 80 μm from the soma only the main dendrite was present and no branching of secondary or tertiary dendrites was observed. Staining for the *cis*-Golgi marker GM130 showed a reduction in the extension of the GA into the main dendrite, as well as a reduction in the percentage of cells with an extended Golgi (Figure 28C). Synapse development and maturation in hippocampal primary culture takes place after DIV 5 and is mostly finished around DIV14 (Frese et al., 2017). To analyze the effect of Calneuron loss on synaptic development the Calneuron KD construct was expressed during this critical phase of development. Transfection of the KD from DIV 9 to DIV14 had little effect on the density of synapses on primary dendrites in close proximity to the soma. However, the density of synapses was dramatically reduced on tertiary dendrites, complementary to results observed in the KD at early development (Figure 28G).

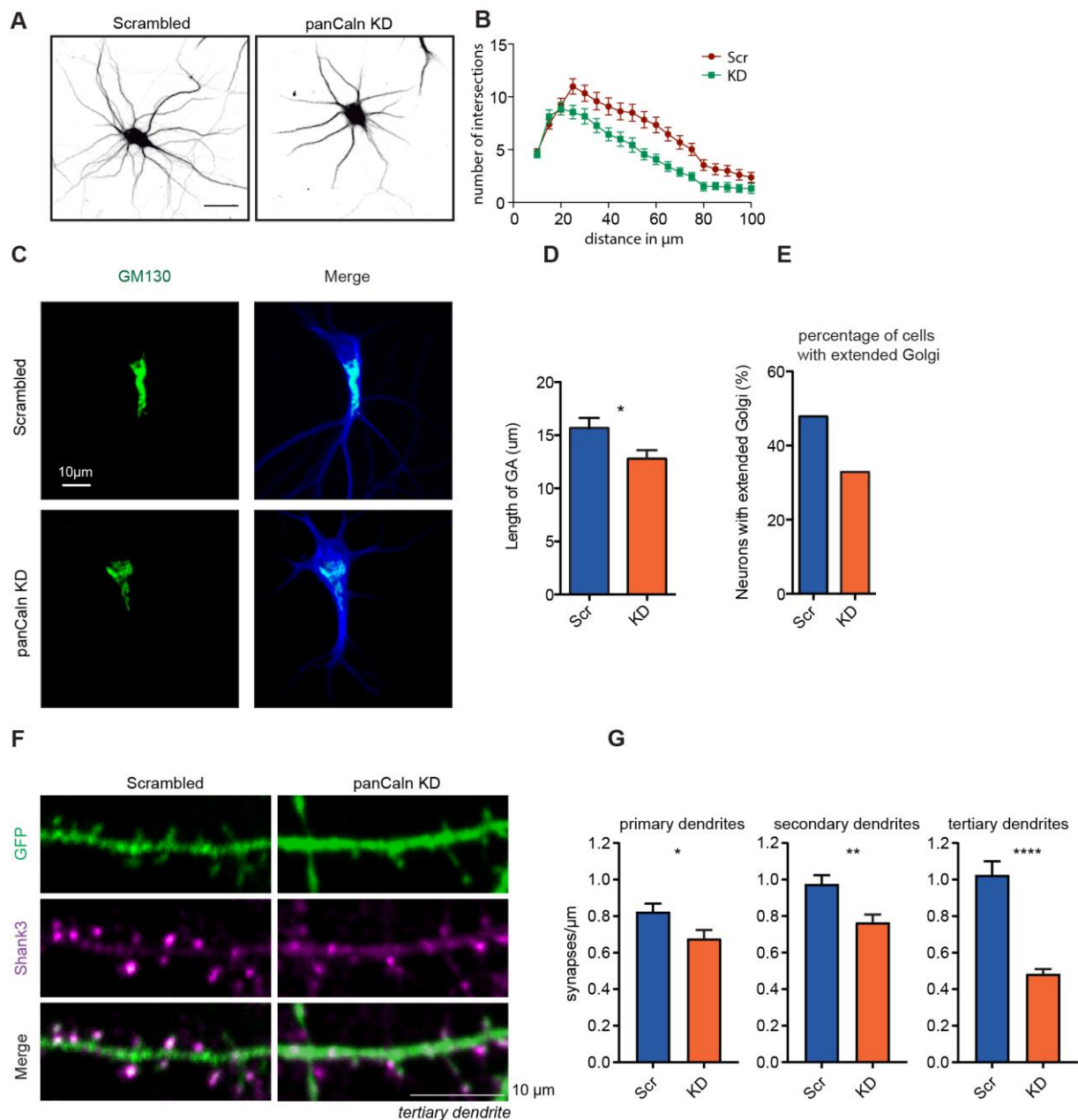


Figure 28. Characterization of the pan Calneuron KD

- A:** Hippocampal primary neurons were transfected with the pan Calneuron KD or a scrambled control construct at DIV 3 and fixed at DIV 8. Scale bar: 10 μm
- B:** The cells were stained for MAP2. The complexity of the dendritic arbor was controlled by Sholl analysis.
- C:** The cells were stained for GM130 (green) scale bar: 10 μm
- D:** The length of the GA was measured from the center of the nucleus to the furthest extend of the GM130 staining.
- E:** The number of cells with an extended Golgi was counted.
- F:** Hippocampal primary neurons were transfected with the pan Calneuron KD or a scrambled control construct at DIV 9 and fixed at DIV 14. Scale bar: 10 μm
- G:** The cells were stained with an antibody against the synaptic marker Shank3. The number of synapses was counted in primary, secondary and tertiary dendrites.
Data information: Data are presented as mean + SEM.

The Calneuron 1 KO line was generated by removing the second exon from the CALN1 gene using the CRISPR-Cas9 system. The CALN1-gene contains two possible start codons, the second ATG is located on the second exon, and removal of the second exon induces a frame shift for the first start codon, so that a complete KO is achieved. 7 founders were generated, of which one was selected for further breeding. Breeding of the line followed normal Mendelian distribution with heterozygous matings resulting in ~25% KO, 50% heterozygous and 25% WT offspring. The ratio of male to female was 1 to 1 over all matings. The KO animals had a normal birth weight of 1.1 grams and gained weight at the same rate as their WT littermates. The line showed no obvious physical abnormalities or increased mortality and was registered as unburdened (unbelastet), as defined by German animal welfare legislation. The KO was confirmed by PCR and Western blot (WB). The WB revealed the complete absence of both Calneuron 1 isoforms in both the hippocampus and the cerebellum (Figure 35A). The morphology of Calneuron 1 KO brains was analyzed by Nissl-staining. Calneuron 1 KO did not result in large scale anatomical abnormalities, in both the hippocampus and the cerebellum (Figure 35B).

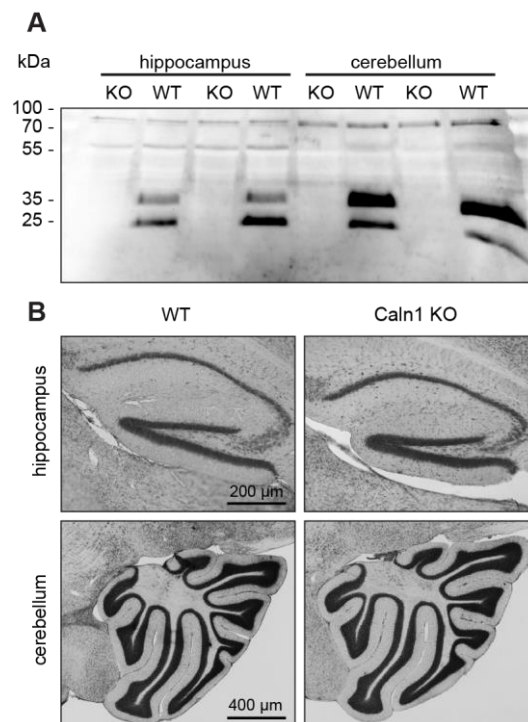


Figure 29. Characterization of the Caln1 KO

- A:** The Calneuron 1 KO was controlled by WB of lysates from hippocampus and cerebellum of two animals.
- B:** The overall morphology was controlled by Nissl staining performed on 40 μm cryosections of a KO mouse and its littermate.

While overall brain morphology was not altered, the morphology of the neuronal GA was affected by Calneuron 1 KO. Cryosections were prepared from two Calneuron 1 KO animals and two WT animals and labeled for the Golgi-marker Giantin (Figure 30A). The average length of the GA was slightly reduced in hippocampal pyramidal neurons in the hippocampal CA1 area (Figure 30B). Correspondingly, the percentage of cells with an extended GA was reduced in Calneuron 1 KO (Figure 30C). To allow for a more detailed analysis of the Golgi

morphology hippocampal primary neurons were prepared from Calneuron 1 KO pups (P0). At DIV 14 cells were immunolabeled for the *cis*-Golgi marker GM130 and the *trans*-Golgi marker Syntaxin 6 (Figure 30D). The GA in pyramidal cells is typically pyramid-shaped with an extension of varying length into the main dendrite. An extension of the GA into the apical dendrite typical for pyramidal neurons was found in 80% of WT, but only 20% of KO neurons (Figure 30F). The length of the GA was reduced and it was organized closer to the nucleus and adapted a compact round shape. The size of the *cis*- and the *trans*-Golgi was slightly reduced in the KO (Figure 30G, H).

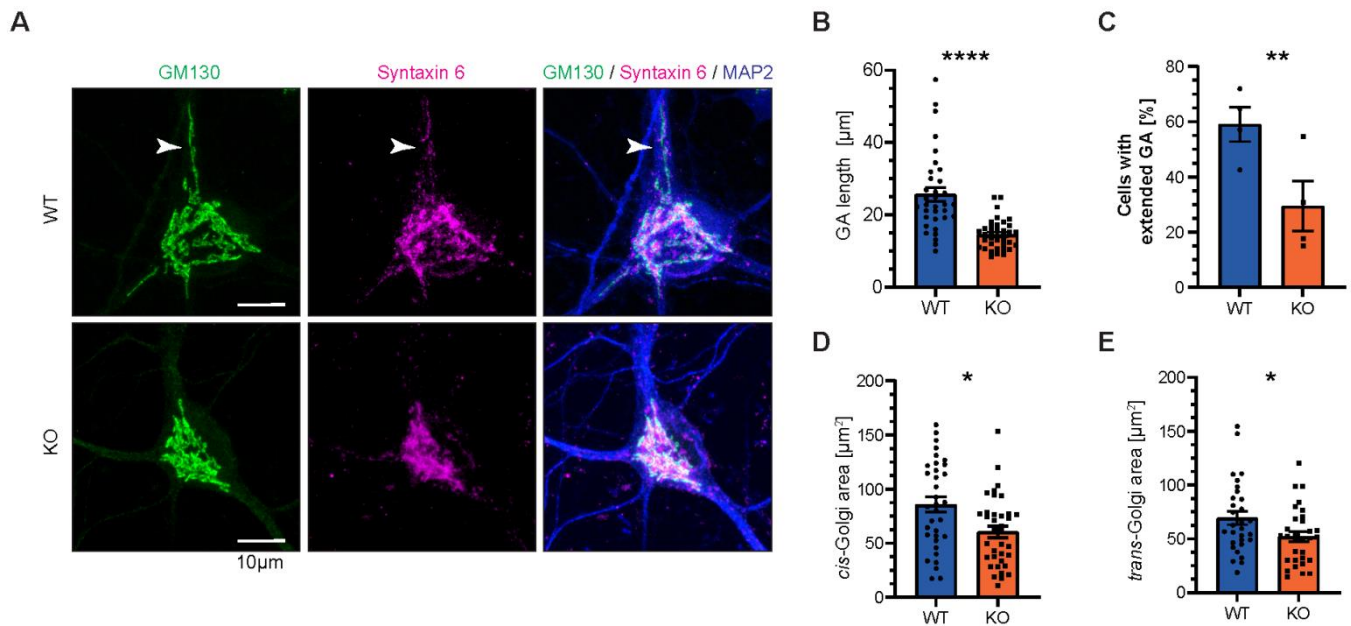


Figure 30. Influence of the Caln1KO on the somatic Golgi

A-E: Hippocampal primary cultures were prepared from Calneuron 1 KO mice and WT littermates at P0 or P1. The cells were fixed at DIV 14 or 15 and stained with antibodies against GM130 (green), Syntaxin 6 (magenta) and MAP2 (blue). The length of the GA was measured from the center of the nucleus to the furthest extend of the GM130 staining (B). Scale bar: 10 μm

C: The percentage of cells with GM130 staining extending into one or more dendrites was counted.

D, E: The area of the total area of the *cis*-Golgi was measured in the GM130 staining (D). The area of the *trans*-Golgi was measured in the Syntaxin 6 staining (E).

Data information: Data are presented as mean \pm SEM.

The mGolt line was crossed with the Calneuron 1 KO, generating a Calneuron 1 KO with transgenic expression of mGolt. This allowed analyzing the effect of Calneuron 1 deficiency on the generation and stability of GS. The frequency of GS was reduced in main dendrites of stratum oriens, stratum radiatum and stratum lacunosum moleculare (Figure 31A, B). This effect was most pronounced in the most distal dendrites localized to the stratum lacunosum moleculare.

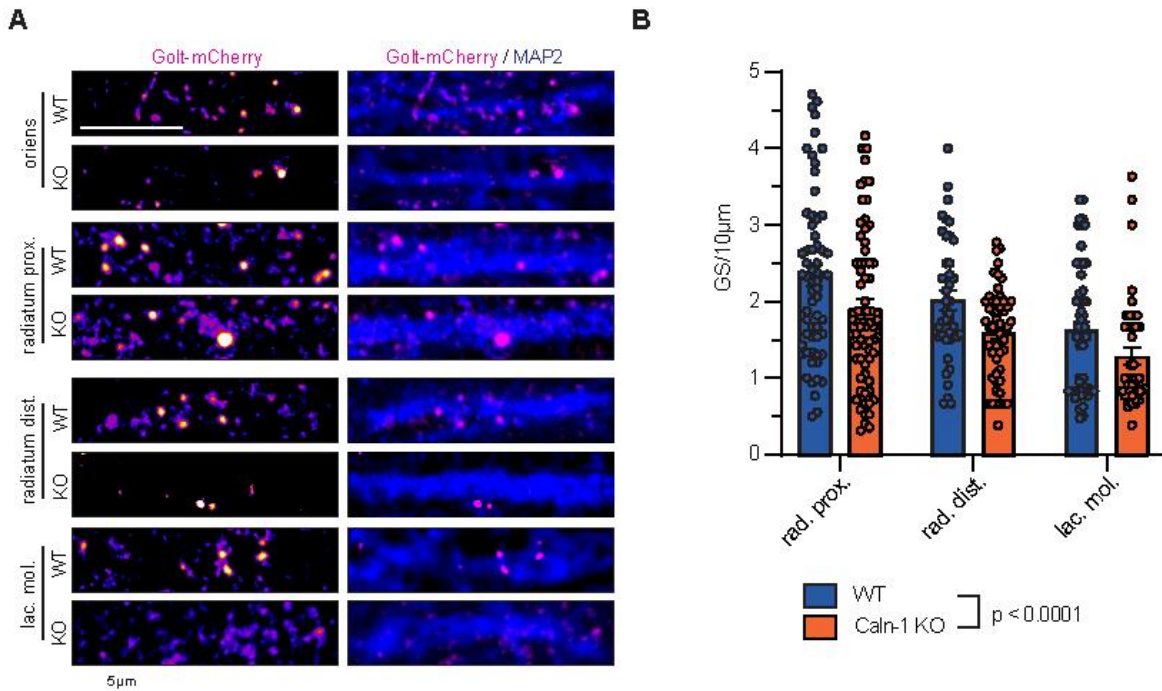


Figure 31. Loss of Calneuron 1 leads to reduced number of GS.

- A:** Cryosections from Calneuron 1 KO animals and WT littermates both expressing mGolt were stained for mGolt and MAP2. Scale bar: 5 μ m
- B:** The number of GS was counted in proximal and distal dendrites of the stratum radiatum and the lacunosum moleculare of the CA1 region. $n > 42$ dendrites from 2 litter pairs. Statistics by two-way ANOVA.
- The data presented in this figure was analyzed with support from Jakob Lormann

3.2.3 Polysialylation of NCAM in GS

Polysialylation of NCAM is a crucial step in both LTD and LTP. It was previously shown that a subset of GS contains polysialylated NCAM, this result was confirmed *in vivo* by immunostainings. This raises the question if NCAM is transported through GS to be polysialylated during plasticity induction. To investigate this idea, three independent systems were used. The trafficking of NCAM immediately following ER exit was studied using the FK506 binding protein (FKBP) system. Live imaging of primary hippocampal neurons showed that NCAM is transported to recycling endosomes following ER exit (Figure 32).

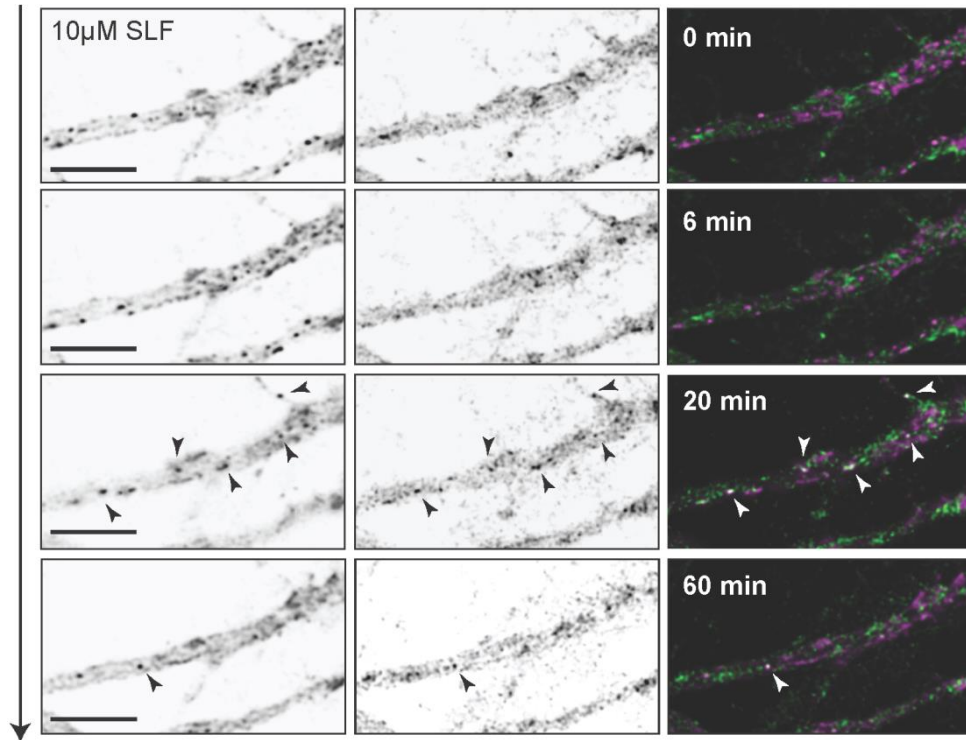


Figure 32. ER-release of NCAM using the FKBP system

Time lapse of FM-NCAM and the recycling endosome marker Tfr1. At T0 10 μ M SLF was added to the medium. Scale bar: 5 μ m

As an alternative method the RUSH system was implemented: The RUSH system consists of two parts, GFP-SBP-HA-NCAM and the hook fused to Streptavidin in the ER. Streptavidin was retained in the ER by an ER localizing STIM1 (Stromal interaction molecule 1) transmembrane domain and the ER retention motif KDEL. NCAM was bound to the hook by a Streptavidin binding protein. The binding was eluted by adding 40 μ M biotin. The construct was first tested in HEK cells by co-expressing the hook, NCAM-RUSH and pGolt-mCherry (Figure 33A). The addition of biotin resulted in a rapid release of NCAM from the ER into the GA. Following verification in HEK cells, the ER release was tested in mature hippocampal neurons. To measure the speed of NCAM release to the cells surface the cells were live stained with an antibody against the Human influenza hemagglutinin (HA)-tag during release and fixed at different time points. The intensity of the surface staining increased rapidly in the time window from 20 min to 2 h after release (Figure 33C). Half maximal surface intensity was reached after 1 hour. The maximum surface intensity was reached 2 h after release, the surface intensity then remained stable at the maximum level (Figure 39C). The RUSH system was co-expressed with pGolt-mCherry. In the unreleased state, NCAM was trapped in the ER and showed no colocalization with pGolt-mCherry in the dendrite (Figure 33D, E). After 1 h more than 60% of GS contained NCAM. Polysialylation (PSA) of NCAM takes place in the Golgi and is crucial for the formation of both LTP and LTD. GS have been shown to contain PSA-NCAM suggesting that the reaction might take place there. Polysialylation is carried out by three Sialyltransferases that localize to the Golgi. The dominant enzyme catalyzing the reaction in young neurons is ST8SiaII. A truncated version of ST8SiaII lacking the enzymatically active domain was overexpressed together with pGolt-mCherry in hippocampal

primary neurons. AT DIV 16 80% of GS contained ST8SiaII, further supporting the hypothesis that polysialylation can take place in GS.

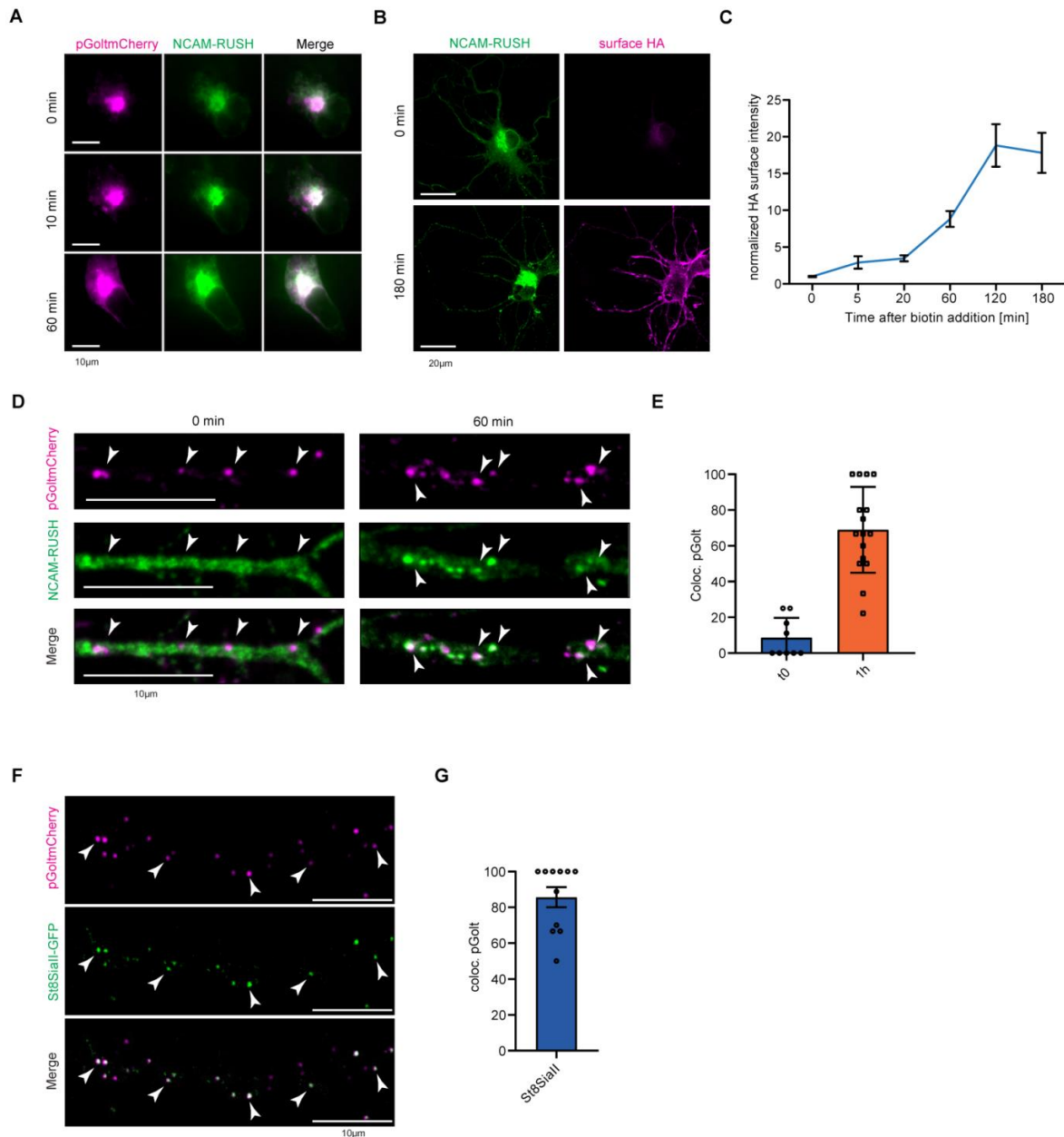


Figure 33. Trafficking of NCAM through GS

- A:** HEK cells expressing pGolt-mCherry, NCAM-SBP-GFP-HA hooked to the ER by streptavidin KDEL were treated with 40 μ M biotin and live imaged for 1 h.
- B:** Primary hippocampal neurons DIV 14 expressing NCAM-SBP-GFP-HA hooked to the ER by streptavidin KDEL were treated with 40 μ M biotin at T0. Surface labeling was conducted for 15 min with an HA antibody.
- C:** Surface intensity was normalized to the GFP signal, to correct for varying expression levels. 0 min: n=15; 5 min: n=17 20 min: n=18 60 min: n=18 120 min: n=26 180 min: n=27.
- D:** Primary neurons expressing NCAM-SBP-GFP-HA hooked to the ER by streptavidin. KDEL and pGolt-mCherry were treated with 40 μ M biotin for 1 h.
- E:** The percentage of GS positive for NCAM was quantified (n=12)
- F:** Primary hippocampal neurons transfected with St8SiaII-GFP and pGolt-mCherry.
- G:** Colocalization of pGolt-mCherry with St8SiaII.
Data information: Data are presented as mean +/- SEM.

To analyze the effect of Calneuron 1 deficiency and the subsequent loss of GS especially in distal dendrites, cryosections from Calneuron 1 KO animals and WT controls were immunolabeled for PSA-NCAM (Figure 34A). The level of PSA-NCAM was measured in proximal and distal dendrites of the stratum radiatum, as well as the stratum lacunosum moleculare of the hippocampal CA1 region (Figure 34B). The PSA-NCAM levels were not changed in proximal regions but were reduced by 50% in distal regions. To control for a possible change in total NCAM expression, not related to Golgi-dependent polysialylation, following KO of Calneuron 1, cryosections were stained with an antibody against unpolysialylated NCAM (Figure 34C). Levels of unpolysialylated NCAM were not significantly changed in any of the strata suggesting that the expression of NCAM was not changed and that the reduction in PSA-NCAM is a result of a reduction in polysialylation.

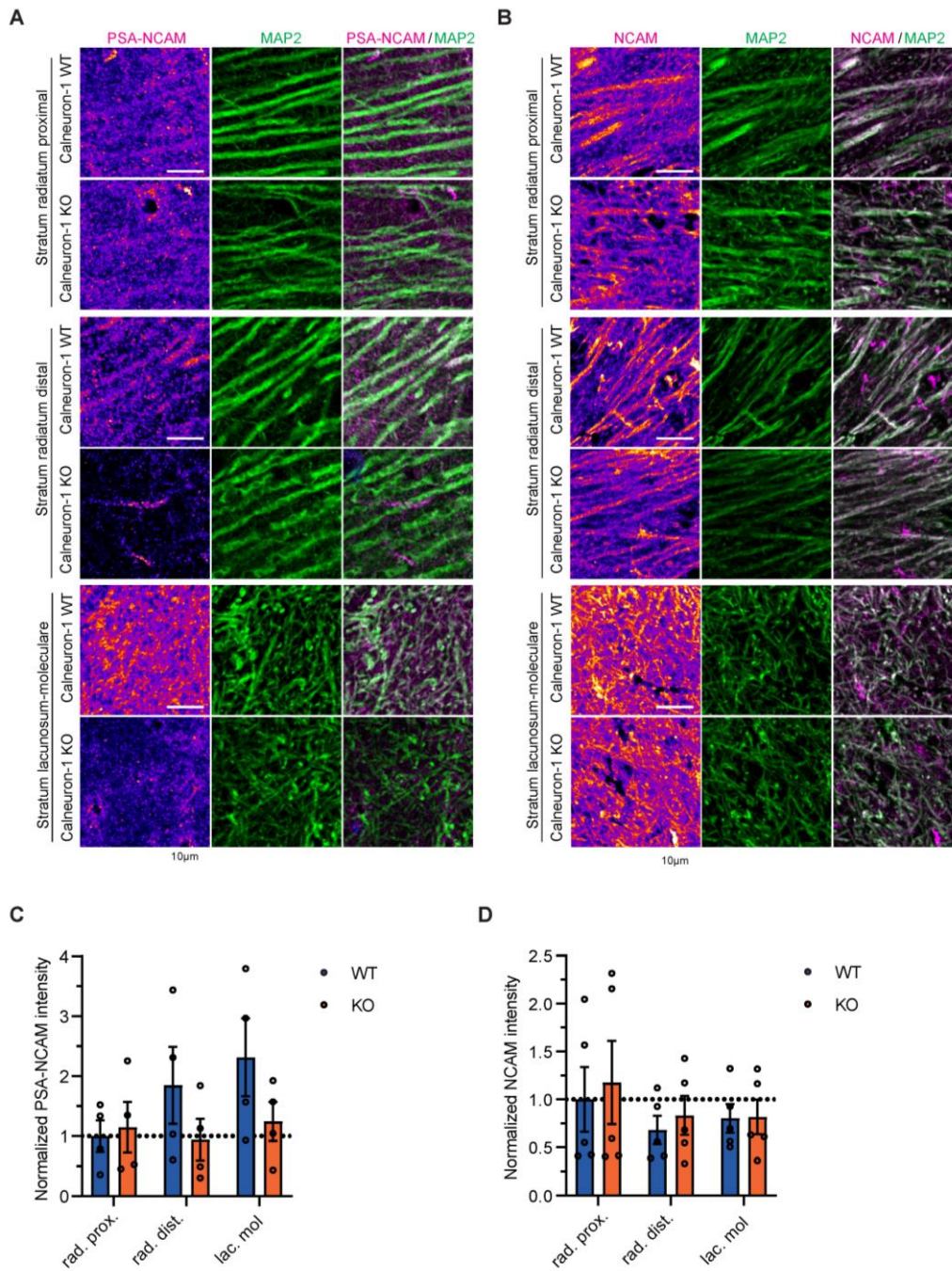


Figure 34. Loss of Calneuron 1 leads to reduced polysialylation of NCAM.

A: Cryosections from Calneuron 1 KO animals and WT littermates were stained for MAP2 (green) and PSA-NCAM (magenta). Scale bar = 10 µm

B: Cryosections from Calneuron 1 KO animals and WT littermates were stained for MAP2 (green) and NCAM (magenta). Scale bar = 10 µm

C: Quantification of A. Levels of PSA-NCAM were measured in the dendrites of the stratum radiatum and the stratum lacunosum moleculare. n > 16 regions from 3 litter pairs. Statistics by two-way ANOVA: genotype: p=0.0050; stratum x genotype: p= 0.0301

D: Quantification of A. Levels of total NCAM were measured in the dendrites of the stratum radiatum and the stratum lacunosum moleculare. n > 16 regions from 3 litter pairs. Statistics by two-way ANOVA: genotype: p=0.1103; stratum x genotype: p= 0.5786
The data presented in this figure was analyzed with support from Jakob Lormann

4 Discussion

In this study we tested a novel multiomics approach on synaptosomes prepared from mice raised in enriched environment (EE). We show that retrograde endocannabinoid signaling (ECS) was altered on both lipid and protein levels following EE as compared to standard environment (SE) control animals (Figure 6). The synaptic levels of the main CB1R agonist in the hippocampus 2-AG were significantly reduced following EE, while the levels of the enzyme FAAH, which degrades 2-AG and AEA, were increased. The levels of a second degradatory enzyme of 2-AG, ABHD6 were reduced following EE. Since ABHD6 has a second function, i.e. as an auxiliary subunit of AMPARs, this resulted in a change in AMPAR surface expression specifically at CB1R positive synapses. The surface delivery and posttranslational modification of synaptic receptors, such as AMPARs and cell adhesion molecules like NCAM, is crucial for synaptic function. To understand this process in more detail we studied local Golgi-transport in hippocampal dendrites. By generating a mouse line expressing a Golgi satellite (GS) marker we could demonstrate the presence of GS *in vivo*. We could further show that both N- and O-glycosylation occur at GS. Characterization of a Calneuron 1 KO line which was also generated during this thesis showed that Calneuron 1 plays an important role in the maintenance and function of GS.

4.1 Synaptoneurolipidomics is a novel research area and multiomics is well suited to generate novel hypothesis on synaptic function in plasticity

The brain is an exceptionally lipid-rich organ with a presumably complex lipid composition. Neurolipidomics aims to understand the chemical diversity of lipids in its interplay with protein composition to reveal the basic dynamics of the neuronal lipidome and its metabolism. Lipids play a central role in several neuronal processes including membrane formation and fusion (Chernomordik and Kozlov, 2003; Puchkov and Haucke, 2013), myelin packing (Fledrich et al., 2018) and lipid mediated signal transmission (Piomelli et al., 2007; McCartney et al., 2014). The synaptic junction is the central building block of a chemical synapse. It mediates cell-cell contact and signal transduction. Compelling evidence suggests a specific role of lipids in synaptic neurotransmission where trace lipids, including phosphatidylinositol phosphates (PtdInsPs) and negatively charged phosphatidylserine (PtdSer) are essential at the plasma membrane for multiple steps of the synaptic vesicle cycle. In addition, lipids determine membrane shape; regulate ion channel activity (Li et al., 2015) and protein interactions (Caccin et al., 2015) and control endocytosis machinery as well as receptor activity (Kononenko and Haucke, 2015). Since most lipid mediators are direct or indirect products of polyunsaturated phospholipids, sufficient molar content of complex polyunsaturated lipids must be located at synaptic junctions to guarantee lipid mediator formation and neurotransmitter release (Han, 2007). Finally, several lines of evidence suggest that the lipid composition of synapses might be dynamic (Jurado et al., 2010; Martin et al., 2014b). But up to now neither a quantitative lipid inventory nor a detailed proteome map of the lipid metabolism of the synaptic junction was available.

The existence of more than 40 different lipids known to modulate signaling and/or to influence membrane geometry in neurons, synapses, and synaptic vesicles (Dieterich and Kreutz, 2016) demanded for a systematic large-scale study of lipid abundance and functional regulation in neuronal subcompartments. Understanding the complexity of brain function and

plasticity requires a deep understanding of all molecular components of the synapse. While the main focus of most studies lies on the protein composition of neurons and their synapses, the plethora of functions carried out by lipids should not be sidelined. Dysregulation of lipid metabolism is a major component of common neurodegenerative diseases such as Alzheimer's and Parkinson's disease (Xu and Huang, 2006). Alterations in the processing of lipids is also at the core of some rare genetic conditions such as the salt and pepper syndrome, which is caused by a mutation in the sialyltransferase ST3Gal5 that is localized to somatic and dendritic Golgi-membranes and is responsible for the sialylation of membrane lipids (Boccutto et al., 2014).

Here, we employed in collaboration with researchers of the Leibniz Institute for Analytical Sciences in Dortmund a multiomics extraction strategy (Coman et al., 2016) and quantitative MS to determine the general molecular composition of the rodent forebrain synaptic junctions. Furthermore, we executed the SIMPLEX workflow on mouse hippocampal synaptic junctions to monitor alterations of lipid metabolism induced by an EE (Coman et al., 2016). Based on SIMPLEX we then generated and initially tested a hypothesis on a molecular and cellular mechanism that might contribute to changes in synaptic plasticity elicited by environmental stimuli. My own contribution was limited to the latter part, I was not involved in the Simplex workflow as such, only in generating tissue specimens as well as testing and generating hypotheses based on this workflow.

In this study we provide a comprehensive quantitative inventory of the rodent synaptic junction at both levels. 416 lipid species covering a concentration range over seven orders of magnitude were quantified, and in parallel an assessment of over 5428 proteins of the proteome was conducted. This analysis uniquely permits a systematic assessment of the lipid metabolic network in synaptic junctions. Phospholipids and cholesterol constitute 90% of the membrane composition whereas SLs together with cholesterol were identified as critical elements defining the composition of synaptic junctions. Altogether, 527 molecules were identified in lipid metabolic networks comprising of glycerol-, glycerophospho-, sphingo-, mediator- and endocannabinoid-lipid metabolism.

To underscore the heuristic value of SIMPLEX to generate novel hypotheses we compared the lipidome and proteome of synaptic junctions of mice raised in EE or SE. We chose environmental stimulation to test whether our approach might be suitable to uncover signaling pathways that are altered by physiological interventions relevant for learning and memory. It should be stressed that we only followed up on one hypothesis and that other interesting and testable hypotheses might be delineated from the data set (accessible under PXD017997, MTBLS1531). Thus, evaluation of the data under different aspects of altered protein interactions in other networks might yield further insights. For instance, the levels of high abundant short chain ceramides such as Cer 18:0;2/16:0, Cer 18:0;2/18:0 and their corresponding long chain base 18:1 and 18:2 derivatives are increased dramatically in synaptic junctions. At this point, we can only speculate about their impact but an increase of abundant ceramide species was shown to enlarge the diameters of ceramide rich platforms (CRP) (Burgert et al., 2017) and combined with a decreased length of these ceramides this could change the solubility of proteins in such domains (Bock and Gulbins, 2003) and thus influence partitioning of proteins and signaling at the junction.

Surprisingly, we also observed a cholesterol phospholipid ratio shift to 1:4, a shift that has the potential to increase membrane fluidity and lateral pressure. Membrane fluidity is strongly influenced by cholesterol which is impeding acyl chain packing (Laude and Prior, 2012; Goñi, 2014) due to its inflexibility and therefore directly increases membrane rigidity (Laude and Prior, 2012). These physical characteristics are shaping the underlying basis for curvature, thickness, and tension that influence cell signaling and microdomain formation (Sohn et al., 2018). Therefore, it is no surprise that higher cholesterol level e.g. induced by postsynaptic trafficking defects leads to an impaired long-term plasticity (LTP) with cognitive deficits (Mitroi et al., 2019), whereas a reduced cholesterol level can lead to a mobilization of AMPARs (Brachet et al., 2015). It is tempting to speculate that this will ease lateral diffusion and exchange of transmembrane proteins.

4.2 ECS is altered in mice exposed to an EE

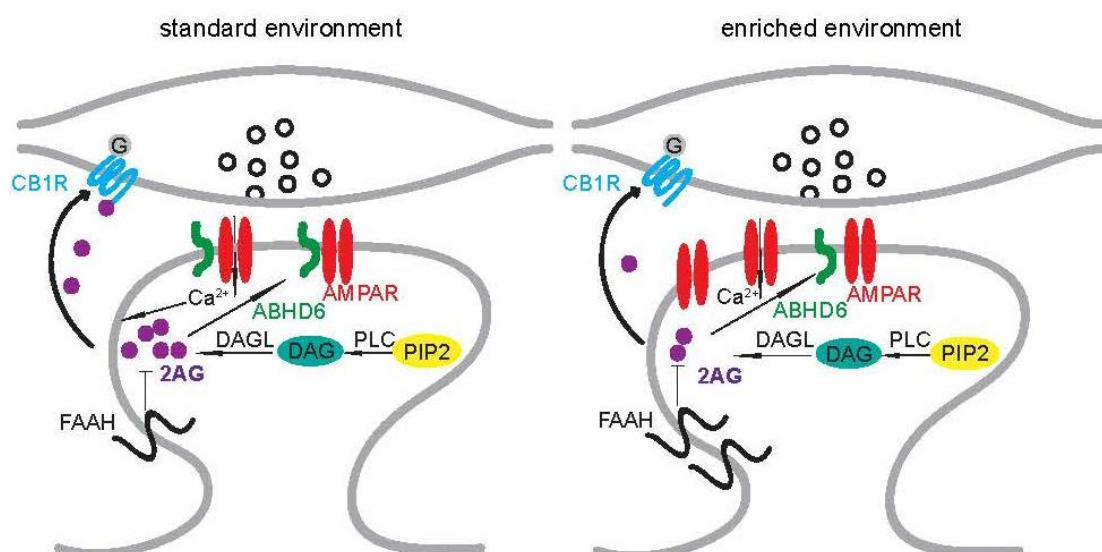
Based on alterations in the synaptic lipidome and proteome we identified ECS to be altered by EE. ECS has previously not been linked to the effects of EE on hippocampal function. I here propose a mechanism by which alterations in the postsynaptic association of ABHD6 and FAAH interact with lowered levels of 2-AG to facilitate an ECS-sensitive form of TBS-LTP at a subset of synapses (Cartoon 8). Thus, this approach revealed that in mice exposed to EE reduced endocannabinoid synthesis and signaling is linked to increased surface expression of AMPAR in a subset of CB1R-positive synapses (Figure 23, 24). This mechanism in turn regulates synaptic strength in an input-specific manner since only 30% of all excitatory synapses in pyramidal neurons of the CA1 region express presynaptic CB1R (Fig. 29). Moreover, altered ECS in response to EE is restricted to Schaffer collaterals and absent in the stratum lacunosum moleculare (Figure 14, 23). At present it is unclear what could be the basis of this input specificity. An intriguing possibility concerns the presence of ER and a spine apparatus in spines (Figure 18). I found that this presence requires CB1R signaling. This has not been previously reported and suggests a coupling of a presynaptic signaling event with the anchoring of ER membrane in spine synapses. The spine apparatus is found in spines of all layers of the hippocampal CA1 region. The highest percentage of spines containing a spine apparatus is found in the stratum lacunosum moleculare, it would be interesting to see if these regulation of spine apparatus formation is different between the hippocampal layers (Deller et al., 2000, 2003, 2007), since different signaling mechanisms might be in place in the different strata of the hippocampus. ABHD6 is clearly resident in the ER of spines and retraction of the ER might underlie its retraction from spines (Figure 19). Therefore, future investigations should focus on the effect of EE on the presence of spinous ER in pyramidal neurons of the CA1 region of the hippocampus.

It is also not known how exactly lower postsynaptic 2-AG levels negatively influence the postsynaptic localization of ABHD6 and why in mechanistic terms this positively affects surface expression of AMPA receptors (Figures 21, 22, 23). In the scenario outlined above it is difficult to isolate the initial trigger for the observed changes, but it might be that generally elevated synaptic activity following EE results in elevated postsynaptic FAAH levels as well as FAAH activity. Although FAAH has a clearly dominant role in catabolism of anandamide, which is much lower abundant in the hippocampus than 2-AG (Figure 10) (Guggenhuber et al., 2016), it is also enzymatically active in the degradation of 2-AG (Goparaju et al., 1998). Lower 2-AG levels will then reduce CB1R signaling and a reduction of CB1R signaling then

concomitantly reduces the postsynaptic expression of ABHD6. Moreover, presynaptic CB1R signaling is positively coupled to the postsynaptic production of 2-AG and this positive feedback loop will be also interrupted. Alternatively, the activity of DAGL might be downregulated in response to EE. The latter possibility can be easily tested in future research. It is important to note that MAGL is most likely not involved given the presynaptic localization of this enzyme in presynapses that I could confirm with immunocytochemical staining. MAGL is the principal enzyme in the degradation of 2-AG but its protein levels were not altered after EE. A further control that is currently lacking would be to determine MAGL enzyme active in synaptosomes of mice subjected to EE.

Taken together, this scenario provides a plausible explanation how ECS is linked to excitatory signaling at a subset of synapses in EE, and this link, in turn, might explain why in contrast to home-caged controls a weak θ -burst protocol in EE mice is under negative control of CB1R signaling. In the latter case ABHD6 will likely relocate to CB1R positive synapses, which then should result in reduced surface expression of GluA1. Of note, since these changes will only affect a very limited number of synapses of the Schaffer collateral pathway, this further underscores the sensitivity of SIMPLEX to detect even subtle pathway alterations. It is quite likely that reduced depolarization-induced suppression of inhibition (DSI) and excitation (DSE) (Katona et al., 2006) are part of this scenario and that highly localized changes in excitation/inhibition balance might occur due to changes in synaptic strength in CB1R positive synapses. Since the major aim was to showcase that testable hypothesis can be derived from SIMPLEX analysis further analysis is at this stage outside of the scope of this thesis. Nonetheless, although open questions remain the experimental data point to a plausible scenario how EE might impact synaptic plasticity at a subset of CB1R-positive excitatory synapses (Cartoon 8).

In summary, in this study we provided the first comprehensive lipid inventory of synaptic junctions. In addition, we have introduced the SIMPLEX workflow that has potential to decipher interactions between synaptic lipid and protein composition and signaling. Collectively, this approach should pave the way for a deeper appreciation of lipid function and signaling in synaptic processes.



Cartoon 8. Schematic of molecular dynamics in CB1R positive excitatory synapses in SE as compared to EE.

A subset of excitatory synapses in the hippocampus contains the CB1R (blue).

The level of FAAH (black) in the synapse is increased following EE. In turn 2AG (purple) levels are reduced. The ABHD6 levels are reduced, resulting in an increase in AMPARs (red).

4.2 Further characterization of Golgi-satellites in dendrites

Calneuron 1 and 2 are EF-hand Ca^{2+} -sensor proteins of the neuronal Calcium-binding protein (nCaBP) family with the highest Ca^{2+} -binding affinity (Wu et al., 2001; Mikhaylova et al., 2006, 2009, 2010). In contrast to other calmodulin (CaM)-like Ca^{2+} -sensors, they are type II tail-anchored transmembrane proteins that, following posttranslational insertion into the endoplasmic reticulum (ER) with assistance of a TRC40/Asna1 chaperone, accumulate at the *trans*-Golgi network (TGN) (Mikhaylova et al., 2009; McCue et al., 2010; Hradsky et al., 2011). Calneurons differ from other family members in terms of their EF-hand domain organization, with a first functional Ca^{2+} -binding domain (EF-hand 1+2) and a non-functional second EF-hand domain (EF-hand 3+4) that is incapable of Ca^{2+} -binding. In functional terms, Calneurons regulate Golgi-to-plasma membrane trafficking via an interaction with Phosphatidylinositol 4-OH kinase III β (PI-4KIII β), one of the key enzymes for production of phosphatidylinositol 4-phosphate at the TGN (Mikhaylova et al., 2009). Calneurons impose a Ca^{2+} -threshold for trafficking of synaptic vesicles as well as axonal Piccolo-Bassoon transport vesicles, probably owing to their strong inhibition of PI-4KIII β activity, with markedly attenuated PI-4KIII β activity at low to moderate $[\text{Ca}^{2+}]_i$ (Mikhaylova et al., 2009).

In vitro protein-lipid overlay assays indicated that Calneuron 1 associates strongly with lipids that are enriched in the TGN and the plasma membrane, namely PI(4)P, PI(4,5)P₂, and PI(3,4,5)P₃ (Hradsky et al., 2011). Indeed, Calneuron 1 is not exclusively resident at the TGN and a fraction of protein can be transported to the plasma membrane (Mikhaylova et al., 2009; Hradsky et al., 2011) where it associates with G protein coupled receptors (GPCRs), such as CB1R (Angelats et al., 2018). In addition, I found in this thesis that ABHD6 colocalizes and might traffic through Golgi-satellites. In previous work of the lab we took advantage of the Golgi targeting properties of the neuronal EF-hand calcium sensor protein Calneuron 2 to develop a simple but efficient plasmid-based system called pGolt to study Golgi organelles in neurons (Mikhaylova et al., 2009, 2016; Bera et al., 2016). With this tool we found the presence of Golgi-related organelles in all dendrites of pyramidal neurons in close proximity to ERGIC and retromer (Mikhaylova et al., 2016). This Golgi-Satellite secretory system (GS) in dendrites is much more widespread than previously described Golgi-outposts GOs, it is positive for Calneuron 1 and it contains at least part of the cellular glycosylation machinery but as opposed to GOs lacks many protein components for sorting and organization of Golgi cisternae. A broad spectrum of synaptic transmembrane proteins (including GluA1, GluN1, GluN2B, NCAM and Neuroligin-1) might pass and even recycle through these organelles (Mikhaylova et al., 2016). Thus, GS might enable local glycosylation of proteins, which can then be recruited to membranes in spatially confined dendritic segments. At present it is unclear how they are assembled and stabilized and which type of glycosylation is possible. In addition, the previous work is driving the question what the role of Calneuron 1 in the assembly, maintenance and function of GS is.

GS are relatively small and exhibit high dynamics of vesicle trafficking. Thus, mechanisms must be in place for assembly and stabilization of this organelle and Calneuron 1 is a likely candidate to mediate such a function. To address this question, I have employed shRNA knockdown of Calneuron 1 and generated a Calneuron 1 KO mouse. To study GS in brain I have generated a transgenic mouse line expressing mGolt in neurons.

In my work I have observed reduced dendrite complexity, a reduced number of synapses in particular in tertiary dendrites and a reduced size of extended Golgi in apical dendrites following protein knockdown of Calneuron. A similar phenotype was observed in Calneuron 1 KO mice. Interestingly, this is correlated with a reduced number of GS in distal dendrites. Collectively this work showed that the presence of Calneuron 1 affects the assembly and presence of GS in dendrites and it suggests that this impact neuronal morphology.

4.3 The needs of a synapse: How Golgi satellites serve synaptic function

What could be the reason for these phenotypes? Based on my results I hypothesize that this might have to do with local glycosylation of transmembrane proteins. In one set of experiments I have used lectins for hybrid and complex N-glycans and could answer the question that a specific set of N-glycans is found at GS as well as O-glycosylation as evidenced by the *Helix pomatia* agglutinin (HPL) that binds prominently to terminal alpha-linked GalNAc residues attached to Ser or Thr residues. Thus, complex glycosylation is possible at GS. It will be interesting to see whether there is a preferential route for recycling for core, hybrid and complex N-glycans. At present it is unclear whether N-glycosylation is at all necessary for trafficking through GS to the plasma membrane. I have used tunicamycin, a drug that completely blocks all N-glycosylation by preventing the transfer of the N-glycan precursor to target proteins in the ER and found reduced N-glycosylation at GS and in future experiments it will be important to verify whether N-glycosylated candidate proteins still pass through GS. Moreover, I found that sialylation of NCAM in distal dendrites depends on the presence of GS. This is interesting in light of previous findings where it was shown that NCAM can be polysialylated (PSA) in response to synaptic activity and staining with a PSA-specific antibody showed that about 38% of pGolt-mCherry labeled GS contain PSA-NCAM whereas ER-Golgi intermediate compartment (ERGIC) showed no co-localization with PSA-NCAM immunofluorescence (Mikhaylova et al., 2016). Thus, based on these still somewhat preliminary results it can be concluded polysialylation of NCAM occurs locally and that mice deficient in GS in distal dendrites might show highly localized phenotypes.

Finally, these results have relevance for an ongoing debate. In a recent study, it was shown that hundreds of neuronal surface membrane proteins are only core-glycosylated (Hanus et al., 2016). Thus, surprisingly high levels of glycosylation profiles that are classically associated with immature intracellular proteins are displayed at the surface of neuronal membranes. It was argued that this atypical glycosylation of surface neuronal proteins can be attributed to a bypass of the GA, indicating that the canonical secretory pathway is not only absent in dendrites but also hypofunctional in the soma. My results contradict this prediction but there are several explanations for these discrepant results. Conclusive evidence was found for the existence of a satellite microsecretory system in dendrites that even allows for local synthesis and processing of synaptic TM proteins (Ye et al., 2007; Ramirez and Couve, 2011; Cui-Wang et al., 2012). Since the vast majority of proteins are synthesized in the soma, and it was speculated that at most 20% of synaptic TM proteins can be synthesized locally in dendrites

(Hanus and Schuman, 2013; Dieterich and Kreutz, 2016) it might be that this small fraction is glycosylated in an activity-dependent manner at GS.

In addition to proteins the Golgi also supplies specifically modified lipids to the synaptic membrane it would be of great interest to further connect the two parts of this study. There is strong evidence to suggest that sialylation of lipids can be carried out locally in GS (Mikhaylova et al., 2016). One could test whether the insertion of lipids sialylated by ST3Gal5 into the synaptic membrane requires GS-function. This would be of high relevance since dysfunction of St3Gal5 has been shown to lead to cognitive impairment (Boccutto et al., 2014).

Similarly, one could study the distribution and function of the sialyltransferase ST6 Beta-Galactoside Alpha-2,6-Sialyltransferase 1 (ST6Gal1) in neuronal dendrites. St6Gal1 catalyzes the sialylation of galactose-containing substrates, including cell-surface signaling lipids and proteins. Polymorphisms in St6Gal1 have been associated with conditions from mild cognitive impairment to Alzheimer's disease (Moll et al., 2020). Since a large number of lipid targeting glycosyltransferases have been implicated in neurodegenerative diseases and at least some of them are found at GS, it would be of great interest to understand if these lipids require local processing in GS (Mikhaylova et al., 2016; Moll et al., 2020).

Future studies are ultimately warranted that address the molecular machinery underlying fast and direct insertion of synaptic membrane proteins and lipids in synapses undergoing plasticity. Moreover, previous work was focused on N-glycosylation of membrane proteins but ignored O-glycosylation, which is reversible and occurs in GS (Mikhaylova et al., 2016). Finally, it might be that two pathways exist for local secretory membrane trafficking and that only a few TM-proteins might pass through GS and synaptic signals might induce a switch of the trafficking route for certain proteins. These intriguing possibilities can now be tested with the tools that I have generated in this thesis.

5 References

- Abraham WC, Robins A (2005) Memory retention - The synaptic stability versus plasticity dilemma. *Trends Neurosci* 28:73–78.
- Anderson GR, Aoto J, Tabuchi K, Földy C, Covy J, Yee AX, Wu D, Lee SJ, Chen L, Malenka RC, Südhof TC (2015) β -Neurexins Control Neural Circuits by Regulating Synaptic Endocannabinoid Signaling. *Cell* 162:593–606.
- Angelats E, Requesens M, Aguinaga D, Kreutz MR, Franco R, Navarro G (2018) Neuronal calcium and cAMP cross-talk mediated by cannabinoid CB1 receptor and EF-hand calcium sensor interactions. *Front Cell Dev Biol* 6:1–9.
- Arroyo AI, Camoletto PG, Morando L, Sassoe-Pognetto M, Giustetto M, Van Veldhoven PP, Schuchman EH, Ledesma MD (2014) Pharmacological reversion of sphingomyelin-induced dendritic spine anomalies in a Niemann Pick disease type A mouse model. *EMBO Mol Med* 6:398–413.
- Banker G, Churchill L, Cotman CW (1974) Proteins of the postsynaptic density. *J Cell Biol* 63:456–465.
- Bär J, Kobler O, Van Bommel B, Mikhaylova M (2016) Periodic F-actin structures shape the neck of dendritic spines. *Sci Rep* 6:1–9 Available at: <http://dx.doi.org/10.1038/srep37136>.
- Barlowe CK, Miller EA (2013) Secretory protein biogenesis and traffic in the early secretory pathway. *Genetics* 193:383–410.
- Bayés A, Grant SGN (2009) Neuroproteomics: Understanding the molecular organization and complexity of the brain. *Nat Rev Neurosci* 10:635–646.
- Bera S, Raghuram V, Mikhaylova M, Kreutz MR (2016) A plasmid-based expression system to study protein-protein interactions at the Golgi in vivo. *Anal Biochem* 502:50–52 Available at: <http://dx.doi.org/10.1016/j.ab.2016.02.016>.
- Bergmann E, Zur G, Bershadsky G, Kahn I (2016) The organization of mouse and human cortico-hippocampal networks estimated by intrinsic functional connectivity. *Cereb Cortex* 26:4497–4512.
- Biever A, Glock C, Tushev G, Ciirdaeva E, Dalmay T, Langer JD, Schuman EM (2020) Monosomes actively translate synaptic mRNAs in neuronal processes. *Science* 367.
- Bissen D, Foss F, Acker-Palmer A (2019) AMPA receptors and their minions: auxiliary proteins in AMPA receptor trafficking. *Cellular and Molecular Life Sciences* volume 76, 2133–2169
- Blomberg F, Cohen RC, Siekevitz P (1977) The structure of postsynaptic densities isolated from dog cerebral cortex. II. Characterization and arrangement of some of the major proteins within the structure. *J Cell Biol* 74:204–225.
- Boccuto L, Aoki K, Flanagan-Steet H, Chen CF, Fan X, Bartel F, Petukh M, Pittman A, Saul R, Chaubey A, Alexov E, Tiemeyer M, Steet R, Schwartz CE (2014) A mutation in a ganglioside biosynthetic enzyme, *ST3GAL5*, results in salt & pepper syndrome, a

- neurocutaneous disorder with altered glycolipid and glycoprotein glycosylation. *Hum Mol Genet* 23:418–433.
- Bock J, Gulbins E (2003) The transmembranous domain of CD40 determines CD40 partitioning into lipid rafts. *FEBS Lett* 534:169–174.
- Boncompain G, Divoux S, Gareil N, De Forges H, Lescure A, Latreche L, Mercanti V, Jollivet F, Raposo G, Perez F (2012) Synchronization of secretory protein traffic in populations of cells. *Nat Methods* 9:493–498.
- Brachet A, Norwood S, Brouwers JF, Palomer E, Helms JB, Dotti CG, Esteban JA (2015) LTP-triggered cholesterol redistribution activates Cdc42 and drives AMPA receptor synaptic delivery. *J Cell Biol* 208:791–806.
- Brechet A et al. (2017) AMPA-receptor specific biogenesis complexes control synaptic transmission and intellectual ability. *Nat Commun* 8, 15910
- Breckenridge WC, Gombos G, Morgan IG (1972) The lipid composition of adult rat brain synaptosomal plasma membranes. *BBA - Biomembr* 266:695–707.
- Burgert A, Schlegel J, Bécam J, Doose S, Bieberich E, Schubert-Unkmeir A, Sauer M (2017) Characterization of Plasma Membrane Ceramides by Super-Resolution Microscopy. *Angew Chemie - Int Ed* 56:6131–6135.
- Caccin P, Scorzeto M, Damiano N, Marin O, Megighian A, Montecucco C (2015) The synaptotagmin juxtamembrane domain is involved in neuroexocytosis. *FEBS Open Bio* 5:388–396 Available at: <http://dx.doi.org/10.1016/j.fob.2015.04.013>.
- Capitani M, Sallese M (2009) The KDEL receptor: New functions for an old protein. *FEBS Lett* 583:3863–3871 Available at: <http://dx.doi.org/10.1016/j.febslet.2009.10.053>.
- Carrasco P, Sahún I, McDonald J, Ramírez S, Jacas J, Gratacós E, Sierra AY, Serra D, Herrero L, Acker-Palmer A, Hegardt FG, Dierssen M, Casals N (2012) Ceramide levels regulated by carnitine palmitoyltransferase 1C control dendritic spine maturation and cognition. *J Biol Chem* 287:21224–21232.
- Castillo PE, Younts TJ, Chávez AE, Hashimoto-dani Y (2012) Endocannabinoid Signaling and Synaptic Function. *Neuron* 76:70–81.
- Chavko M, Nemoto EM, Melick JA (1993) Regional lipid composition in the rat brain. *Mol Chem Neuropathol* 18:123–131.
- Chen KE, Healy MD, Collins BM (2019) Towards a molecular understanding of endosomal trafficking by Retromer and Retriever. *Traffic* 20:465–478.
- Chernomordik L V., Kozlov MM (2003) Protein-Lipid Interplay in Fusion and Fission of Biological Membranes. *Annu Rev Biochem* 72:175–207.
- Coman C, Solari FA, Hentschel A, Sickmann A, Zahedi RP, Ahrends R (2016) Simultaneous metabolite, protein, lipid extraction (SIMPLEX): A combinatorial multimolecular omics approach for systems biology. *Mol Cell Proteomics* 15:1453–1466.
- Cui-Wang T, Hanus C, Cui T, Helton T, Bourne J, Watson D, Harris KM, Ehlers MD (2012) Local zones of endoplasmic reticulum complexity confine cargo in neuronal dendrites. *Cell* 148:309–321 Available at: <http://dx.doi.org/10.1016/j.cell.2011.11.056>.

- DA S (1953) Dendritic organization in the neurons of the visual and motor cortices of the cat. *J Anat* 87:387–406.
- Deller T, Bas Orth C, Del Turco D, Vlachos A, Burbach GJ, Drakew A, Chabanis S, Korte M, Schwegler H, Haas CA, Frotscher M (2007) A role for synaptopodin and the spine apparatus in hippocampal synaptic plasticity. *Ann Anat* 189:5–16.
- Deller T, Korte M, Chabanis S, Drakew A, Schwegler H, Stefani GG, Zuniga A, Schwarz K, Bonhoeffer T, Zeller R, Frotscher M, Mundel P (2003) Synaptopodin-deficient mice lack a spine apparatus and show deficits in synaptic plasticity. *Proc Natl Acad Sci U S A* 100:10494–10499.
- Deller T, Mundel P, Frotscher M (2000) Potential role of synaptopodin in spine motility by coupling actin to the spine apparatus. *Hippocampus* 10:569–581.
- Di Marzo V, Maccarrone M (2008) FAAH and anandamide: is 2-AG really the odd one out? *Trends Pharmacol Sci* 29:229–233.
- Diana MA, Marty A (2004) Endocannabinoid-mediated short-term synaptic plasticity: Depolarization-induced suppression of inhibition (DSI) and depolarization-induced suppression of excitation (DSE). *Br J Pharmacol* 142:9–19.
- Dieterich DC, Kreutz MR (2016) Proteomics of the synapse - A quantitative approach to neuronal plasticity. *Mol Cell Proteomics* 15:368–381.
- Distler U, Schmeisser MJ, Pelosi A, Reim D, Kuharev J, Weiczner R, Baumgart J, Boeckers TM, Nitsch R, Vogt J, Tenzer S (2014) In-depth protein profiling of the postsynaptic density from mouse hippocampus using data-independent acquisition proteomics. *Proteomics* 14:2607–2613.
- Dotti CG, Esteban JA, Ledesma MD (2014) Lipid dynamics at dendritic spines. *Front Neuroanat* 8:1–11.
- Dumont F (2012) FK506, An Immunosuppressant Targeting Calcineurin Function. *Curr Med Chem* 7:731–748.
- Duncan BW, Murphy KE, Maness PF (2021) Molecular Mechanisms of L1 and NCAM Adhesion Molecules in Synaptic Pruning, Plasticity, and Stabilization. *Front Cell Dev Biol* 9:1–13.
- Ellis SR, Paine MRL, Eijkel GB, Pauling JK, Husen P, Jervelund MW, Hermansson M, Ejsing CS, Heeren RMA (2018) Automated, parallel mass spectrometry imaging and structural identification of lipids. *Nat Methods* 15:515–518 Available at: <http://dx.doi.org/10.1038/s41592-018-0010-6>.
- Eric R. Kandel, John D. Koester, Sarah H. Mack SAS (2013) *Principles of Neural Science*, Fifth Edition.
- Fledrich R et al. (2018) Targeting myelin lipid metabolism as a potential therapeutic strategy in a model of CMT1A neuropathy. *Nat Commun* 9: 3025.
- Frank C, Rufini S, Tancredi V, Forcina R, Grossi D, D’Arcangelo G (2008) Cholesterol depletion inhibits synaptic transmission and synaptic plasticity in rat hippocampus. *Exp Neurol* 212:407–414.

- Frese CK, Mikhaylova M, Stucchi R, Gautier V, Liu Q, Mohammed S, Heck AJR, Altelaar AFM, Hoogenraad CC (2017) Quantitative Map of Proteome Dynamics during Neuronal Differentiation. *Cell Rep* 18:1527–1542 Available at: <http://dx.doi.org/10.1016/j.celrep.2017.01.025>.
- Gao Y et al. (2010) Loss of retrograde endocannabinoid signaling and reduced adult neurogenesis in diacylglycerol lipase knock-out mice. *J Neurosci* 30:2017–2024.
- Gaoni Y, Mechoulam R (1964) Isolation, Structure, and Partial Synthesis of an Active Constituent of Hashish. *J Am Chem Soc* 86:1646–1647.
- Gascon E, Vutskits L, Kiss JZ (2007) Polysialic acid-neural cell adhesion molecule in brain plasticity: From synapses to integration of new neurons. *Brain Res Rev* 56:101–118.
- Gee CE, Ohmert I, Wiegert JS, Oertner TG (2017) Preparation of slice cultures from rodent hippocampus. *Cold Spring Harb Protoc* 2017:126–130.
- Goñi FM (2014) The basic structure and dynamics of cell membranes: An update of the Singer-Nicolson model. *Biochim Biophys Acta - Biomembr* 1838:1467–1476 Available at: <http://dx.doi.org/10.1016/j.bbamem.2014.01.006>.
- Goparaju SK, Ueda N, Yamaguchi H, Yamamoto S (1998) Anandamide amidohydrolase reacting with 2-arachidonoylglycerol, another cannabinoid receptor ligand. *FEBS Lett* 422:69–73.
- Grønborg M, Pavlos NJ, Brunk I, Chua JJE, Münster-Wandowski A, Riedel D, Ahnert-Hilger G, Urlaub H, Jahn R (2010) Quantitative comparison of glutamatergic and GABAergic synaptic vesicles unveils selectivity for few proteins including MAL2, a novel synaptic vesicle protein. *J Neurosci* 30:2–12.
- Guan F, Wang X, He F (2015) Promotion of cell migration by neural cell adhesion molecule (NCAM) is enhanced by PSA in a polysialyltransferase-specific manner. *PLoS One* 10:1–14.
- Guggenhuber S, Romo-Parra H, Bindila L, Leschik J, Lomazzo E, Remmers F, Zimmermann T, Lerner R, Klugmann M, Pape HC, Lutz B (2016) Impaired 2-AG signaling in hippocampal glutamatergic neurons: Aggravation of anxiety-like behavior and unaltered seizure susceptibility. *Int J Neuropsychopharmacol* 19:1–13.
- Haeussler M, Schönig K, Eckert H, Eschstruth A, Mianné J, Renaud JB, Schneider-Maunoury S, Shkumatava A, Teboul L, Kent J, Joly JS, Concordet JP (2016) Evaluation of off-target and on-target scoring algorithms and integration into the guide RNA selection tool CRISPOR. *Genome Biol* 17:1–12 Available at: <http://dx.doi.org/10.1186/s13059-016-1012-2>.
- Han X (2007) Neurolipidomics: Challenges and developments. *Front Biosci* 12:2601–2615.
- Hanahan D (1983) Studies on transformation of *Escherichia coli* with plasmids. *J Mol Biol* 166:557–580.
- Hanus C, Geptin H, Tushev G, Garg S, Alvarez-Castelao B, Sambandan S, Kochen L, Hafner A-S, Langer JD, Schuman EM (2016) Unconventional secretory processing diversifies neuronal ion channel properties. *Elife* 5:1–27.
- Hanus C, Schuman EM (2013) Proteostasis in complex dendrites. *Nat Rev Neurosci* 14:638–

648.

- Harvey Lodish, Arnold Berk, S Lawrence Zipursky, Paul Matsudaira, David Baltimore and JD (2013) *Molecular Cell Biology*, 4th edition.
- Hashimotodani Y, Ohno-Shosaku T, Kano M (2007) Ca²⁺-assisted receptor-driven endocannabinoid release: mechanisms that associate presynaptic and postsynaptic activities. *Curr Opin Neurobiol* 17:360–365.
- Hashimotodani Y, Ohno-Shosaku T, Tsubokawa H, Ogata H, Emoto K, Maejima T, Araishi K, Shin HS, Kano M (2005) Phospholipase C β serves as a coincidence detector through its Ca²⁺ dependency for triggering retrograde endocannabinoid signal. *Neuron* 45:257–268.
- Hasin Y, Seldin M, Lusic A (2017) Multi-omics approaches to disease. *Genome Biol* 18:1–15.
- Henley JM, Wilkinson KA (2016) Synaptic AMPA receptor composition in development, plasticity and disease. *Nat Rev Neurosci* 17:337–350.
- Herring BE, Nicoll RA (2016) Long-Term Potentiation: From CaMKII to AMPA Receptor Trafficking. *Annu Rev Physiol* 78:351–365.
- Herzog R, Schwudke D, Schuhmann K, Sampaio JL, Bornstein SR, Schroeder M, Shevchenko A (2011) A novel informatics concept for high-throughput shotgun lipidomics based on the molecular fragmentation query language. *Genome Biol* 12:1–25.
- Horton AC, Ehlers MD (2003) Dual modes of endoplasmic reticulum-to-Golgi transport in dendrites revealed by live-cell imaging. *J Neurosci* 23:6188–6199.
- Horváth E, Woodhams SG, Nyilas R, Henstridge CM, Kano M, Sakimura K, Watanabe M, Katona I (2014) Heterogeneous presynaptic distribution of monoacylglycerol lipase, a multipotent regulator of nociceptive circuits in the mouse spinal cord. *Eur J Neurosci* 39:419–434.
- Hradsky J, Raghuram V, Reddy PP, Navarro G, Hupe M, Casado V, McCormick PJ, Sharma Y, Kreutz MR, Mikhaylova M (2011) Post-translational membrane insertion of tail-anchored transmembrane EF-hand Ca²⁺ sensor calneurons requires the TRC40/Asn1 protein chaperone. *J Biol Chem* 286:36762–36776.
- Jurado S, Benoist M, Lario A, Knafo S, Petrok CN, Esteban JA (2010) PTEN is recruited to the postsynaptic terminal for NMDA receptor-dependent long-term depression. *EMBO J* 29:2827–2840.
- Kandel MB, Yamamoto S, Midorikawa R, Morise J, Wakazono Y, Oka S, Takamiya K (2018) N-glycosylation of the AMPA-type glutamate receptor regulates cell surface expression and tetramer formation affecting channel function. *J Neurochem* 147:730–747.
- Kang Y, Ge Y, Cassidy RM, Lam V, Luo L, Moon KM, Lewis R, Molday RS, Wong ROL, Foster LJ, Craig AM (2014) A combined transgenic proteomic analysis and regulated trafficking of neuroligin-2. *J Biol Chem* 289:29350–29364.
- Kano M (2014) Control of synaptic function by endocannabinoid-mediated retrograde signaling. *Proc Japan Acad Ser B Phys Biol Sci* 90:235–250.

- Karpova A, Mikhaylova M, Bera S, Bär J, Reddy PP, Behnisch T, Rankovic V, Spilker C, Bethge P, Sahin J, Kaushik R, Zuschratter W, Kähne T, Naumann M, Gundelfinger ED, Kreutz MR (2013) Encoding and transducing the synaptic or extrasynaptic origin of NMDA receptor signals to the nucleus. *Cell* 152:1119–1133.
- Katona I, Urbán GM, Wallace M, Ledent C, Jung KM, Piomelli D, Mackie K, Freund TF (2006) Molecular composition of the endocannabinoid system at glutamatergic synapses. *J Neurosci* 26:5628–5637.
- Kempermann G (2019) Environmental enrichment, new neurons and the neurobiology of individuality. *Nat Rev Neurosci* 20:235–245 Available at: <http://dx.doi.org/10.1038/s41583-019-0120-x>.
- Knierim JJ (2015) The hippocampus. *Curr Biol* 25:R1116–R1121.
- Kochlamazashvili G, Senkov O, Grebenyuk S, Robinson C, Xiao MF, Stummeyer K, Gerardy-Schahn R, Engel AK, Feig L, Semyanov A, Suppiramaniam V, Schachner M, Dityatev A (2010) Neural cell adhesion molecule-associated polysialic acid regulates synaptic plasticity and learning by restraining the signaling through GluN2B-containing NMDA receptors. *J Neurosci* 30:4171–4183.
- Kononenko NL, Haucke V (2015) Molecular mechanisms of presynaptic membrane retrieval and synaptic vesicle reformation. *Neuron* 85:484–496 Available at: <http://dx.doi.org/10.1016/j.neuron.2014.12.016>.
- Koopmans F et al. (2019) SynGO: An Evidence-Based, Expert-Curated Knowledge Base for the Synapse. *Neuron* 103:217-234.e4.
- Koudinov AR, Koudinova N V. (2001) Essential role for cholesterol in synaptic plasticity and neuronal degeneration. *FASEB J* 15:1858–1860.
- Kröcher T, Malinovskaja K, Jürgenson M, Aonurm-Helm A, Zharkovskaya T, Kalda A, Röckle I, Schiff M, Weinhold B, Gerardy-Schahn R, Hildebrandt H, Zharkovsky A (2013) Schizophrenia-like phenotype of polysialyltransferase ST8SIA2-deficient mice. *Brain Struct Funct* 220:71–83.
- Lacaille JC, Schwartzkroin PA (1988) Statum lacunosum-moleculare interneurons of hippocampal CA1 region. I. Intracellular response characteristics, synaptic responses, and morphology. *J Neurosci* 8:1400–1410.
- Laude AJ, Prior IA (2012) Plasma membrane microdomains : organisation , function and trafficking. *Mol Membr Biol* 21:193–205.
- Lerner R, Post JM, Ellis SR, Naomi Vos DR, Heeren RMA, Lutz B, Bindila L (2018) Simultaneous lipidomic and transcriptomic profiling in mouse brain punches of acute epileptic seizure model compared to controls. *J Lipid Res* 59:283–297.
- Li J, Lü S, Liu Y, Pang C, Chen Y, Zhang S, Yu H, Long M, Zhang H, Logothetis DE, Zhan Y, An H (2015) Identification of the conformational transition pathway in PIP 2 Opening Kir Channels. *Sci Rep* 5.
- Liu SJ, Zukin RS (2007) Ca²⁺-permeable AMPA receptors in synaptic plasticity and neuronal death. *Trends Neurosci* 30:126–134.
- Marrs WR et al. (2010) The serine hydrolase ABHD6 controls the accumulation and efficacy

- of 2-AG at cannabinoid receptors. *Nat Neurosci* 13:951–957 Available at: <http://dx.doi.org/10.1038/nn.2601>.
- Martin MG, Ahmed T, Korovaichuk A, Venero C, Menchón SA, Salas I, Munck S, Herreras O, Balschun D, Dotti CG (2014a) Constitutive hippocampal cholesterol loss underlies poor cognition in old rodents. *EMBO Mol Med* 6:902–917.
- Martin MG, Ahmed T, Korovaichuk A, Venero C, Menchón SA, Salas I, Munck S, Herreras O, Balschun D, Dotti CG (2014b) Constitutive hippocampal cholesterol loss underlies poor cognition in old rodents. *EMBO Mol Med* 6:902–917.
- Matsuda LA, Lolait SJ, Brownstein MJ, Young AC, Bonner TI (1990) Structure of a cannabinoid receptor and functional expression of the cloned cDNA. *Nature* 346:561–564.
- McCartney AJ, Zolov SN, Kauffman EJ, Zhang Y, Strunk BS, Weisman LS, Sutton MA (2014) Activity-dependent PI(3,5)P₂ synthesis controls AMPA receptor trafficking during synaptic depression. *Proc Natl Acad Sci U S A* 111:E4896–E4905.
- McCue H V., Haynes LP, Burgoyne RD (2010) Bioinformatic analysis of CaBP/calneuron proteins reveals a family of highly conserved vertebrate Ca²⁺-binding proteins. *BMC Res Notes* 3.
- Mikhaylova M, Bär J, van Bommel B, Schätzle P, YuanXiang PA, Raman R, Hradsky J, Konietzny A, Loktionov EY, Reddy PP, Lopez-Rojas J, Spilker C, Kobler O, Raza SA, Stork O, Hoogenraad CC, Kreutz MR (2018) Caldendrin Directly Couples Postsynaptic Calcium Signals to Actin Remodeling in Dendritic Spines. *Neuron* 97:1110-1125.e14.
- Mikhaylova M, Bera S, Kobler O, Frischknecht R, Kreutz MR (2016) A Dendritic Golgi Satellite between ERGIC and Retromer. *Cell Rep* 14:189–199 Available at: <http://dx.doi.org/10.1016/j.celrep.2015.12.024>.
- Mikhaylova M, Reddy PP, Kreutz MR (2010) Role of neuronal Ca²⁺-sensor proteins in Golgi-cell-surface membrane traffic. *Biochem Soc Trans* 38:177–180.
- Mikhaylova M, Reddy PP, Munsch T, Landgraf P, Suman SK, Smalla KH, Gundelfinger ED, Sharma Y, Kreutz MR (2009) Calneurons provide a calcium threshold for trans-Golgi network to plasma membrane trafficking. *Proc Natl Acad Sci U S A* 106:9093–9098.
- Mikhaylova M, Sharma Y, Reissner C, Nagel F, Aravind P, Rajini B, Smalla KH, Gundelfinger ED, Kreutz MR (2006) Neuronal Ca²⁺ signaling via caldendrin and calneurons. *Biochim Biophys Acta - Mol Cell Res* 1763:1229–1237.
- Missler M, Südhof TC, Biederer T (2012) Synaptic cell adhesion. *Cold Spring Harb Perspect Biol* 4:1–18.
- Mitroi DN, Pereyra-Gómez G, Soto-Huelin B, Senovilla F, Kobayashi T, Esteban JA, Ledesma MD (2019) NPC 1 enables cholesterol mobilization during long-term potentiation that can be restored in Niemann–Pick disease type C by CYP 46A1 activation . *EMBO Rep* 20:1–18.
- Molenaar MR, Jeucken A, Wassenaar TA, Van De Lest CHA, Brouwers JF, Helms JB (2019) LION/web: A web-based ontology enrichment tool for lipidomic data analysis. *Gigascience* 8:1–10.

- Moll T, Shaw PJ, Cooper-Knock J (2020) Disrupted glycosylation of lipids and proteins is a cause of neurodegeneration. *Brain* 143:1332–1340.
- Monzo HJ, Coppieters N, Park TIH, Dieriks B V., Faull RLM, Dragunow M, Curtis MA (2017) Insulin promotes cell migration by regulating PSA-NCAM. *Exp Cell Res* 355:26–39 Available at: <http://dx.doi.org/10.1016/j.yexcr.2017.03.029>.
- Morise J, Yamamoto S, Midorikawa R, Takamiya K, Nonaka M, Takematsu H, Oka S (2020) Distinct cell surface expression patterns of n-glycosylation site mutants of ampa-type glutamate receptor under the homo-oligomeric expression conditions. *Int J Mol Sci* 21:1–11.
- Mühlenhoff M, Eckhardt M, Bethe A, Frosch M, Gerardy-Schahn R (1996) Polysialylation of NCAM by a single enzyme. *Curr Biol* 6:1188–1191.
- Muller D, Wang C, Skibo G, Toni N, Cremer H, Calaora V, Rougon G, Kiss JZ (1996) PSA-NCAM is required for activity-induced synaptic plasticity. *Neuron* 17:413–422.
- Mundhenk J, Fusi C, Kreutz MR (2019) Caldendrin and calneurons—EF-hand CaM-like calcium sensors with unique features and specialized neuronal functions. *Front Mol Neurosci* 12:1–9.
- Neuhoff H, Roeper J, Schweizer M (1999) Activity-dependent formation of perforated synapses in cultured hippocampal neurons. *Eur J Neurosci* 11:4241–4250.
- O’Brien JS, Sampson EL (1965) Lipid composition of the normal human brain: gray matter, white matter, and myelin. *J Lipid Res* 6:537–544 Available at: [http://dx.doi.org/10.1016/S0022-2275\(20\)39619-X](http://dx.doi.org/10.1016/S0022-2275(20)39619-X).
- Ohline SM, Abraham WC (2019a) Environmental enrichment effects on synaptic and cellular physiology of hippocampal neurons. *Neuropharmacology* 145:3–12 Available at: <https://doi.org/10.1016/j.neuropharm.2018.04.007>.
- Ohline SM, Abraham WC (2019b) Environmental enrichment effects on synaptic and cellular physiology of hippocampal neurons. *Neuropharmacology* 145:3–12 Available at: <https://doi.org/10.1016/j.neuropharm.2018.04.007>.
- Ostroff LE, Watson DJ, Cao G, Parker PH, Smith H, Harris KM (2018) Shifting patterns of polyribosome accumulation at synapses over the course of hippocampal long-term potentiation. *Hippocampus* 28:416–430.
- Park M (2018) AMPA receptor trafficking for postsynaptic potentiation. *Front Cell Neurosci* 12:1–10.
- Peng B, Geue S, Coman C, Münzer P, Kopczynski D, Has C, Hoffmann N, Manke MC, Lang F, Sickmann A, Gawaz M, Borst O, Ahrends R (2018) Identification of key lipids critical for platelet activation by comprehensive analysis of the platelet lipidome. *Blood* 132(5):e1–e12.
- Peng B, Weintraub ST, Coman C, Ponnaiyan S, Sharma R, Tews B, Winter D, Ahrends R (2017) A Comprehensive High-Resolution Targeted Workflow for the Deep Profiling of Sphingolipids. *Anal Chem* 89:12480–12487.
- Per Andersen, Richard Morris, David Amaral, John O’Keefe TB (2007) *The Hippocampus Book*.

- Piomelli D, Astarita G, Rapaka R (2007) A neuroscientist's guide to lipidomics. *Nat Rev Neurosci* 8:743–754.
- Plant K, Pelkey KA, Bortolotto ZA, Morita D, Terashima A, McBain CJ, Collingridge GL, Isaac JTR (2006) Transient incorporation of native GluR2-lacking AMPA receptors during hippocampal long-term potentiation. *Nat Neurosci* 9:602–604.
- Puchkov D, Haucke V (2013) Greasing the synaptic vesicle cycle by membrane lipids. *Trends Cell Biol* 23:493–503 Available at: <http://dx.doi.org/10.1016/j.tcb.2013.05.002>.
- Ramirez OA, Couve A (2011) The endoplasmic reticulum and protein trafficking in dendrites and axons. *Trends Cell Biol* 21:219–227.
- Riccio P, Fasano A, Borenshtein N, Bleve-Zacheo T, Kirschner DA (2000) Multilamellar packing of myelin modeled by lipid-bound MBP. *J Neurosci Res* 59:513–521.
- Rosenberg T, Gal-Ben-Ari S, Dieterich DC, Kreutz MR, Ziv NE, Gundelfinger ED, Rosenblum K (2014) The roles of protein expression in synaptic plasticity and memory consolidation. *Front Mol Neurosci* 7:1–14.
- Rutishauser U (2008) Polysialic acid in the plasticity of the developing and adult vertebrate nervous system. *Nat Rev Neurosci* 9:26–35.
- Savinainen JR, Saario SM, Laitinen JT (2012) The serine hydrolases MAGL, ABHD6 and ABHD12 as guardians of 2-arachidonoylglycerol signalling through cannabinoid receptors. *Acta Physiol* 204:267–276.
- Schindelin J, Arganda-Carreras I, Frise E, Kaynig V, Longair M, Pietzsch T, Preibisch S, Rueden C, Saalfeld S, Schmid B, Tinevez JY, White DJ, Hartenstein V, Eliceiri K, Tomancak P, Cardona A (2012) Fiji: An open-source platform for biological-image analysis. *Nat Methods* 9:676–682.
- Schwenk J, Boudkkazi S, Kocylowski MK, Brechet A, Zolles G, Bus T, Costa K, Kollwe A, Jordan J, Bank J, Bildl W, Sprengel R, Kulik A, Roeper J, Schulte U, Fakler B (2019) An ER Assembly Line of AMPA-Receptors Controls Excitatory Neurotransmission and Its Plasticity. *Neuron* 104:680-692.e9 Available at: <https://doi.org/10.1016/j.neuron.2019.08.033>.
- Seaman MNJ (2009) Enhanced SnapShot: Endosome-to-Golgi Retrieval. *Cell* 139:10–11.
- Seaman MNJ, Marcusson EG, Cereghino JL, Emr SD (1997) Endosome to Golgi retrieval of the vacuolar protein sorting receptor, Vps10p, requires the function of the VPS29, VPS30, and VPS35 gene products. *J Cell Biol* 137:79–92.
- Seidenbecher CI, Landwehr M, Smalla KH, Kreutz M, Dieterich DC, Zuschratter W, Reissner C, Hammarback JA, Böckers TM, Gundelfinger ED, Kreutz MR (2004) Caldendrin but not Calmodulin Binds to Light Chain 3 of MAP1A/B: An Association with the Microtubule Cytoskeleton Highlighting Exclusive Binding Partners for Neuronal Ca²⁺-sensor Proteins. *J Mol Biol* 336:957–970.
- Shepherd JD (2012) Memory, plasticity, and sleep - A role for calcium permeable AMPA receptors? *Front Mol Neurosci* 5:1–5.
- Shonesy BC, Winder DG, Patel S, Colbran RJ (2015) The initiation of synaptic 2-AG mobilization requires both an increased supply of diacylglycerol precursor and increased

- postsynaptic calcium. *Neuropharmacology* 91:57–62 Available at: <http://dx.doi.org/10.1016/j.neuropharm.2014.11.026>.
- Sohn J, Lin H, Fritch MR, Tuan RS (2018) Influence of cholesterol/caveolin-1/caveolae homeostasis on membrane properties and substrate adhesion characteristics of adult human mesenchymal stem cells. *Stem Cell Res Ther* 9:1–15.
- Steindel F, Lerner R, Häring M, Ruehle S, Marsicano G, Lutz B, Monory K (2013) Neuron-type specific cannabinoid-mediated G protein signalling in mouse hippocampus. *J Neurochem* 124:795–807.
- Takeuchi Y, Morise J, Morita I, Takematsu H, Oka S (2015) Role of site-specific N-glycans expressed on GluA2 in the regulation of cell surface expression of AMPA-type glutamate receptors. *PLoS One* 10:1–14.
- Tanaka H, Takafuji K, Taguchi A, Wiriyasermkul P, Ohgaki R, Nagamori S, Suh PG, Kanai Y (2012) Linkage of N-cadherin to multiple cytoskeletal elements revealed by a proteomic approach in hippocampal neurons. *Neurochem Int* 61:240–250.
- Tanimura A, Yamazaki M, Hashimotodani Y, Uchigashima M, Kawata S, Abe M, Kita Y, Hashimoto K, Shimizu T, Watanabe M, Sakimura K, Kano M (2010) The Endocannabinoid 2-Arachidonoylglycerol Produced by Diacylglycerol Lipase α Mediates Retrograde Suppression of Synaptic Transmission. *Neuron* 65:320–327 Available at: <http://dx.doi.org/10.1016/j.neuron.2010.01.021>.
- Taverna E, Francolini M, Jeromin A, Hilfiker S, Roder J, Rosa P (2002) Neuronal calcium sensor 1 and phosphatidylinositol 4-OH kinase β interact in neuronal cells and are translocated to membranes during nucleotide-evoked exocytosis. *J Cell Sci* 115:3909–3922.
- Tsuriel S, Geva R, Zamorano P, Dresbach T, Boeckers T, Gundelfinger ED, Garner CC, Ziv NE (2006) Local sharing as a predominant determinant of synaptic matrix molecular dynamics. *PLoS Biol* 4:1572–1587.
- Tucholski J, Simmons MS, Pinner AL, Haroutunian V, McCullumsmith RE, Meador-Woodruff JH (2013) Abnormal N-linked glycosylation of cortical AMPA receptor subunits in schizophrenia. *Schizophr Res* 146:177–183 Available at: <http://dx.doi.org/10.1016/j.schres.2013.01.031>.
- Vaithianathan T, Matthias K, Bahr B, Schachner M, Suppiramaniam V, Dityatev A, Steinhäuser C (2004) Neural cell adhesion molecule-associated polysialic acid potentiates α -amino-3-hydroxy-5-methylisoxazole-4-propionic acid receptor currents. *J Biol Chem* 279:47975–47984.
- Vorhees C V., Williams MT (2014) Assessing spatial learning and memory in rodents. *ILAR J* 55:310–332.
- Wang Y, Gu N, Duan T, Kesner P, Blaskovits F, Liu J, Lu Y, Tong L, Gao F, Harris C, MacKie K, Li J, Tan Q, Hill MN, Yuan Z, Zhang X (2017) Monoacylglycerol lipase inhibitors produce pro- or antidepressant responses via hippocampal CA1 GABAergic synapses. *Mol Psychiatry* 22:215–226.
- Wei M, Jia M, Zhang J, Yu L, Zhao Y, Chen Y, Ma Y, Zhang W, Shi YS, Zhang C (2017) The inhibitory effect of α/β -hydrolase domain-containing 6 (ABHD6) on the surface

- targeting of GluA2- and GluA3-containing AMPA receptors. *Front Mol Neurosci* 10:1–12.
- Weinhold B, Seidenfaden R, Röckle I, Mühlenhoff M, Schertzinger F, Conzelmann S, Marth JD, Gerardy-Schahn R, Hildebrandt H (2005) Genetic ablation of polysialic acid causes severe neurodevelopmental defects rescued by deletion of the neural cell adhesion molecule. *J Biol Chem* 280:42971–42977.
- Wiegert JS, Gee CE, Oertner TG (2017) Viral vector-based transduction of slice cultures. *Cold Spring Harb Protoc* 2017:131–134.
- Wu YQ, Lin X, Liu CM, Jamrich M, Shaffer LG (2001) Identification of a human brain-specific gene, calneuron 1, a new member of the calmodulin superfamily. *Mol Genet Metab* 72:343–350.
- Xu Q, Huang Y (2006) Lipid metabolism in Alzheimer’s and Parkinson’s disease. *Future Lipidol* 1:441–453.
- Yang X, Annaert W (2021) The nanoscopic organization of synapse structures: a common basis for cell communication. *Membranes* 11(4), 248.
- Yang Z, Sun L (2021) Recent technical progress in sample preparation and liquid-phase separation-mass spectrometry for proteomic analysis of mass-limited samples. *Anal Methods* 13:1214–1225.
- Ye B, Zhang Y, Song W, Younger SH, Jan LY, Jan YN (2007) Growing Dendrites and Axons Differ in Their Reliance on the Secretory Pathway. *Cell* 130:717–729.
- Yoshino H, Miyamae T, Hansen G, Zambrowicz B, Flynn M, Pedicord D, Blat Y, Westphal RS, Zaczek R, Lewis DA, Gonzalez-Burgos G (2011) Postsynaptic diacylglycerol lipase α mediates retrograde endocannabinoid suppression of inhibition in mouse prefrontal cortex. *J Physiol* 589:4857–4884.
- Yu J, Rao P, Clark S, Mitra J, Ha T, Gouaux E (2021) Hippocampal AMPA receptor assemblies and mechanism of allosteric inhibition. *Nature* 594 Available at: <http://dx.doi.org/10.1038/s41586-021-03540-0>.
- Zhang H, Huang T, Hong Y, Yang W, Zhang X, Luo H, Xu H, Wang X (2018) The retromer complex and sorting nexins in neurodegenerative diseases. *Front Aging Neurosci* 10:1–11.
- Zhang J, Liu Q (2015) Cholesterol metabolism and homeostasis in the brain. *Protein Cell* 6:254–264.
- Zheng M, Hu Y, Gou R, Wang J, Nie X, Li X, Liu Q, Liu J, Lin B (2019) Integrated multi-omics analysis of genomics, epigenomics, and transcriptomics in ovarian carcinoma. *Aging (Albany NY)* 11:4198–4215.
- Zimmermann T, Bartsch JC, Beer A, Lomazzo E, Guggenhuber S, Lange MD, Bindila L, Pape HC, Lutz B (2019) Impaired anandamide/palmitoylethanolamide signaling in hippocampal glutamatergic neurons alters synaptic plasticity, learning, and emotional responses. *Neuropsychopharmacology* 44:1377–1388 Available at: <http://dx.doi.org/10.1038/s41386-018-0274-7>.
- Züllig T, Trötz Müller M, Köfeler HC (2020) Lipidomics from sample preparation to data

analysis: a primer. *Anal Bioanal Chem* 412:2191–2209.

6 Abbreviations

| | |
|---------------|--|
| 2-AG | 2-Arachidonoylglycerol |
| 4-AP | 4-Aminopyridine |
| AA | Arachidonic Acid |
| AAL | <i>Aleuria aurantia</i> lectin |
| AAV | adeno-associated virus |
| ABHD6 | alpha/beta-Hydrolase domain containing 6 |
| AEA | N-arachidonylethanolamine |
| AM251 | 1-(2,4-Dichlorophenyl)-5-(4-iodophenyl)-4-methyl-N-1-piperidinyl-1H-pyrazole-3-carboxamide |
| AMPAR | α -amino-3-hydroxy-5-methyl-4-isoxazolepropionic acid receptor |
| ARF | GTPase ADP-ribosylation factor |
| BIC | bicuculline |
| BSA | bovine serum albumin |
| CA (1,2,3) | <i>cornu ammonis</i> (1,2,3) |
| CaMKII | Ca ²⁺ /calmodulin-dependent protein kinase II |
| CB1R | cannabinoid receptor 1 |
| CB2R | cannabinoid receptor 2 |
| CNQX | 6-cyano-7-nitroquinoxaline-2,3-dione |
| ConA | Concanavalin A |
| COP1 | coat protein complex I |
| COP2 | coat protein complex II |
| CRP | ceramide rich platforms |
| DAB | 3,3'-Diaminobenzidine |
| DAG | diacylglycerol |
| DAGL | diacylglycerol lipase |
| Dam-methylase | DNA adenine methylase |
| DAP | 2-Amino-5-phosphonovaleriansäure |
| DAPI | 4',6-Diamidin-2-phenylindol |
| DG | dentate gyrus |
| DIV | day <i>in vitro</i> |
| DMEM | Dulbecco's Modified Eagle Medium |
| DMSO | dimethylsulfoxid |
| DNA | Deoxyribonucleic acid |
| dNTPs | Deoxynucleoside Triphosphate set |
| DSE | depolarization-induced suppression of excitation |
| DSI | depolarization-induced suppression of inhibition |
| E/I | excitation/inhibition |
| EC | endocannabinoids |
| ECS | endocannabinoid signaling |
| EDTA | Ethylenediaminetetraacetic acid |
| EE | enriched environment |
| EF-hand 1+2 | Ca ²⁺ -binding domain |
| EM | electron-microscopy |
| ER | endoplasmic reticulum |
| ERGIC | ER-Golgi intermediate compartment |
| FA | Fatty Acid |
| FAAH | fatty acid amide hydrolase |

| | |
|-----------------|--|
| FBS | fetal bovine serum |
| FK506 | Tacrolimus |
| FKBP | FK506 binding protein domain |
| GA | Golgi apparatus |
| GDP | guanosine diphosphate |
| GluA1-4 | Glutamate receptor 1-4 |
| GluN2B | NMDA-receptor subunit <i>N</i> -methyl D-aspartate receptor subtype 2B |
| GM130 | Golgi matrix protein 130 |
| GO | Golgi-outpost |
| GPCRs | G protein coupled receptors |
| Gq | G protein subunit alpha q |
| GS | Golgi Satellites |
| GTP | guanosine-5'-triphosphate |
| H3 | Histone binding protein 3 |
| HBSS | Hanks' Balanced Salt Solution |
| HEK cells | Human embryonic kidney 293 cells |
| HPL | <i>Helix pomatia</i> agglutinin |
| ICC | Immunocytochemistry |
| IHC | Immunohistochemistry |
| IP3 | Inositol triphosphate |
| IP3R | Inositol triphosphate Receptor |
| KD | knockdown |
| KO | knockout |
| LB | lysogeny broth |
| LTD | long term depression |
| LTP | long term potentiation |
| M1R | muscarinic acetylcholine receptor M1 |
| MAG | monoacylglycerol |
| MAGL | Monoacylglycerinlipase |
| MAGUK | membrane-associated guanylate kinases |
| Man2 | Mannosidase 2 |
| MAPK | mitogen-activated protein kinase |
| MARCKS | Myristoylated alanine-rich C-kinase substrate |
| MEM | Modified Eagle Medium |
| mGluRs | metabotropic glutamate receptors |
| MRC5 | Medical Research Council cell strain 5 |
| MS | Mass spectrometry |
| nCaBP | Calcium-binding protein |
| NCAM | Neural cell adhesion molecule |
| NCS1 | Neuronal Calcium Sensor 1 |
| NMDAR | <i>N</i> -methyl-D-aspartate receptor |
| P2 | heavy membrane fraction |
| PB | phosphate buffer |
| PEI | polyethylenimine |
| PFA | Paraformaldehyd |
| PI | protease inhibitor cocktail |
| PI4KIII β | Phosphatidylinositol 4-kinase III beta |
| PIP2 | Phosphatidylinositol |
| PLC β | PhospholipaseC- β |
| PLL | poly-L-lysin |

| | |
|------------|--|
| PSA | Polysialylation |
| PSD | postsynaptic density |
| PSD95 | Postsynaptic density protein 95 |
| PtdInsPs | phosphatidylinositol phosphates |
| PtdSer | phosphatidylserine |
| RNA | ribonucleic acid |
| ROIs | regions of interest |
| RT | room temperature |
| RUSH | retention using selective hooks |
| Sar1 | secretion associated Rasrelated GTPase 1A |
| SBP | Streptavidin binding peptide |
| SE | standard environment |
| sgRNA | single guide RNA |
| SGZ | sub granular zone |
| SJ | synaptic junctions |
| SLF | synthetic ligand of FKBP |
| SM | Sphingomyellin |
| So | synaptosomes |
| SOB | Super Optimal Broth |
| ST3Gal5 | Lactosylceramide alpha-2,3-sialyltransferase |
| ST8Sia2 | alpha-2,8-sialyltransferase 8B |
| ST8Sia4 | CMP-N-acetylneuraminase-poly-alpha-2,8-sialyltransferase |
| STED | Stimulated Emission Depletion |
| SV2B | Synaptic vesicle protein 2B |
| SYP | Synaptophysin |
| TAE | Tris-acetate-EDTA |
| TBS | theta-burst stimulation |
| TBS buffer | Tris-buffered saline |
| TBS-LTP | theta-burst stimulation long-term plasticity |
| TEM | transmission electron microscope |
| TfB1 | Transfer buffer 1 |
| TfB2 | Transfer buffer 2 |
| TGN | <i>trans</i> -Golgi network |
| THC | tetrahydrocannabinol |
| TIRF | Total internal reflection fluorescence |
| TM | <i>trans</i> membrane |
| TTX | Tetrodotoxin |
| VPS | vacuolar protein sorting-associated protein |
| WGA | Wheat germ agglutinin |

Selbstständigkeitserklärung

Ich versichere hiermit, dass ich die vorliegende Arbeit zu dem Thema “Regulation of synaptic signaling following environmental enrichment and local secretory trafficking in neuronal dendrites“ ohne unzulässige Hilfe Dritter und ohne Benutzung anderer als der angegebenen Hilfsmittel angefertigt habe; verwendete fremde und eigene Quellen sind als solche kenntlich gemacht.

Ich habe insbesondere nicht wissentlich:

- Ergebnisse erfunden oder widersprüchliche Ergebnisse verschwiegen,
- statistische Verfahren absichtlich missbraucht, um Daten in ungerechtfertigter Weise zu interpretieren,
- fremde Ergebnisse oder Veröffentlichungen plagiiert,
- fremde Forschungsergebnisse verzerrt wiedergegeben.

Mir ist bekannt, dass Verstöße gegen das Urheberrecht Unterlassungs- und Schadensersatzansprüche des Urhebers sowie eine strafrechtliche Ahndung durch die Strafverfolgungsbehörden begründen kann.

Ich erkläre mich damit einverstanden, dass die Arbeit ggf. mit Mitteln der elektronischen Datenverarbeitung auf Plagiate überprüft werden kann.

Die Arbeit wurde bisher weder im Inland noch im Ausland in gleicher oder ähnlicher Form als Dissertation eingereicht und ist als Ganzes auch noch nicht veröffentlicht.